Fall 2012

Factors Influencing the Spatial and Temporal Distrubtion of Primary Productivity and Community Respiration in the Mississippi Coastal Estuarine Region

Ryan Anthony Vandermeulen
University of Southern Mississippi

The University of Southern Mississippi

FACTORS INFLUENCING THE SPATIAL AND TEMPORAL DISTRIBUTION OF PRIMARY PRODUCTIVITY AND COMMUNITY RESPIRATION IN THE MISSISSIPPI COASTAL ESTUARINE REGION

by

Ryan Anthony Vandermeulen

A Thesis
Submitted to the Graduate School
of The University of Southern Mississippi
in Partial Fulfillment of the Requirements
for the Degree of Master of Science

Approved:

Dean of the Graduate School

August 2012

ABSTRACT

FACTORS INFLUENCING THE SPATIAL AND TEMPORAL DISTRIBUTION OF PRIMARY PRODUCTIVITY AND COMMUNITY RESPIRATION IN THE MISSISSIPPI COASTAL ESTUARINE REGION

by Ryan Vandermeulen

August 2012

This study describes the spatial and temporal distribution of net primary productivity (NetPP) and respiration (RESP) in relation to the biogeochemical, optical, and hydrographic variability in the Mississippi Sound and Mississippi Bight over the course of one year. Surface *in-situ* measurements of NetPP and RESP were regularly determined at two stations by a time-course detection of dissolved oxygen (DO) using novel optode technology. In addition, various biogeochemical, optical, and hydrographic parameters were examined over 14 stations throughout the estuary over a year, using ground and satellite (MODIS Aqua) measurements.

In this study, consistently low dissolved inorganic N:P ratios (average N:P < 4.3 for all stations) suggest that rates of NetPP were nitrogen limited, while the NetPP rates measured in the Mississippi Sound showed periodic growth limitation due to low water-column light availability. Measured RESP rates were partially correlated to both allochthonous (POM, $r^2 = 0.78$, $p < 0.01$, $n = 20$) and authochthonous (chlorophyll-a, $r^2 = 0.74$, $p < 0.01$, $n = 23$) proxies for organic matter sources. There was also some evidence that ambient seasonal light levels may have driven some enhanced light-dependent respiration. Time and depth integrations of NetPP and RESP indicate that net heterotrophic conditions persisted in Mississippi waters through most of the year, and

that both integrated rates tended to be higher in the Mississippi Bight compared to the Mississippi Sound.

As light availability appears to play an important role in regulating biological activity in this estuary, an empirical model (derived from multiple regression analysis) for predicting the downwelling light attenuation coefficient [K_d(PAR)] is proposed for Mississippi waters. The model is based on contributing biogeochemical parameters [suspended particulate matter (SPM), chromophoric dissolved organic matter (CDOM), and chlorophyll-a] and the partitioning of each biogeochemical parameter using the empirical model reveals that SPM was the dominant contributor to K_d(PAR). However, relative contribution of SPM (as well as values of K_d) diminished in the Mississippi Bight as the fraction of Particulate Inorganic Matter (PIM) to total SPM decreased.

Finally, the extrapolation of biologically significant parameters to larger spatial scales via satellite remote sensing was assessed for the study area. Comparisons of measured chlorophyll-a, SPM, CDOM, K_d, euphotic depth (Z_{eu}), and photosynthetically available radiation (PAR) to various products derived from the MODIS time-series showed high correlations ($r^2 > 0.8$), with the exception of chlorophyll-a ($r^2 \leq 0.6$). Overall, a quasi-analytical algorithm (QAA) approach was better suited for measuring the distribution of light (i.e. K_d and Z_{eu}) using satellite remote sensing methods in these optically complex waters, while simpler remote sensing reflectance (R_{rs}) and band ratios tended to predict SPM and CDOM distribution better. The results of this study demonstrate that the drivers of biogeochemical variability as well as the balance between NetPP and RESP are determined by a multitude of factors.

ACKNOWLEDGMENTS

I am extremely grateful to my academic advisor, Dr. Kjell Gundersen, for his unwavering help, support, and patience through my graduate studies. His personal and professional mentorship were paramount in guiding me through my academic endeavors, and have made me a better scientist. Thank you for everything Dr. Gundersen. I would also like to thank my thesis committee members, Dr. Karen Orcutt, Dr. Bruce Spiering, and lead advisor Dr. Stephan Howden for their technical advice. A special thanks is in order for Dr. Bruce Monger for teaching me the fine art of programming, enabling me to become at peace with satellite remote sensing. Also, I am deeply appreciative to Dr. Steve Lohrenz for his financial support of my external coursework.

I would like to acknowledge the technical support of the University of Southern Mississippi staff and technicians, specifically the efforts of Allie Mojzis for providing quality data, as well as Kevin Martin and Curtis Caruthers for safely operating the boat during sampling. A sincere debt of gratitude goes out to my colleagues Sumit Chakraborty, Paul Burnett, and Amy Glover. Thank you all for your technical advice, relentless encouragement and above all, your friendship through this process.

Finally, I would like to thank my wife Miranda for her personal support and great patience at all times, and for loving me unconditionally through my successes and failures. I am also grateful to my parents, Leo and Tammy, and my brother, Jon, for their confidence in me and encouragement from birth to set no limits to my ambition. Admittedly, a mere expression of thanks to all the above contributors does not begin to describe the depth of my gratitude. This work was funded by the NASA Graduate Student Research Program (GSRP) fellowship (grant no. NNX10AL05H).

TABLE OF CONTENTS

LIST OF TABLES

Table

LIST OF ILLUSTRATIONS

Figure

LIST OF ABBREVIATIONS

Apparent Optical Property.....AOP

Colored Dissolved Organic Matter.....CDOM

Chlorophyll-*a*.....chl-*a*

Dissolved Inorganic Nitrogen.....DIN

Dissolved Inorganic Phosphorous.....DIN

Dissolved Organic Matter.....DOM

Dissolved Organic Carbon .....DOC

Dissolved Oxygen.....DO

Gross Primary Productivity.....GPP

Inherent Optical Property.....IOP

Moderate Resolution Imaging Spectroradiometer.....MODIS

Net Ecosystem Productivity.....NEP

Net Primary Productivity.....NetPP

Particulate Organic Carbon .....POC

Particulate Inorganic Matter .....PIM

Particulate Organic Matter.....POM

Particulate Nitrogen….....PN

Particulate Total Phosphorous .....PTP

Photosynthetically Available Radiation.....PAR

Quasi-Analytical Algoritm.....QAA

Remote Sensing Reflectance.....R_{rs}

Respiration .....RESP

Suspended Particulate Matter.....SPM

CHAPTER I

INTRODUCTION

Functioning as the ultimate transition from land to sea, estuaries are dynamic ecosystems characterized by regular fluctuations in several biogeochemical parameters. These regions generally receive copious amounts of allochthonous materials (i.e. inorganic nutrients and organic matter from rivers), and while estuaries comprise a relatively small fraction of total water volume of Earth, they contain extremely productive biological communities. As such, there is a disproportionally high amount of biogeochemical cycling that occurs in these regions compared to the open ocean. In order to understand the flow of energy and materials through an estuary and the ecological consequences, however, it becomes necessary to examine the balanced contribution of several community members over spatial and temporal scales.

The measurement of Net Ecosystem Production (NEP) attempts to determine whether a particular estuary is a net source or sink of carbon by quantifying the relationship between two fundamental processes that affect its distribution, namely primary productivity (P) and respiration (R). The NEP is defined as the difference between P and R, and is a direct indicator of the ecological status of any given community, and indirectly, the water quality (del Giorgio and Williams 2005). While these processes tend to influence the activity of one another, they are not always closely coupled as one might expect, therefore, on a small scale, ecosystems can become net autotrophic ($P > R$) or net heterotrophic ($P < R$) based on community composition, as well as the quantity and quality of available energy source material (Blight et al. 1995, Caffrey 2003, Hopkinson and Smith 2005). This, in turn, affects the potential for transfer

of carbon to higher trophic levels and is significant on global scales (Smith and Kemp 1995).

Certainly, as with any open aquatic system, there are seldom any clear linear relationships that can be used to definitively predict the interactions among community members, and this is especially true for estuaries. The reactants and products of both primary productivity and respiration are closely linked. However, in an ever-changing ecosystem influenced by much greater proportions of allochthonous material than open water ecosystems, there are ultimately many environmental factors that control each of these processes independently (Carlson 2002, Smith and Kemp 2003). Given the influence of tidal fluctuations, these factors have the potential to change dramatically on diel as well as seasonal scales (Fuhrman et al. 1985, Smith and Kemp 1995). In order to resolve this variability, this project will assess net ecosystem productivity through a multi-spatial scale time-series monitoring of dissolved oxygen, light, chlorophyll-a, and several dynamic hydrographic, optical, and chemical parameters that influence metabolic activity in Mississippi waters.

Background

Since the introduction of the ^{14}C method by Steeman Nielsen in 1952, traditional research has focused a great deal on primary productivity in coastal regions, while vastly neglecting the contribution of heterotrophic respiration to whole ecosystem metabolism. Recently, however, there has been a surge of interest in additionally quantifying respiration measurements, in part, due to the increased precision in methodology (Smith and Kemp 2003, Williams and del Giorgio 2005). In addition, there has been an increased awareness to the role that microheterotrophs play in biogeochemical cycling, not merely

as decomposers, but as active participants in the regeneration of nutrients via the microbial loop (Pomeroy 1974, Azam et al. 1983). Thus, primary productivity and respiration can affect an ecosystem in very different ways, and therefore have been recognized as distinct processes with variable contributions to the distribution of organic matter in aquatic ecosystems (Carlson 2002).

From an ecological perspective, the flux of oxygen in a given parcel of water is a direct indicator of the *in situ* production and oxidation of organic matter (Williams 1981, Biddanda et al. 1994). Although oxygen evolution is a function of autotrophic activity, it is important to note that in natural waters, it is also affected by the net pool of organic matter being added to the environment, as there is simultaneous consumption of organic matter and oxygen taking place (Ryther 1956). These measurements are of ecological significance, but yield limiting information about all the energy being utilized by a system since the organic matter produced is not necessarily consumed in the time or place it originates (Pomeroy and Johannes 1968). However, respiration (oxygen consumption) is common to all organisms and the addition of this measurement is a direct indication of energy utilization within the community at a particular time and location. It should be noted that some energy obtained for respiration is ultimately utilized in creating new cell bodies, and therefore not respired, possibly leading to slight underestimates of organic matter consumption on shorter time scales (Geider 1992, del Giogio and Cole 1998). Nevertheless, while all current methods are subject to some degree of uncertainty, using oxygen monitoring to examine the flow of organic matter through a community is ultimately advantageous for ecological questions as it incorporates various sources of

carbon found in natural systems while simultaneously assessing the activity of both autotrophs and heterotrophs.

Oxygen concentrations have conventionally been measured using the Winkler technique, originally developed in 1888, and several improvements to the method have been made since (Williams and Jenkinson 1982, Outdot et al. 1988). While this procedure yields very accurate results, it is a destructive method, thus it is difficult to obtain high resolution data on short-term patterns (i.e. diel variability) without sacrificing several samples over a given time interval, which can present logistical challenges. Due to the intensity of labor involved, therefore, the use of Winkler titrations is generally limited to the analysis of a beginning and end point, while data points in between must be extrapolated. This becomes a problem when measuring respiration because rates of oxygen consumption have been shown to become non-linear within minutes to hours of dark measurements (Weger et al. 1989, Hopkinson and Smith 2005, Falkowski and Raven 2007). Recently, the use of polarographic oxygen sensors has allowed the continuous monitoring of dissolved oxygen in the environment, however, these sensors consume some oxygen in the process (Kanwisher 1959, Falkowski and Owens 1978, Griffith 1988, Beardall et al. 1994). Even more recently, the sophistication of dissolved oxygen optodes has vastly improved the precision of real-time measurements even under low oxygen conditions, while leaving samples completely unaltered and available for subsequent sampling. The use of these sensors has yet to become mainstream in oceanographic research, however, one of the goals of this thesis is to establish the viability of dissolved oxygen optode sensors in measurements of biological activity. In

many cases, an increase in data points using real-time measurements can shed light on processes occurring on shorter time scales.

For example, when measuring primary productivity, several authors argue that the dark measurements used to correct for oxygen loss in the light do not include some light-dependent and oxygen-consuming processes such as photorespiration and the Mehler reaction, thus providing some underestimate of net productivity (Williams and del Giorgio 2005, Falkowski and Raven 2007). Photorespiration occurs as oxygen concentrations accumulate in the cell at high light intensities, causing ribulose-1,5-bis-phosphate carboxylase/oxygenase (RuBisCO) to cease carbon fixation and instead consumes oxygen to form glycolate and glycerate (Falkowski and Raven 2007). The Mehler reaction involves the photoreduction of oxygen as electrons are transported along photosystems 2 and 1 (Gazeau et al. 2007). While neither of these processes are involved in the cycling of organic matter through the ecosystem, the potential for the alteration of net productivity measurements has significant implications (Gazeau et al. 2007). However, lab experiments using *Skeletonema costatum* show a dramatic change in the rate of oxygen consumption following the instantaneous removal of light, suggesting that light-dependent processes may continue to occur for several minutes following a dark period (Figure 1). On longer time scales (i.e. hours), dark respiration rates continue a non-linear trajectory as the pool of carbohydrate within a bottle is utilized (Falkowski and Raven 2007). With real-time analysis of biological activity, optodes can allow for greater resolution than can be obtained with comparable methodology.

Neither P nor R are static measurements and will tend to change throughout the day based on internal substrate availability and the demand for cellular pathway

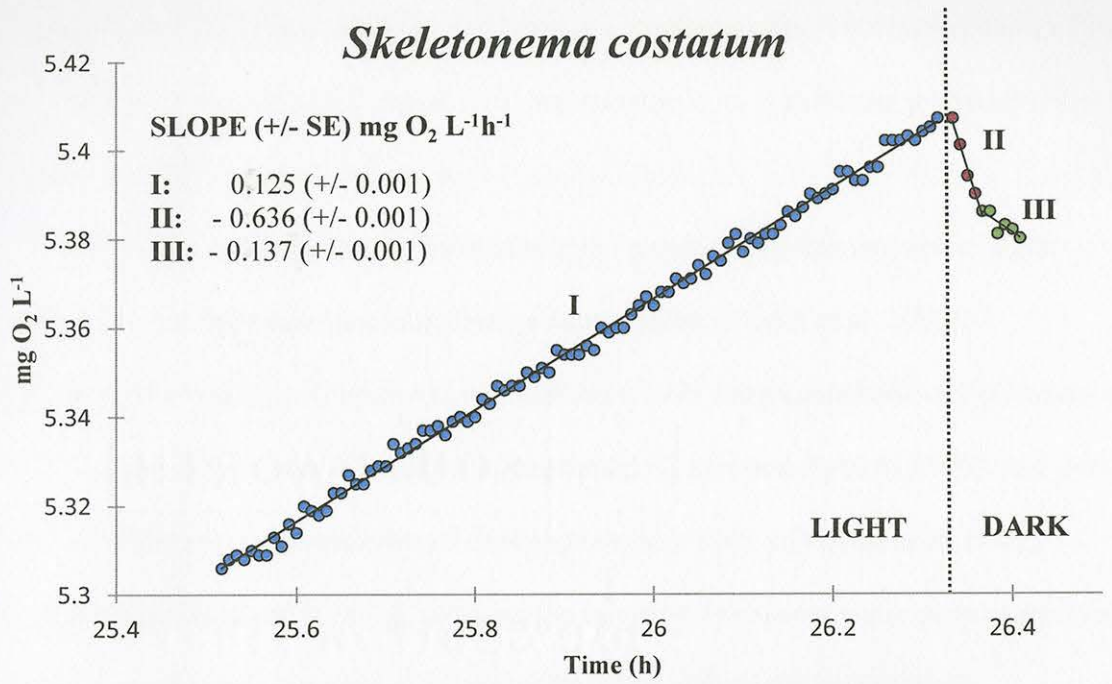

Figure 1. Oxygen concentration measurements over time and computed rates of pure *Skeletonema costatum* culture (Gundersen and Vandermeulen unpublished).

intermediates (Geider 1992). The most important control on the daily availability of the afore mentioned products is the availability of photosynthetically available radiation (PAR, 400-700 nm), which changes not only on a regular diel basis, but may change in response to cloud shading and turbulent wave activity in natural environments (Cloern 1987, Kirk 1992, Falkowski and Raven 2007). Changes in light intensity throughout the day have been shown to have a significant effect on the rates of photosynthesis, and subsequently on rates of phytoplankton respiration as more substrate becomes available (Falkowski and Owens 1978, Weger et al. 1989, Beardall et al. 1994, Lewitus and Kana 1995). While physiological responses within individual cells are not often of interest to ecologists looking at large scale patterns, nutrient dynamics and differences in seasonal community composition have the potential to significantly change the rate of both primary production and respiration on varying time scales (Geider 1992). According to

Weger et al. (1989), accounting for diel changes alone can alter P/R ratio estimates by up to 25%. Therefore, when looking at NEP measurements, it is pertinent to quantify these changes to retain accurate estimates.

Besides regulating the amount of primary productivity that can occur, light availability can influence plankton species composition (Floder et al. 2002), morphology/physiology (Falkowski and LaRoche 1991), organism behavior (Graham et al. 2001), the distribution of subaquatic vegetation (Carter and Rybicki 1990), and can even contribute to the breakdown of dissolved organic matter (Moran et al. 2000). Modeling the distribution of light attenuation and its contributing water parameters is of utmost importance to examining the dynamics of an ecosystem, especially in environments where light limitation is ubiquitous. As light enters the water column, it is absorbed and scattered by various constituents within the water, thereby leading to the diffuse attenuation of light with depth (Kirk 1994). These various constituents include water itself, phytoplankton, suspended particulate material (SPM; both inorganic and organic), and chromophoric dissolved organic matter (CDOM), all of which modify the spectral and geometrical distribution of light in water and contribute to its overall optical properties (Kirk 1992, Lewis 1992).

The mathematical description of this attenuation is described by the diffuse attenuation coefficient, K_d, and is frequently modeled as a function of the Beer-Lambert Law: $E_z = E_o e^{-kz}$ where E is downwelling irradiance at depth (z), declining in an exponential manner (-k) from the irradiance level just under the surface (E_o). The diffuse attenuation coefficient is known as an apparent optical property (AOP), because its value is dependent on both the concentration of constituents in the water, as well as the angular

distribution of the underwater light field (Morel and Smith 1982). This is distinguished from Inherent Optical Properties (IOPs), which describe the scattering and absorption terms that contribute to K_d, and are solely a function of the water content (Kirk 1994). Besides characterizing the underwater light field, K_d is also used to calculate the euphotic depth (Z_{eu}), or the depth at which 1% of the surface light is available. The euphotic depth defines the threshold for photosynthetic activity based on light availability and is significant for integrated calculations of primary productivity. In addition, heterotrophic respiration is not strongly dependent on light availability, therefore the ratio of photic depth to water depth may be a large factor in resolving the spatial distribution of NEP within a given community (Cloern 1987, Caffrey et al. 1998). Given the variable nature of estuarine environments, the underwater distribution of light is likely to change drastically on spatial and temporal scales and affect the distribution of ecosystem productivity.

One unavoidable aspect of any ship-based *in situ* sampling procedure is that the data offers little or no input into spatial variability, as measurements only apply to the sample being collected. Hence, in order to understand the influence of biogeochemical cycles on larger scales, it follows that there must exist some observation of these cycles on expanded scales. With recent advances in technology, there has been an interest in potentially monitoring biogeochemical processes via ocean color on larger spatial scales using satellite remote sensing (Johnson et al. 2009). The principle of ocean color observation relies on the upwelling of light from the ocean surface after it has been backscattered by the afore mentioned constituents in the water (Kirk 1994). An observed body of water will display spatial and temporal variation in both AOPs and IOPs, which

subsequently correspond to a change in ocean color as observed from satellite radiometers. In this way, information is frequently gathered over global scales, allowing a comprehensive view of large aquatic ecosystems with greater efficiency than shipboard measurements (Kirk 1994). However, the analytical retrieval of biogeochemistry from radiance measurements can be challenging, especially in waters where light absorption is dominated by factors that do not covary with phytoplankton, also known as Case 2 waters (Mroel and Prieur 1977). Several published data products exist that allow the quantification of biologically significant parameters within Case 2 waters, including the diffuse attenuation coefficient (K_d), CDOM, SPM, and in some cases, chlorophyll. These algorithms have yet to be extensively tested in coastal Mississippi waters. However, the careful coupling of *in situ* measurements and satellite data may allow for data validation and extrapolation to larger spatial scales.

Hydrodynamics

The study area resides along a sampling transect that extends from the Bay of St. Louis (located in Hancock County, MS) to the relatively shallow Gulf of Mexico waters (Mississippi Bight) just beyond a chain of narrow barrier islands that enclose the shallow Mississippi Sound. Primary seawater input to the estuarine system occurs through passages located between these six offshore barrier islands. Most of the freshwater introduced to the Mississippi Sound arrives through numerous rivers which cover the entire geographic range of the MS Coast and extend eastward into Mobile Bay. Episodic freshwater input to the western Mississippi Sound occurs via the Bonnet Carré spillway (BCS), a flood-control operation that re-directs water from the Mississippi River to the western Mississippi Sound through Lake Pontchartrain (Christmas 1973).

The Mississippi coastal estuarine system encompasses several salt-influenced bays, the Mississippi Sound, and the Mississippi Bight. This micro-tidal estuary is shallow (average depth of MS Sound = 3 m) and well-mixed, therefore variations in salinity generally extend horizontally from the mouth of the rivers and bays, with no extended periods of vertical stratification north of the barrier island passes (Kjerve 1983, Kjerve and Magill 1989). The presence of sewage treatment plants and chemical/industrial plants along the Gulf Coast can be a potential source of pollution to coastal waterways, depending on the rate of output and tidal levels (Lytle and Lytle 1983). In addition to terrestrial sources of anthropogenic input, the British Petroleum oil spill that occurred on April 20th, 2010 has introduced weathered hydrocarbon products into adjacent waterways and the Mississippi Sound. As of yet, no time-series record of primary productivity and dissolved oxygen consumption is available for this region.

Significance

One of the leading objectives in biological oceanographic research is to determine how carbon flows through a given ecosystem on varying temporal scales. This is especially important for estuaries, as these regions account for nearly 25% of the global estimates of primary productivity (Berger et al. 1989). While on larger time and space scales, primary productivity and respiration must ultimately converge, the potential uncoupling of these two processes directly affects biogeochemical cycling of carbon in aquatic systems, which, in turn, affects the health of an estuary and determines the sustainability of fisheries (Smith and Kemp 2001). Therefore, it is of utmost importance that this cycling be understood at a fundamental level, analyzing all parameters which

may affect the distribution of carbon in order to resolve the calculated budget in coastal ecosystems.

The Mississippi coastal estuarine system is characterized by extensive fluvial input, terrestrial runoff, and high benthic sediment fluxes, resulting in the delivery of both inorganic and organic substrates to fuel biological activity (Lohrenz and Verity 2004). Where these inputs tend to favor heterotrophic activity, and net dissolved oxygen consumption begins to exceed net oxygen production, the system may decline to a state of hypoxia. While the appreciable effect of air-sea diffusion generally keeps the shallow, well-mixed waters of the near-shore communities from becoming hypoxic, there are regions within the Mississippi Bight that can experience seasonal declines in bottom water oxygen concentrations (Brunner et al. 1996, Engle et al. 1999). Ultimately, by examining the relationship between several biogeochemical parameters, a more defined picture of ecosystem metabolism in the Mississippi Estuary will begin to develop, which may be useful to state and federal officials when remotely analyzing the health of these regions.

Research Strategy

The objective of this study is to resolve the variability of ecosystem metabolism and biogeochemistry on relevant temporal and spatial scales, while assessing the possibility of large-scale extrapolation. Ultimately, the processes responsible for estuarine health in this region are driven by light, temperature, salinity, nutrients, and carbon delivery, all of which will be closely monitored over varying spatial and temporal scales. Various statistical methods and direct comparison will be utilized to determine how each of these parameters affect primary productivity and community respiration.

Depth and time-integrations of rate measurements will determine NEP at two different stations, using a combination of lab-derived and *in situ* data. Also, the relationship between measured optically significant parameters (chlorophyll, CDOM, and SPM) and light attenuation will be examined directly though *in* situ measurements to determine if a direct correlation can be derived. Finally, relationships between ground measurements of optical properties and satellite-derived products will be analyzed to determine whether validation criteria can be achieved.

Hypotheses

(1) Measurements of net primary productivity and respiration will vary on seasonal scales and between stations, showing significant correlations with salinity, temperature, biogeochemistry, light attenuation (K_d), and PAR.

(2) The spatial-temporal variability of light attenuation (K_d) measurements can be correlated and partitioned to laboratory-derived measurements of CDOM, SPM, and chlorophyll.

(3) Satellite (MODIS) derived estimates of biologically significant parameters (chlorophyll, SPM, CDOM, K_d(PAR), Z_{eu}, and PAR) can be validated with ground measurements and used to calculate regional primary productivity.

CHAPTER II

MATERIALS AND METHODS

Data Acquisition (all stations)

Data were collected from 14 sampling stations located in and around Bay St. Louis, the Mississippi Sound, and Mississippi Bight. Two separate transects were sampled at regular, fixed intervals between January and December 2011, as weather permitted. The Bonnet Carré Spillway (BCS) transect is a near-shore sampling grid, extending from the mouth of the Pearl River, and eastward to Pass Christian with one station in Bay St. Louis. The Northern Gulf Institute (NGI) transect extends southward from Bay St. Louis, and into the Mississippi Sound and Mississippi Bight, terminating at the 20 meter isobath south of Horn Island. All stations were sampled using the *R/V LeMoyne*, operated by the USM Department of Marine Science.

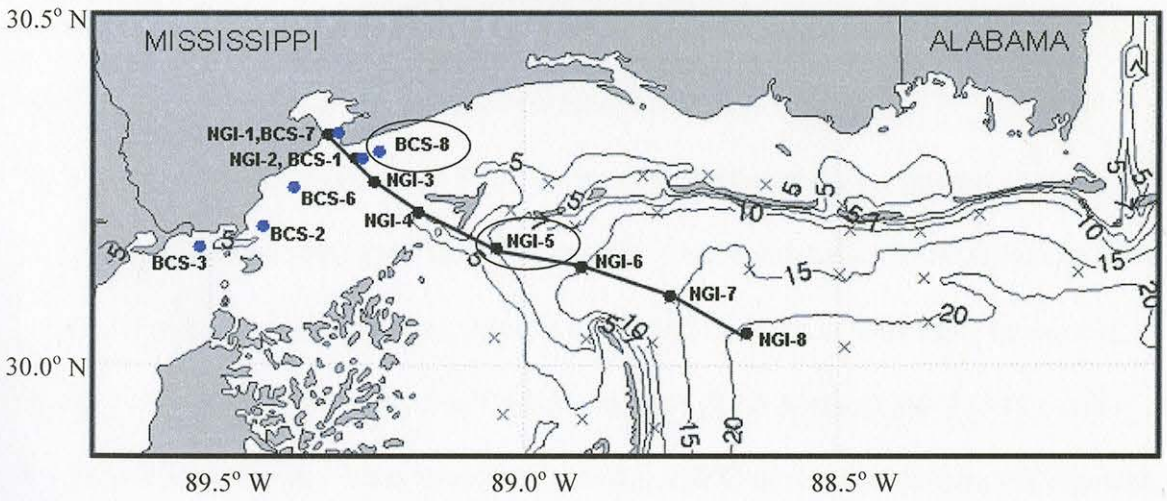

Figure 2. Sampling stations visited monthly by the Department of Marine Science, USM in the Northern Gulf Institute project (NGI, black dots) and the Bonnet Carré Spillway (BCS, blue dots) monitoring programs. The circles show the station locations for the monthly primary productivity incubations.

At each station, salinity and temperature were determined with the use of a Seabird SBE 49 CTD, dissolved oxygen was determined using the Seabird SBE 43 sensor, and chlorophyll fluorescence was determined using the Wetlabs ECO FL-3 fluorometer. Conductivity and dissolved oxygen sensors were consistently calibrated with concurrent water samples that were analyzed in the laboratory (see methods below). In addition, surface water was sampled and analyzed for several biogeochemical and optical parameters, including inorganic nutrients (NO_3, NO_2, NH_4, PO_4, SiO_3), chlorophyll-a, suspended particulate matter (SPM), and chromophoric dissolved organic matter (CDOM).

Dissolved oxygen concentrations were determined chemically using the Winkler titration method (Winkler 1888). Salinity samples were measured against an IAPSO seawater standard on a Guideline Salinometer (AutoSal Model 8400B) according to the manufacturer. Chlorophyll-a samples were extracted in methanol, and sample fluorescence was measured on a Turner Design 10AU Fluorometer (Welschmeyer 1994). Nutrient samples were analyzed fluorometrically (NO_3, NO_2,NH_4) and spectrophotometrically (PO_4, and SiO_3) on an Astoria-Pacific A2+2 nutrient analyzer, according to the manufacturer. The SPM samples were collected on pre-combusted GF/F filters (0.7 μm nominal pore size), dried at 60°C, and weighed at least three times until consecutive readings were less than 0.055% variable (EPA Method 160.2 1979). After the initial measurement, filters were combusted at 450°C for 6 hours to burn off organics, and then re-weighed in order to obtain the particulate inorganic matter (PIM) fraction. Particulate organic matter (POM) was determined as the difference between SPM and PIM.

The CDOM samples were filtered through 47 mm 0.2 μm polycarbonate membrane filters, and the filtrate absorption, *A*, was determined spectrophotometrically between 250 and 800 nm using a Cary 300 Bio UV-visible spectrophotometer. The CDOM slope, *S*, was calculated using a non-linear curve fit of the absorption between 350 – 500 nm. The CDOM absorption coefficient, $a(\lambda)$, was calculated at 412 nm and 440 nm using equation 2-1:

$$a(\lambda) = (2.303 * A(\lambda)) / L, \qquad \text{(Equation 2-1)}$$

where L is the optical path length in meters (Kirk 1994).

Physical Data

Various physical data was obtained over the year-long sampling period, from January to December 2011, as detailed in Table 1. Locations are shown in Figure 3.

Table 1

Ancillary Information on the Physical Data Collected from Government Agencies.

Data Type/Location	Agency	Station	Coordinates	Website
Precipitation (Waveland, MS)	NOAA NCDC	9426	30°18'00"N, 89°22'48"W	ncdc.noaa.gov
Precipitation (Biloxi, MS)	NOAA NCDC	220797	30°24'00"N, 88°51'57"W	ncdc.noaa.gov
Tides (Bay. St. Louis, MS)	NOAA NDBC	WYCM6	30°19'33"N, 89°19'33"W	ndbc.noaa.gov
Wind Vel/Dir. (Bay St. Louis, MS)	NOAA NDBC	WYCM6	30°19'33"N, 89°19'33"W	ndbc.noaa.gov
Wind Vel/Dir. (Ship Island Pass)	NOAA NDBC	GPOM6	30°13'48"N, 88°58'55"W	ndbc.noaa.gov
River Discharge (Wolf River)	USGS	2481510	30°29'02"N, 89°16'26"W	water.usgs.gov
River Discharge (Pearl River)	USGS	2489500	30°47'35"N, 89°49'15"W	water.usgs.gov
River Discharge (Pascagoula River)	USGS	2479000	30°58'41"N, 88°43'37"W	water.usgs.gov
River Discharge (Alabama River)	USGS	2428401	30°36'48"N, 87°33'02"W	water.usgs.gov
Solar Radiation (Grand Bay, MS)	NERR/CDMO	CR	30°21'33"N, 88°25'12"W	nerrscdmo.org

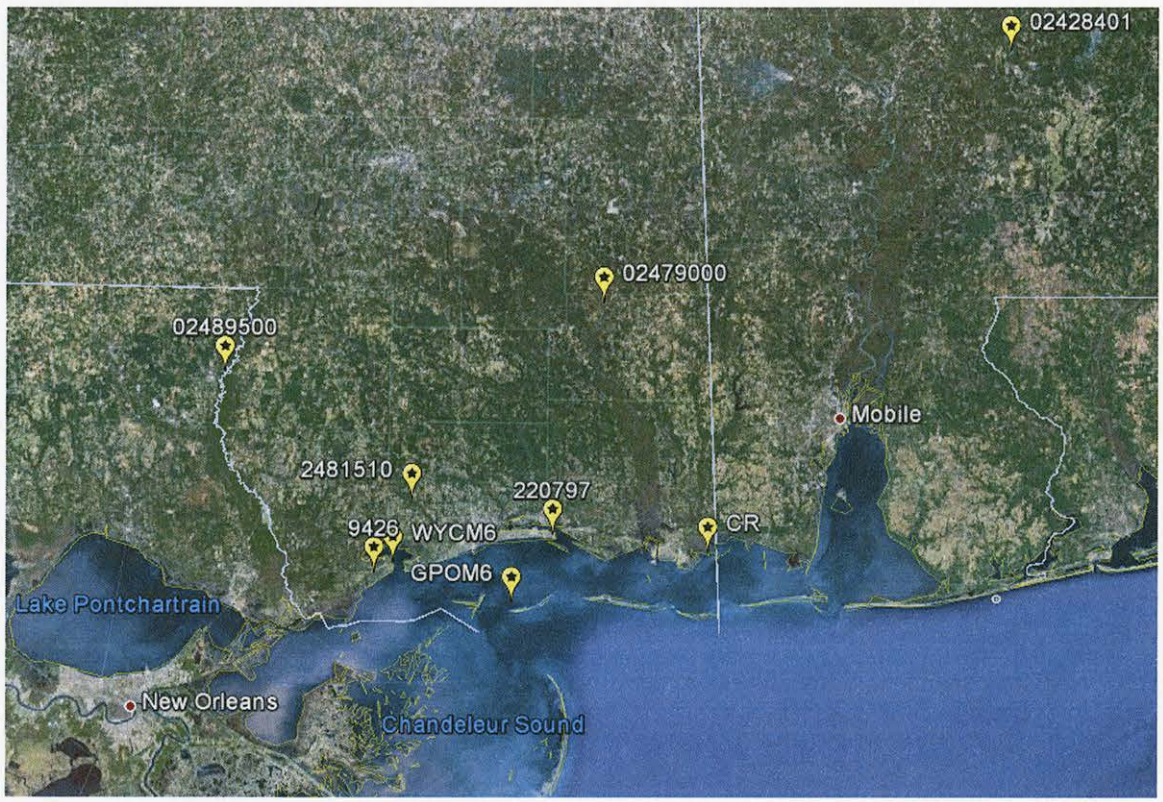

Figure 3. Google Earth image of physical data collection stations.

Net Primary Productivity and Respiration Measurements

Two selected stations were sampled monthly for *in situ* determination of Net Primary Productivity (NetPP) and Community Respiration (RESP) rates. Station NGI-5 (30°09'39"N, 89°02'49"W) is in the Mississippi Bight region, located southeast of Cat Island, with a depth of approximately 7 meters. Station BCS-8 (30°17'52"N, 89°15'43"W) is located within the Mississippi Sound, just outside of Bay St. Louis, with a depth of approximately 3 meters.

For each station, surface waters were collected into a clean 5-gallon bucket. A second bucket, modified with a 200 μm screen mesh bottom, was gently inserted into the sample bucket to eliminate nekton from the incubation. A polycarbonate bottle equipped with a magnetic stir bar was submerged in the filtered water and steps were taken to ensure there were no air bubbles present in the bottle. The incubator was stirred at low speed (125 rpm) to ensure low turbulence that would simulate natural conditions, and restrict the settling of particulates in the bottle. A dissolved oxygen optode sensor (Aanderaa Instruments) was placed inside the bottle (Figure 4), measuring the net development of oxygen every 30 seconds over the course of the incubation. The optode was connected to an environmental sonde (In situ® TROLL 9500), which subsequently measured and recorded temperature and depth in 30 second intervals.

The entire incubation array (Figure 4) was submerged in surface waters using a buoy system fastened to an anchor (Figure 5). After completing the sampling at all other stations (3 – 6 hours), the array was quickly recovered, covered in aluminum foil, and re-deployed for 15 – 45 minutes to obtain respiration rate measurements. A duplicate incubation array was deployed at BCS station 8 at six sampling periods through the year

(June, August, September, October, November, December) to assess the variability between incubation bottles. In addition to oxygen monitoring, sub-surface downwelling light intensity was measured at a frequency of 1/30 seconds during the entire incubation period using a HOBO Pendant® temperature/light data logger (UA-002-08, Onset Computers) attached to the array (Figure 4).

At the completion of an incubation, the content of each bottle was sampled for chlorophyll-a. In addition, un-screened water collected from the same station was sampled for elemental C,N,P and dissolved organic carbon (DOC). Chlorophyll-a was analyzed fluorometrically in accordance with Welschmeyer (1994). Particulate organic carbon and nitrogen (POC, PN) samples were analyzed on ECS 4010 elemental CHN analyzer, using methods outlined in JGOFS (1996). Particulate Total Phosphorous (PTP) samples were combusted, extracted in HCl, and analyzed spectrophotometrically as described by Solorzano and Sharp (1980). Samples for DOC were filtered using pre-combusted GF/F filters, acidified (4 drops of HCl per 60 mL filtrate), and stored at -20°C until analysis. Concentrations of DOC were determined on a Shimadzu TOC-V analyzer.

The dissolved oxygen incubation data was downloaded from the In Situ® TROLL 9500 data logger and displayed in a Microsoft Excel spreadsheet format. Oxygen concentrations were plotted as a function of time, and several linear regressions were used to calculate rate measurements (in units of mg O_2 L^{-1} h^{-1}) over the course of the incubation (rates in light = NetPP, rates after foil covering = RESP). Rates were also converted to carbon equivalents (0.375 mg C mg^{-1} O_2 based on a respiratory quotient of 1: Strickland & Parsons 1972).

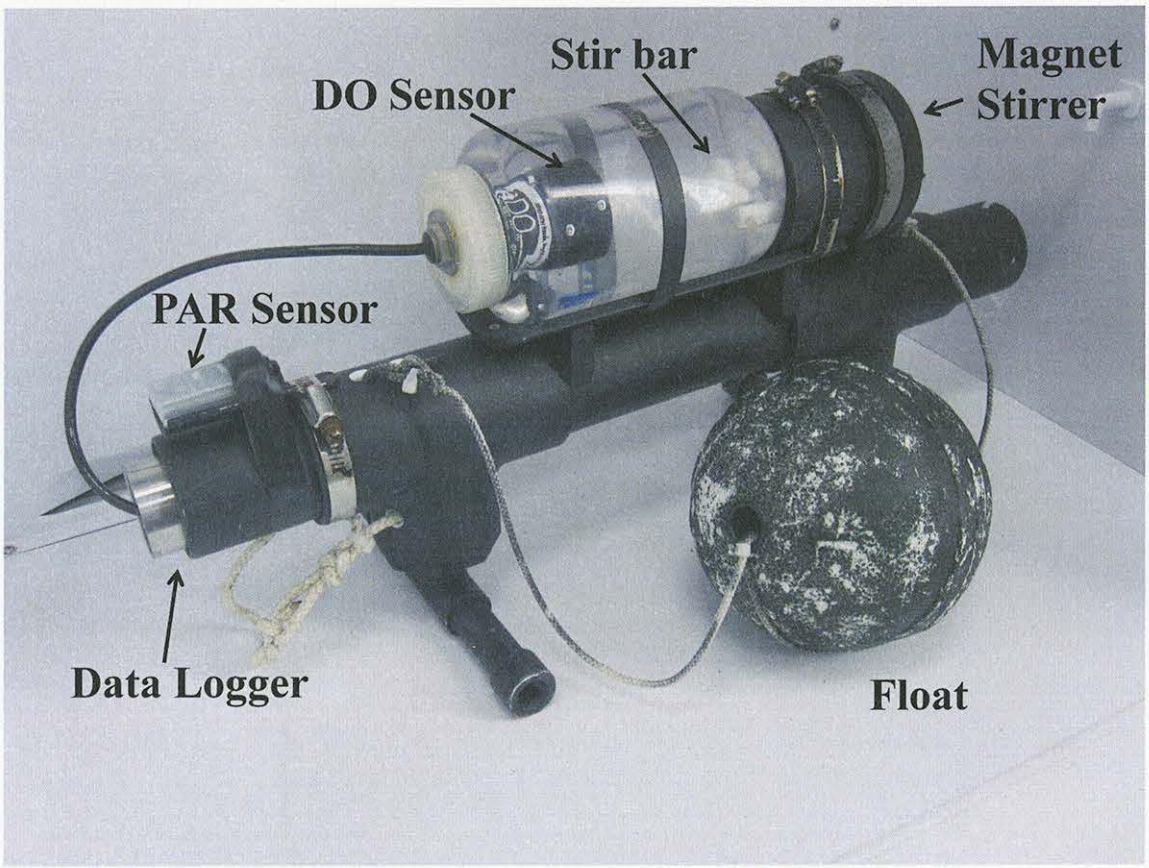

Figure 4. In situ surface incubator equipped with an Aanderra dissolved oxygen optode sensor and Onset HOBO Temperature/Light Pendant. Incubations were deployed for 2- 6 hours in ambient light at approximately 0.25 m depth.

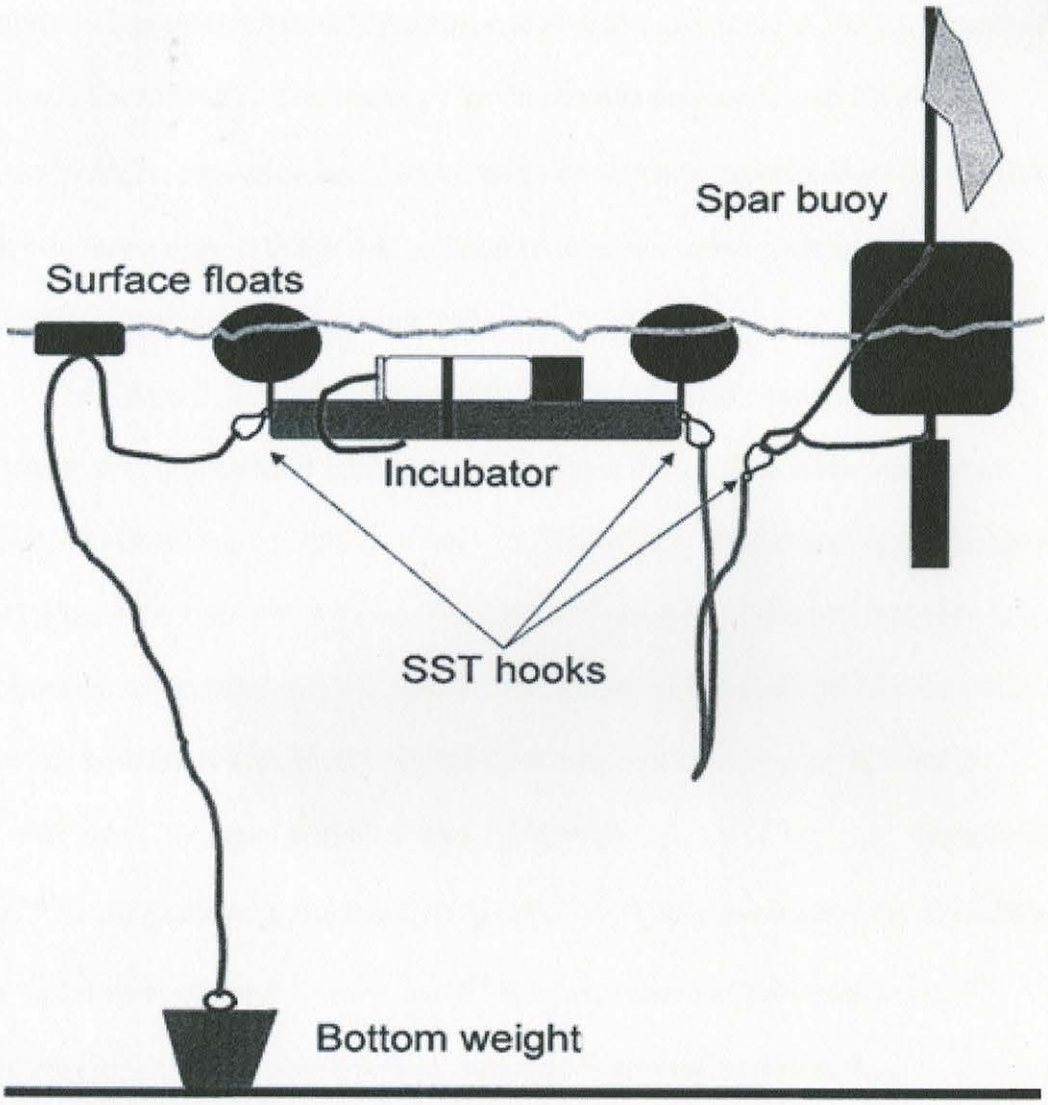

Figure 5. Schematic of dissolved oxygen incubation array used in this study. All elements used to fasten and float the array were painted black in order to ensure minimal reflection.

^{14}C Incubations / Photosynthesis-Irradiance (P-E) Curves

Seawater was also collected from each incubation station and the ^{14}C uptake was measured in a photosynthetron (PAR range 0.04-8.65 mol quanta m^{-2} h^{-1}) as described in Lewis and Smith (1983). The source of irradiance was provided by an ENH-type tungsten-halogen projection lamp, which was subsequently calibrated with a QSL-100 4π scalar irradiance sensor. Water was maintained at *in situ* temperature at the time of collection using a recirculating water bath.

The duration of each incubation was 30 minutes. Upon completion of the incubation, the samples were filtered, acidified (until dry), spiked with scintillation cocktail, and then analyzed two days later for radioactivity (Disintegrations Per Minute, DPM) using a Tri-Carb 2000CA liquid scintillation analyzer. The photosynthetic rates were normalized to chlorophyll to construct a P-E curve (Appendix D). Fitting of the curve was performed with MATLAB, using an equation from Platt et al. (1980):

$$P^B = P^B_s (1- \exp (- \alpha^B E/P^B_s)) (\exp (-\beta^B E/P^B_s)), \qquad \text{(Equation 2-2)}$$

where P^B is the photosynthetic rate (g C [g chl a^{-1}] h^{-1}), E is quantum scalar irradiance, α^B is the initial slope of the P-E curve, and β^B is an expression of photoinhibition. P^B_s represents the maximum photosynthetic rate, and is also referred to as P_{max}.

In order to apply the P-E data to field conditions, a correction factor was applied to the 4π scalar irradiance values to make them comparable to the 2π cosine irradiance. An empirical relationship between 4π and 2π irradiance was derived by measuring the light intensity in the photosynthetron using both types of sensors (Appendix A).

In Situ Irradiance and Light Attenuation [K_d(PAR)] Measurements

In order to obtain attenuation coefficients (K_d) over the wavelength range of Photosynthetically Available Radiation (PAR, 400-700 nm), profiles of downwelling irradiance (E_d^z) were obtained at every station along both transects. Profiles were performed using a hand held unit that included HOBO Temperature/Light Pendant® (recording every 5 s) and TROLL 9500 Data Logger (recording every 5 s), as shown in Figure 6. The profiler was always lowered into the water on the side of the boat facing the sun. Profiling began at the terminal depth and the unit was slowly brought up in 1 foot intervals (1 meter at stations > 7 m), with a sampling time of at least 15 seconds at each depth.

In addition to the water-based profiles, simultaneous measurements of above-surface irradiance (E_d^{0+}) were performed, using an Onset HOBO Temperature/Light Pendant® mounted on top of the boat. The attenuation coefficient was subsequently calculated as the logarithmic slope of the E_d^z profiles as a function of depth as shown in Figure 7 (Kirk 1994). All profiles were normalized to the above-surface E_d^{0+} in order to characterize the percentage of light present at each depth (Figure 8).

The euphotic depth (Z_{eu}) was defined as follows:

$$Z_{eu} = (\ln(0.01)) / K_d(PAR), \qquad \text{(Equation 2-3)}$$

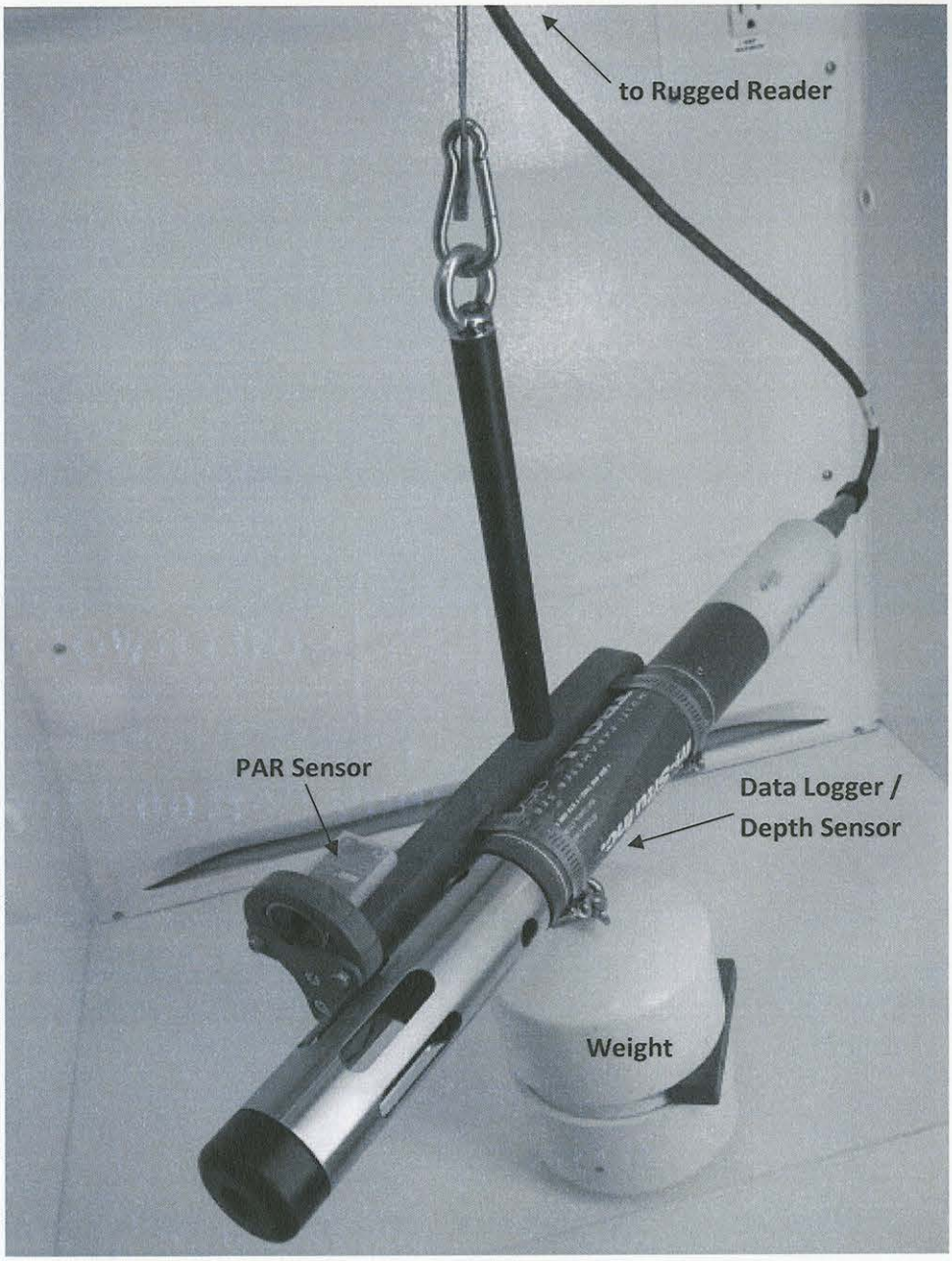

Figure 6. Photosynthetically Available Radiation (PAR) profiling apparatus used to measure the attenuation of downwelling irradiance (E_d^z) for all stations during this study.

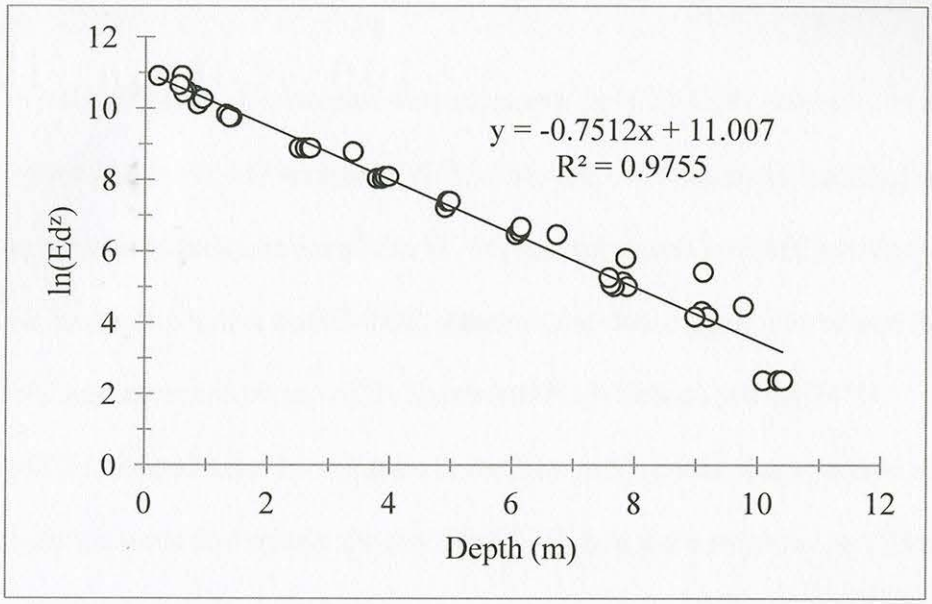

Figure 7. Natural log transformation of downwelling irradiance (E_d^z) as a function of depth. The slope represents the K_d(PAR) value, while the intercept represents log transformed irradiance just below the surface of water (E_d^0).

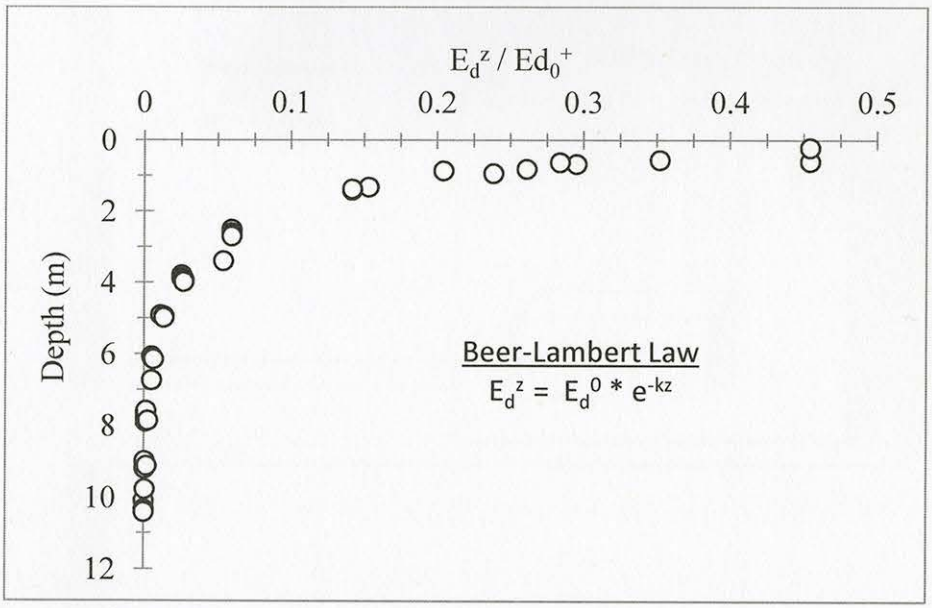

Figure 8. The attenuation of PAR with depth. Normalizing sub-surface irradiance to above-surface irradiance enables the simple calculation of Z_{eu}, and enables the extrapolation of other surface irradiance sensor values to depth.

PAR Time Series

Surface PAR measurements were measured by a LI-COR (LI-190) 2π quantum sensor connected to HOBO 4-channel (U12-006, Onset Computers) data logger. A Universal Transconductance Amplifier (UTA, manufactured by EME systems) was utilized in order to connect the LI-COR sensor to the data logger. The sensor dock (Figure 9) was mounted on top of St. Stanislaus High School (30°18'24"N, 89°19'44"W), located near the entrance to the Bay of St. Louis, and was free of any shading obstructions throughout the day. The PAR data were recorded in 15 minute increments and manually downloaded once every month.

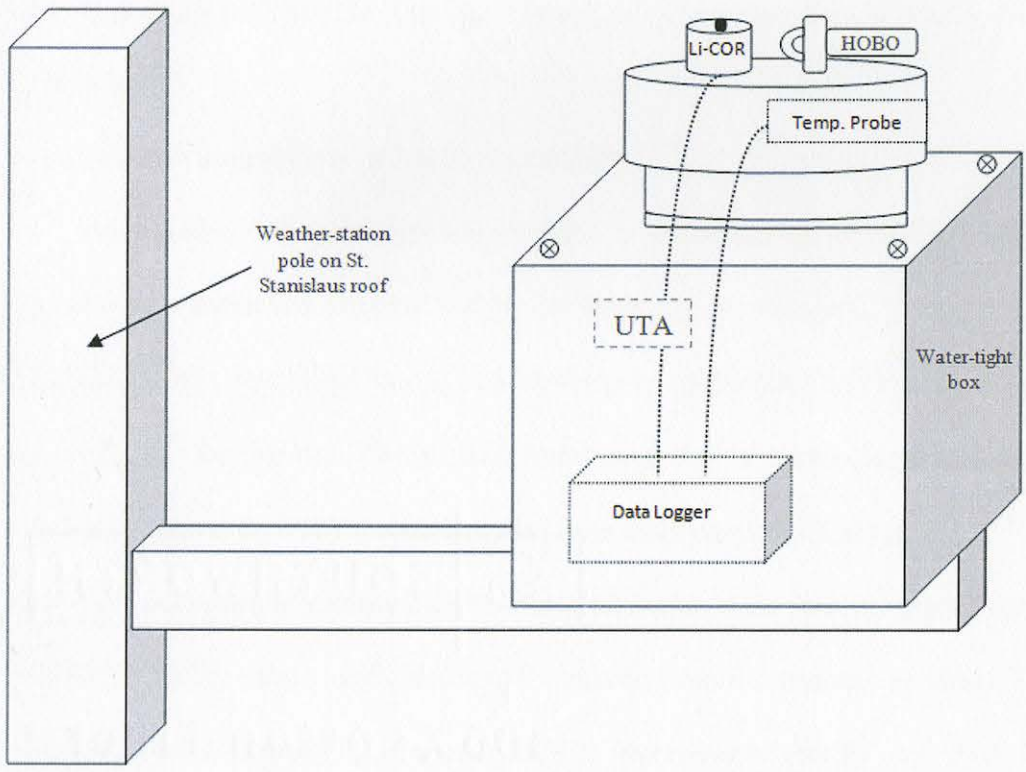

Figure 9. Schematic of PAR sensor dock mounted on the roof of St. Stanislaus High School. The setup was oriented to face south and the apparatus was never shaded by the pole behind it or any other obstruction surrounding it.

After downloading the raw data, voltage output had to be manually converted into PAR readings (μmole photons m^{-2} s^{-1}) by applying a calibration multiplier supplied by LI-COR, and a gain correction factor of 0.16, supplied by EME systems. Ground measurements of Instantaneous PAR (IPAR, (μmole photons m^{-2} s^{-1}) and daily PAR (mole photons m^{-2} d^{-1}) were all derived using this sensor.

All HOBO sensors used were compared with one another prior to the study, and found to agree within 2 – 3 % of each other (Appendix B). In addition, a HOBO sensor was compared to the LI-190 sensor, and found to agree within 2 % of each other (Appendix B). The wavelength response from the HOBO Pendant ® (450-1100 nm at <50% response level), differs from that of the LI-COR sensor (400-700 nm at 100% response level).

Time and depth integrations of NetPP and RESP

Normalized P-E curve data were used to derive *in situ* photosynthetic rates, integrated with depth and over the diel period for every day sampled. It was assumed that the maximum rate calculated for oxygen incubations normalized to chlorophyll in a given day was P_{max}^{DO} for that day. The α and β terms from the ^{14}C incubations were used in conjunction with daily PAR measurements (from stationary LI-COR) and P_{max}^{DO}, to derive daily estimates of surface NetPP. These estimates were then integrated with depth using the K_d(PAR) values, and chlorophyll (derived from fluorometer profiles). For depth integration over calculated Z_{eu} (Equation 2-3), it was assumed that E_d^+ was PAR from the stationary LI-COR sensor. Time and depth integrations for respiration measurements were also made, assuming constant rates in time and vertical space.

Moderate Resolution Imaging Spectroradiometer (MODIS) processing

Level 1a MODIS Aqua data and associated ancillary files were downloaded from NASA's Ocean Color Website (http://oceancolor.gsfc.nasa.gov) for all 24 sampling days in 2011. A series of IDL® programs were called using SeaDAS 6.2 in order to batch process all files from level 1a to level 2 files. These level 2 files were processed to a cylindrical map projection, using the native resolution of the file. All standard flags were used, with the exception of the STRAYLIGHT flag (flag#9), which was removed due to the high sediment load of waters being studied. Standard near infrared (NIR) atmospheric correction was applied to all bands. Two quality control masked files were generated (.flat and .png), bound by the following (N,S,W,E) coordinates: 30.5°, 29.0°, -90.75°, -87.0°. Table 2 summarizes the MODIS data that were collected for this study.

Table 2

Details of MODIS Products Processed for this Study.

MODIS product	Wavelengths	Resolution	Atm. Correction
Rrs	412,443,488,531,547,667,678,748	1 km	NIR
Rrs	645	250 m	NIR
Kd_lee	412,443,488,531,547,667,678,PAR	1 km	NIR
Kd_morel	412,443,488,531,547,667,678,PAR	1 km	NIR
Kd_490	N/A	1 km	NIR
Zeu_lee	N/A	1 km	NIR
Zeu_morel	N/A	1 km	NIR
chlor_a	N/A	1 km	NIR
flh	N/A	1 km	NIR
aph_qaa	412,443,488,531,547,667,678	1 km	NIR
par	N/A	1 km	NIR

As a final step to ensure that satellite data were viable for ground truthing, the optical depth was determined at each station, using *in situ* derived values of K_d(PAR). This value was compared with the physical depth of that station. If the optical depth exceeded the physical depth for that station, data was flagged and not used for satellite comparisons.

The optical depth was defined as follows:

$$\text{Optical Depth} = 1 / K_d(\text{PAR}) \qquad \text{(Equation 2-4)}$$

Data analysis

Trends, averages, standard deviations, and ranges were inspected over the course of this time series to resolve how light, temperature, salinity, nutrients, and carbon delivery change through the year and how the biological community responds. A multiple regression analysis (Microsoft Excel) was utilized to weigh the relative contribution of optically significant parameters (chlorophyll, CDOM, and SPM) to the signal of light attenuation (K_d) and to map this contribution spatially and temporally. Finally, empirical relationships between ground measurements of optical properties and satellite-derived products were analyzed using a Pearson correlation matrix as well as Model II regressions or non-linear fits to determine whether validation criteria could be achieved.

CHAPTER III

RESULTS

Environmental Variability

Climatology

Precipitation data were obtained from Waveland and Biloxi, MS in order to assess the local input of rain and urban runoff into the watershed (Figure 10). The data from 2011 showed a wet winter and early spring at the beginning of the year, followed by an extended dry period into the summer. This is interrupted by a few significant rain events mid-way through the year. The highest daily rain amount recorded in one day for the year was 14.35 cm on July 24, 2011 (Year day 205). Also notable is the signal from Tropical Storm Lee, which passed through Mississippi on September 4, 2011 (Year Day 247). The rest of the year was relatively dry, with intermittent rain events into the winter.

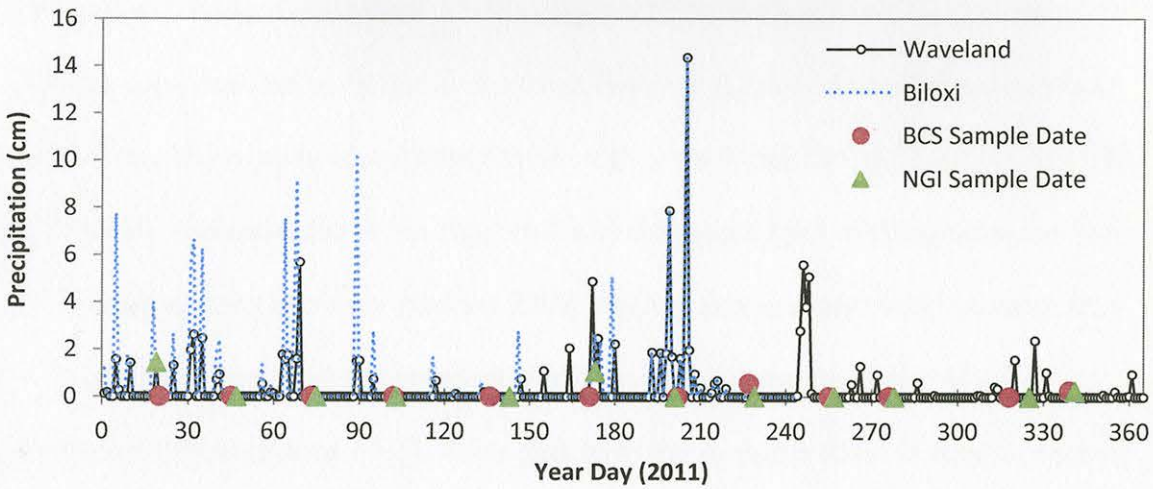

Figure 10. Time-series of precipitation in Waveland and Biloxi, MS. Total daily precipitation on the sampling dates are shown for stations BCS-8 (red dots) and NGI-5 (green triangles). Data for the Biloxi time-series ends at Year day 244

The wind data time series is shown in Figure 11. The continuous data series in Figure 11 represents the daily average wind velocity over a 24 hour period at NOAA station GPMO6. Wind direction data for each day were also collected and shown in Figure 11. Wind direction was highly variable on daily scales, and no seasonal pattern was readily discernible, outside of a weakly consistent southerly wind in the spring. Spring and winter months had higher wind speeds in general, and there appeared to be a reduction in episodic high-wind events during the summer, only disrupted by the arrival of Tropical Storm Lee in September.

River water discharge data were collected from several rivers that influence the Mississippi Gulf Coast. The Wolf River drains into Bay St. Louis, MS and is used as a proxy for fluvial input into the Bay, which also includes inputs from the Jourdan River. The Pearl River lies on the western border of the BCS sampling transect, dividing the Mississippi-Louisiana state lines. The Pascagoula River is a large river to the East of the sampling area, and due to localized westward currents, it has the potential to introduce material into the western Mississippi Sound, with some temporal lag (Boone 1973). This is especially important due to the high level anthropogenic input of phosphates into the Sound located along this river (Sawant 2009). Mobile Bay is a large body of water that also drains westward, and has potential to influence the biogeochemistry of the Mississippi Sound (Boone 1973). River data from the Alabama River is used as a proxy for input from the Mobile Bay.

In general, high discharge was characteristic during the spring months, but dropped off considerably into the late spring and early summer. This summer lull was interrupted by the precipitation event on year day 205 and again by a large input from

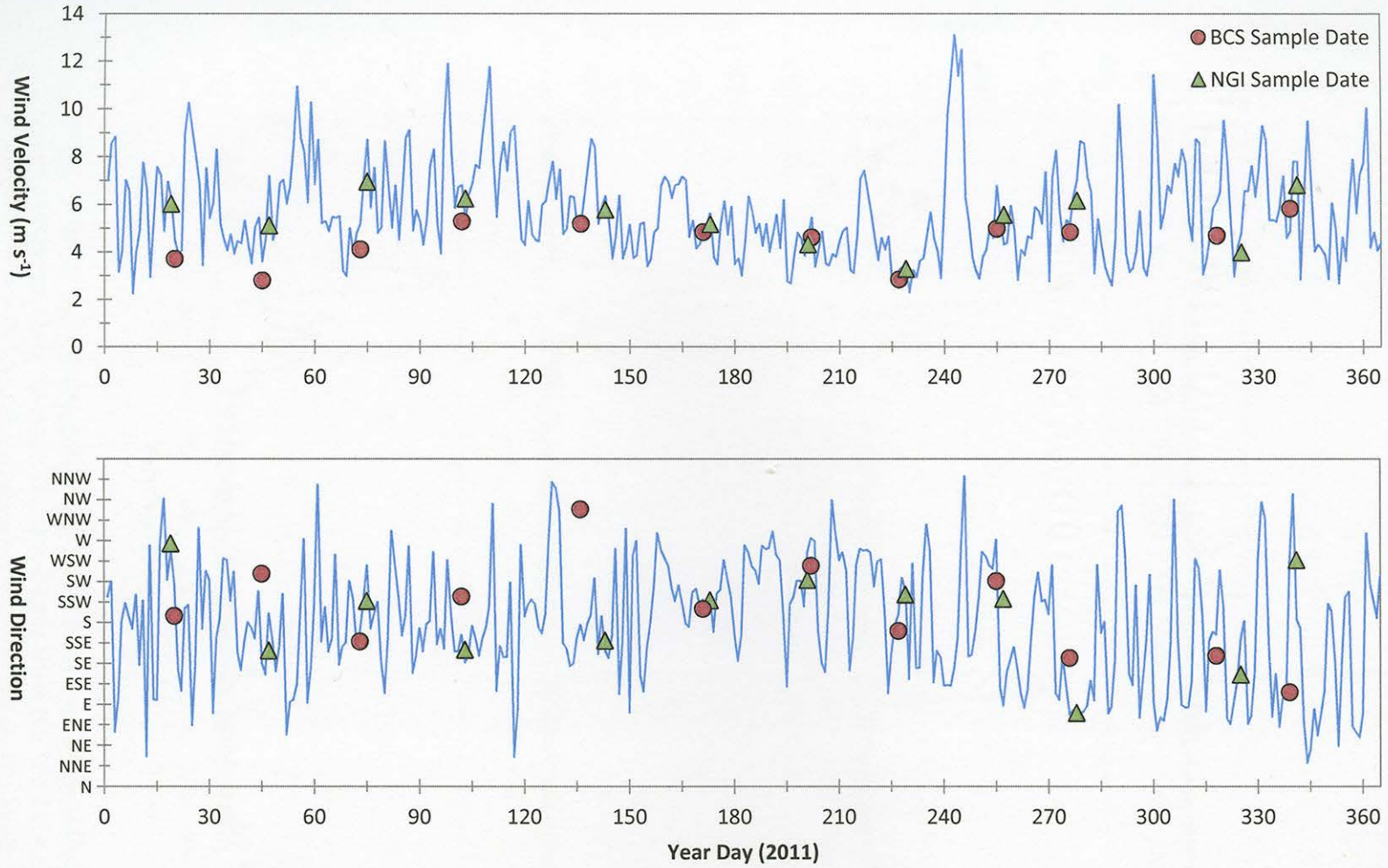

Figure 11. Continuous time-series (blue line) of wind speed and direction at NOAA Station GPOM6. Daily averaged wind velocity and direction on the sampling dates are shown for stations BCS-8 (WYCM6, red dots) and NGI-5 (GPOM6, green triangles).

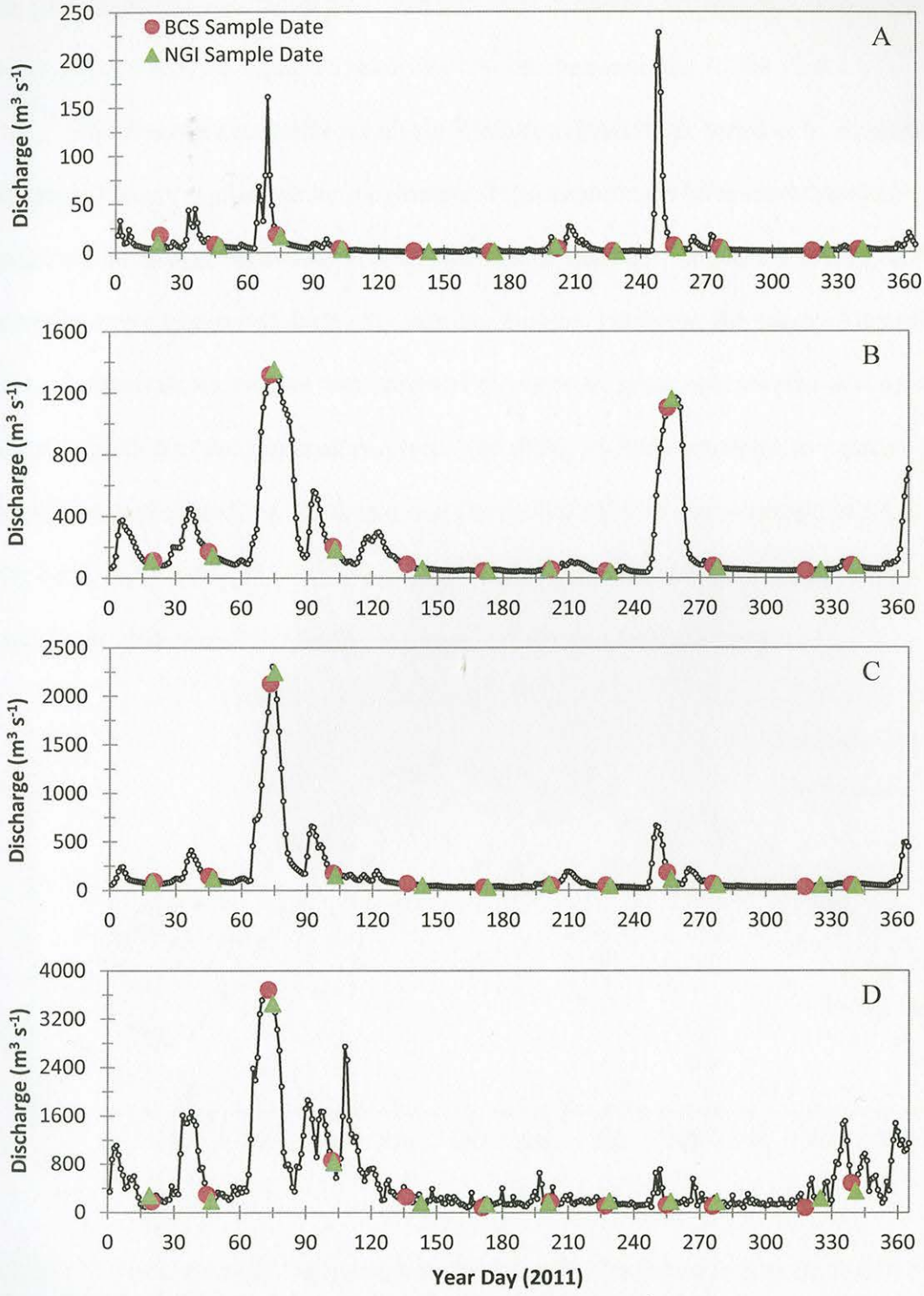

Figure 12. Time series of daily average discharge rates from four rivers influencing the western Mississippi Sound. Daily average discharge rates from the Wolf River (A), Pearl River (B), Pascagoula River (C) and the Alabama River (D) are shown. Note the changes in scale for each river.

the passing of Tropical Storm Lee (year day 247) in stations further west. After this event, discharge rates remained relatively low for the remainder of the year.

The Photosynthetically Available Radiation (PAR) time series at St. Stanislaus is shown in Figure 13, illustrating the gradual shift in maximum solar elevation through the year, as well as high variability as a result of cloud coverage. In general, the highest light intensity was experienced during the summer months. However, the nature of sampling in monthly intervals shows that data retrieved on water sampling dates were not always a direct reflection of the seasonal averages. Variability of PAR between two stations within the Mississippi Sound (St. Stanislaus and Grand Bay NERR) was investigated in Appendix B, showing close agreement on longer time scales (slope = 1.0051), but significant inter-annual variability as a result of the spatial disconnect.

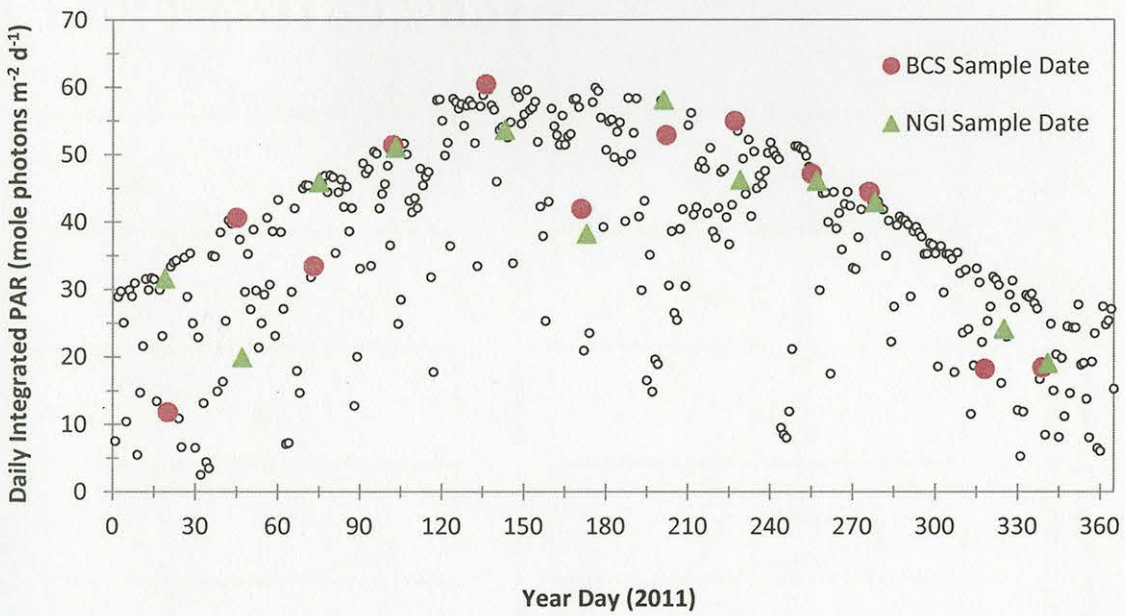

Figure 13. Time-series of Daily integrated PAR at St. Stanislaus in Bay St. Louis, MS. The values for PAR on each sampling date are highlighted in color.

Tidal data is shown in Figure 14 for all sampling dates. During the sampling period in 2011, tides ranged from about -0.4 meters below to 0.8 above the mean lower

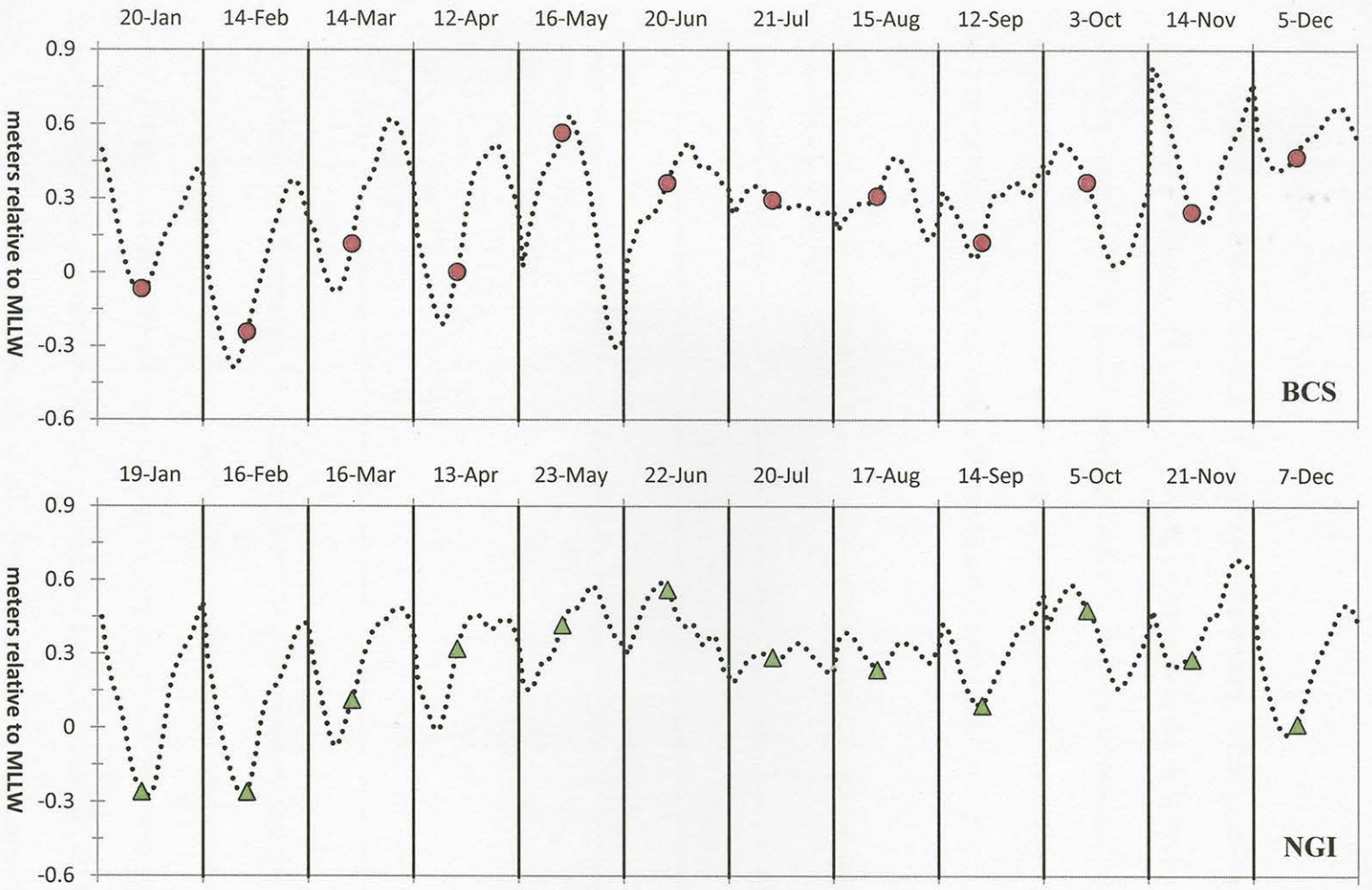

Figure 14. Tidal cycle measured for each sampling day for BCS (top) and NGI (bottom). The tide level corresponding to 1000 h is shown for BCS (red dots) and NGI (green triangles) in 2011.

low water (MLLW) level. Outgoing, incoming, and peak high/low tidal stages were investigated during this study.

Water column properties

Surface and bottom samples of sea water temperature, salinity, and dissolved oxygen content are shown in Figure 15. This figure compares the differences between the Mississippi Sound (BCS-8) and Mississippi Bight (NGI-5) environments, illustrating differences in the stability of the water column and susceptibility to mixing. The annual mean and variability of surface values obtained are shown below in Table 3.

Table 3

Annual Average Concentration of Temperature, Salinity, and Oxygen for Surface and Bottom Waters at Stations BCS-8 and NGI-5.

	BCS-8		NGI-5	
Parameter	Mean	SD	Mean	SD
Temperature_sfc (^{o}C)	21.6	7.3	21.9	7.1
Temperature_btm (^{o}C)	22.9	6.5	21.5	4.7
Salinity_sfc	16.8	7.3	25.5	6.6
Salinity_btm	17.3	6.5	30.4	3.3
Oxygen_sfc (mg L^{-1})	7.4	2.5	8.2	2.4
Oxygen_btm (mg L^{-1})	5.6	2.9	4.1	3.3

Station BCS-8 experienced a minimal amount of temperature and salinity stratification through the year, though some slight stratification did set up in the summer and fall months. Station NGI-5 became stratified very early on in the year, with some indication of the onset as early as March, and remained so until October. Dissolved oxygen concentrations were relatively similar from surface to bottom waters in the Mississippi Sound, though some vertical divergence was shown in the Mississippi Bight.

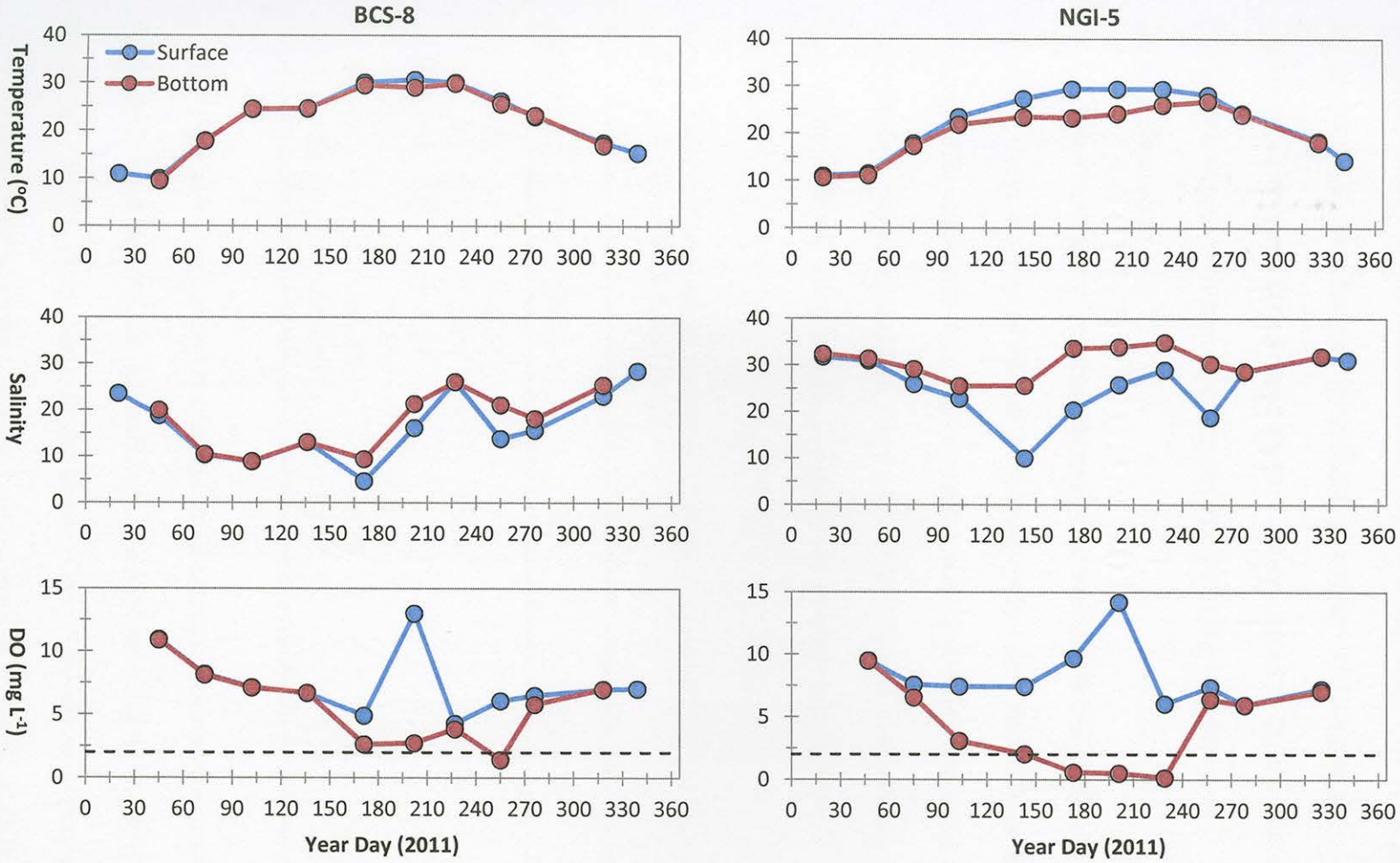

Figure 15. Time-series of surface and bottom temperature, salinity, and dissolved oxygen for Stations BCS-8 (left) and NGI-5 (right). The dashed line on the DO graph represents the threshold for hypoxia (< 2 mg L^{-1}).

At station BCS-8, bottom dissolved oxygen concentrations started to decline relative to the surface in June, and continued to decline into a single hypoxia event in September. Station NGI-5 showed bottom water dissolved oxygen declining as early as the stratification sets up in March, and these values continued to decline into hypoxia in June. The system remained hypoxic for four months, breaking in September.

Nutrient Chemistry

The time-series of nutrient chemistry for stations BCS-8 and NGI-5 is shown in Figure 16. Surface values of all water chemistry parameters tended to be elevated in the Mississippi Sound consistently throughout the year, with a few intermittent exceptions in the nitrite and silicate time series. For a generalized regional comparison, average concentrations for all chemical parameters are shown below in Table 4.

Table 4

Annual Average Concentrations of Nutrients and Dissolved Organic Carbon in Surface Waters at Stations BCS-8 and NGI-5.

Parameter	BCS-8	SD	NGI-5	SD
NO_3 (μM)	0.25	0.25	0.11	0.09
NO_2 (μM)	0.04	0.07	0.06	0.10
NH_4 (μM)	1.54	2.57	0.52	0.47
PO_4 (μM)	0.83	0.59	0.27	0.37
SiO_3 (μM)	44.46	34.16	26.75	27.07
DOC (μM)	380.67	83.47	265.10	87.51

In general, some apparent increase in all nutrient concentrations was discernible in spring for both stations, though station NGI-5 showed a slight drawdown in nitrate, phosphate, and silicate by April. As the Bonnet Carré Spillway was opened (year day 129), some changes in nutrient chemistry were observed. The station BCS-8 samples

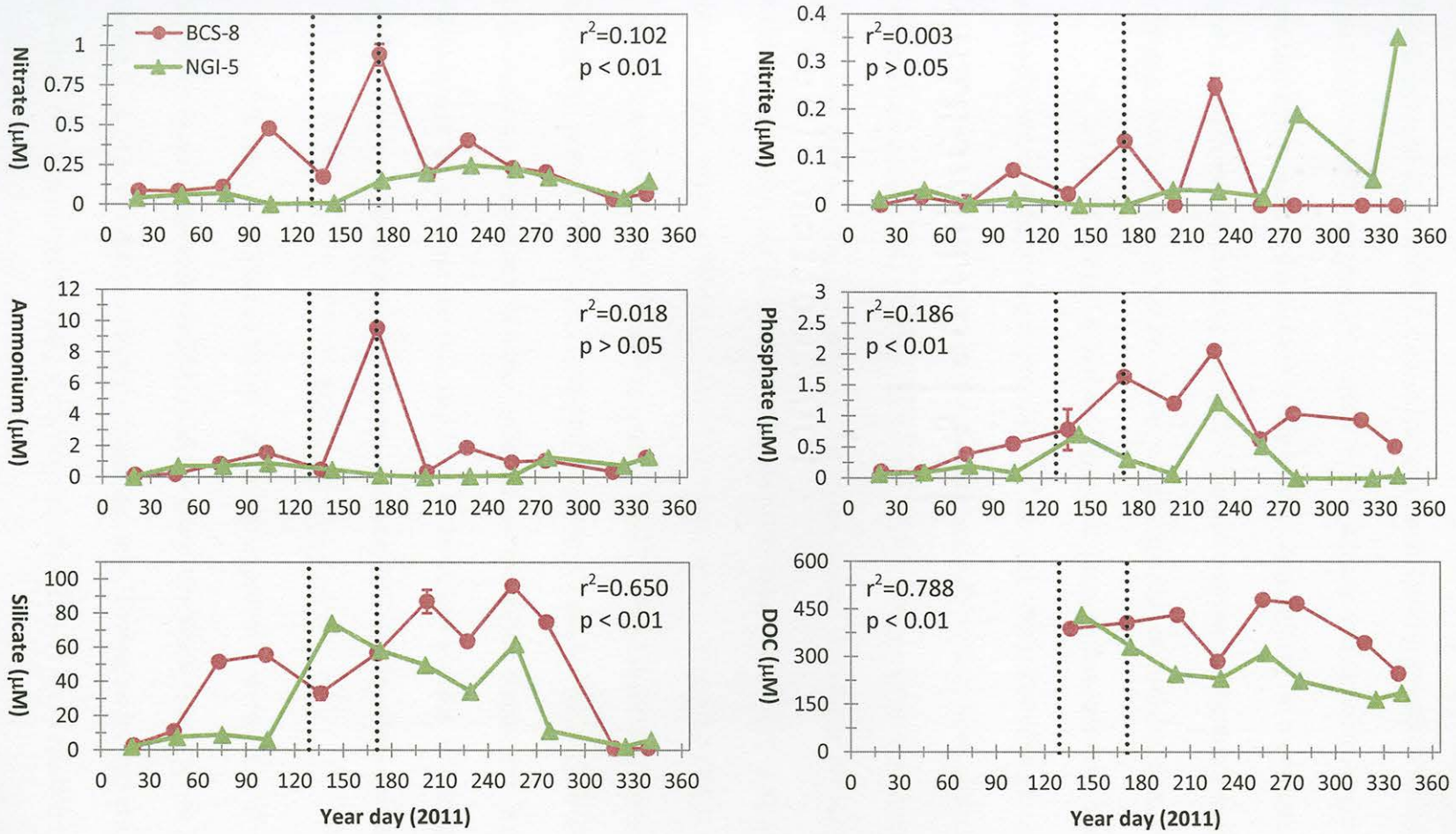

Figure 16. Time-series of surface nutrients for stations BCS-8 (red) and NGI-5 (green). The dotted lines represent the opening and closing of the Bonnet Carré Spillway, starting May 9, 2011 (year day 129) and ending on June 20, 2011 (year day 171). The r^2 and p-values represent the relation of each parameter (all available stations) to salinity.

appeared to experience a decrease in most nutrient concentrations in May, followed by a drastic increase in all nutrient concentrations the following month, with a substantial nitrate and ammonium peak. At station NGI-5, silicate and dissolved organic carbon concentrations were at the highest levels in 2011 during May, in conjunction with an increase in phosphate for that month. By June, all nutrient concentrations at station NGI-5 dropped with the exception of nitrate, which experienced a slight increase.

At station BCS-8, all dissolved inorganic nitrogen concentrations tended to gradually decrease through the remainder of the year. Phosphate and silicate levels for this station were elevated through the summer and fall, with lowest concentrations present during the winter months. At station NGI-5, nitrate levels continued to increase through the summer and fall, dropping off in the winter. A peculiar nitrite spike appeared at this station in the late fall and into the winter months, following the same pattern of other nitrogen species. While the signal appeared greatly magnified compared to previous months, it made up a small fraction (mean = 8%) of the total nitrogen species present. During this period, there was no detectable nitrite present at station BCS-8. Phosphate and silicate concentrations followed a similar pattern to the Mississippi Sound station, with highs in the summer and fall, and lows in the colder months. The highest concentrations of nitrate and phosphate for station NGI-5 were observed in August.

Biological Variability

This section will focus on the variability of *in situ* derived rates of net primary productivity and respiration in 2011, and compare how these rates vary in response to potential biological drivers within the water column. Temperature, salinity, nutrient chemistry and photosynthetically available radiation (PAR) are considered again, but in

direct relation to biological activity, alongside other parameters such as chlorophyll, dissolved organic carbon (DOC), particulate elemental compounds and ratios (C:N:P), and light attenuation (K_d). This section will compare and contrast biological variation between two sampled stations and examine temporal variability within stations. In addition, calculated budgets of Net Ecosystem Productivity (NEP, daily and depth-integrated) are presented.

Net PP and RESP Time Series

A time-series of net primary productivity (NetPP) and respiration (RESP) rates taken from *in situ* incubator measurements alongside sea surface measurements of temperature and salinity is shown in Figure 17. This figure compares the difference in biological activity between the Mississippi Sound (BCS-8) and Mississippi Bight (NGI-5) stations, and demonstrates the variability of this activity in time and space. The negative values indicate consumption of oxygen and are plotted on a negative scale. For detailed monthly data plots of surface NetPP and RESP, refer to Appendix E. The upper and lower ranges of values obtained in 2011 are shown below in Table 5. Rates are shown in units of oxygen and carbon per unit volume and time.

Table 5

Range of Values for Surface NetPP and RESP at Stations BCS-8 and NGI-5.

	BCS-8		NGI-5	
Parameter	Low	High	Low	High
NetPP (mg O_2 L^{-1} h^{-1})	-0.033	1.001	-0.076	0.841
NetPP (mg C L^{-1} h^{-1})	-0.012	0.375	-0.028	0.315
RESP (mg O_2 L^{-1} h^{-1})	-0.118	-0.403	-0.073	-0.390
RESP (mg C L^{-1} h^{-1})	-0.044	-0.151	-0.027	0.146

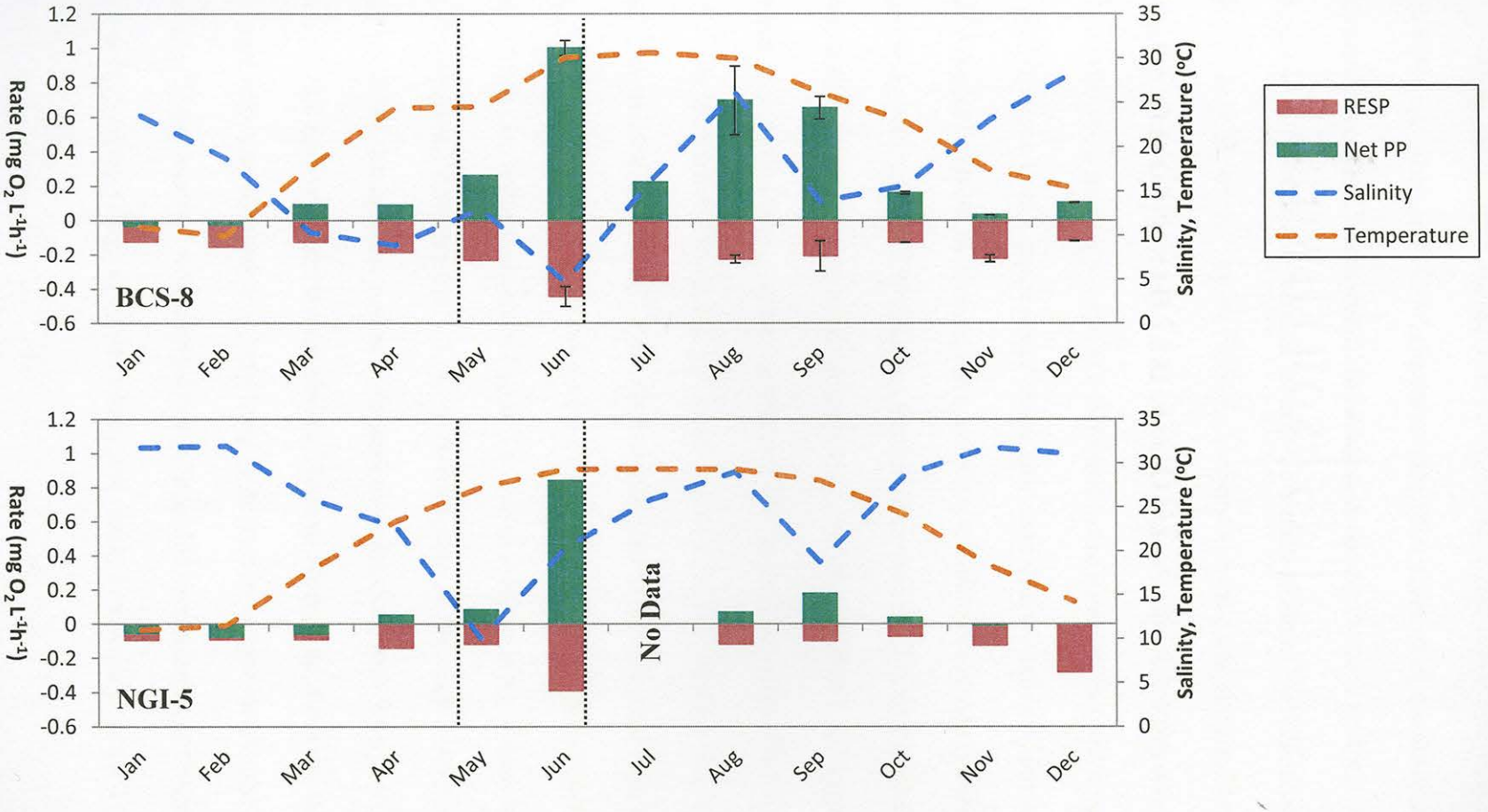

Figure 17. Time-series of surface NetPP and community RESP rates as well as sea surface temperature and salinity measured in the Mississippi Sound (BCS-8) and the Mississippi Bight (NGI-5) from January to December 2011. The dotted vertical lines represent the period of time the Bonnet Carré Spillway was open.

While the relative magnitudes of NetPP and RESP rates measured at stations BCS-8 (higher rates) and NGI-5 (lower rates) differ, there exist some seasonal commonalities. NetPP rates started to increase in spring for both stations, coming to the highest values recorded in the year during the month of June. No data exists for station NGI-5 in July, however, station BCS-8 experienced a dramatic drop in NetPP rates during this month, followed by a subsequent increase in the following months. Station NGI-5 followed a similar pattern of a fall season rate increase, but unlike station BCS-8, this rate increase is of a much lower magnitude than that experienced during the summer peak. Respiration rates at both stations also showed some differences in relative magnitude, with station BCS-8 having higher rates than station NGI-5. Some seasonality in respiration rates was present at both stations, with the gradual buildup and decline of a summer maximum (June), a small increase in November for station BCS-8, and a small increase in November/December at station NGI-5. Rates of respiration were not always directly correlated to rates of NetPP on a monthly basis throughout the year (Figure 17).

Sea surface temperature and salinity are plotted as a reference to the physical conditions in the water column in Figure 17. Salinity values were always higher at station NGI-5 compared to station BCS-8, with the exception of the May. Two major salinity drops occurred through the year at both stations coinciding with the opening of the Bonnet Carré Spillway, and the passing of Tropical Storm Lee. For both stations, the spring months also showed relatively lower salinities in comparison to the rest of the year (Figure 17), the onset of which coincided with higher river discharge (Figure 12) and localized rain events (Figure 10) in March and April. Sea surface temperature throughout

the time series showed a gradual increase towards summer and a decrease in the latter half of the year, with no major variations between both stations.

No strong correlations were derived directly from a first order linear comparison between salinity and NetPP or RESP (Figure 18). However, Figure 18 does show that an apparent non-linear relation exists between biological rates and temperature ($p < 0.01$), while more linear correlations explain the relationship between NetPP and chlorophyll-a ($r^2 = 0.9636$, $p < 0.01$), and to some degree, RESP and chlorophyll-a ($r^2 = 0.7378$, $p < 0.01$).

Nutrients and Biomass

A time-series showing changes in chlorophyll and surface nutrients (total dissolved inorganic nitrogen [DIN] and phosphate) as well dissolved nutrient ratios (NH4/DIN, NO3/DIN) for both stations is shown in Figure 19. Average N:P ratios for station BCS-8 (N:P = 2.2) and NGI-5 (N:P = 6.9) were consistently low through the year. At station BCS-8, there was a minor DIN peak in spring, followed by a more substantial peak in the summer corresponding to the opening of the Bonnet Carré Spillway. Another minor DIN peak appeared in the late summer. Chlorophyll concentrations followed a similar pattern of DIN, most noticeably at the June peak, July decrease, and August increase.

Throughout the year at station BCS-8, the majority of nitrogen (> 60%) in the system was in the form of ammonia. From January to March, ammonia ratios increased while nitrate ratios dropped, followed by an inverse shift in April and May, when nitrate ratios increased and ammonia ratios decreased. The following month, during the June peak of DIN and chlorophyll for the year, 90% of the measured DIN was in the form of

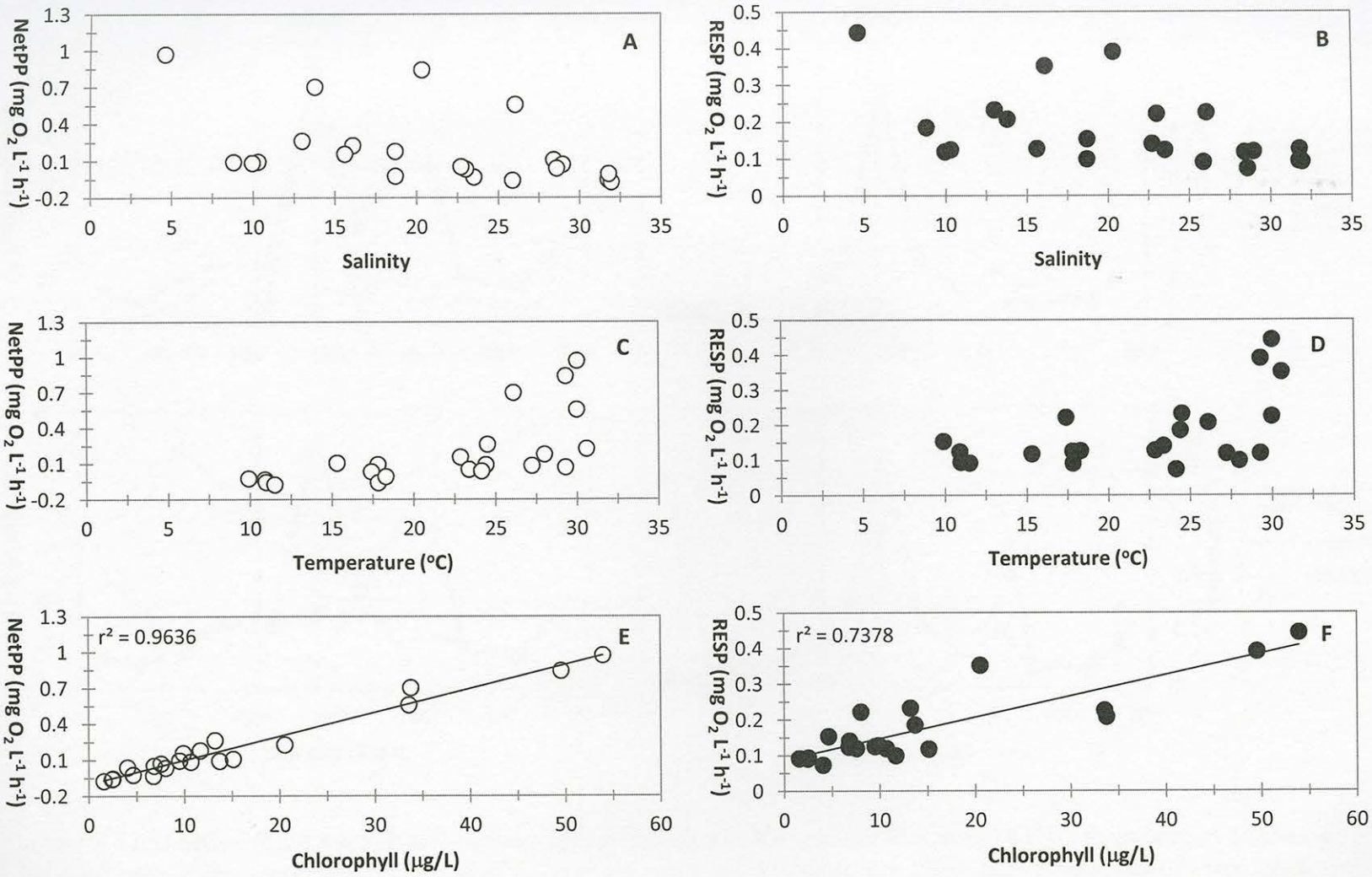

Figure 18. Comparison of NetPP (left) and RESP (right) to salinity, temperature, and chlorophyll for sampled stations.

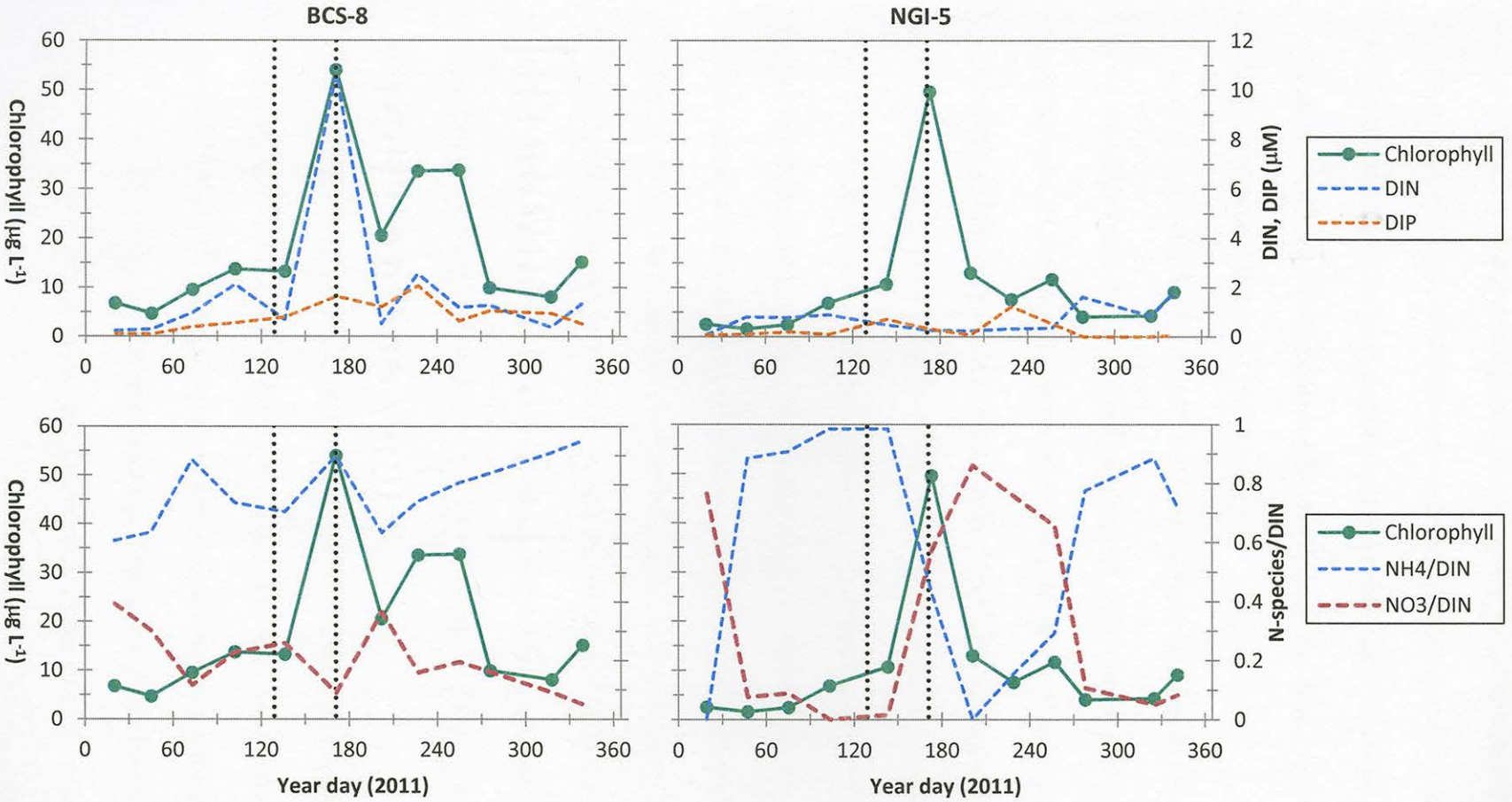

Figure 19. Time-series of chlorophyll and various nutrient parameters for stations BCS-8 and NGI-5 from January to December 2011. The dotted vertical lines represent the period of time the Bonnet Carré Spillway was open. Top: Time series of chlorophyll and dissolved inorganic nitrogen (DIN) and dissolved inorganic phosphorous (DIP). Bottom: Time series of chlorophyll and dissolved nutrient ratios (Percent ammonia and nitrate of total dissolved inorganic nitrogen).

ammonia. While still dominating the DIN signal for July, ammonia concentrations decreased to 63.6% of DIN and nitrate concentrations increased (36.4% of DIN). From August into the end of the year, ammonia ratios continued to increase while nitrate ratios decreased. Nitrite ratios were consistently low through the year, on average contributing less than 2.0% to the DIN.

At station NGI-5 (Figure 19), DIN values were consistently low through the year. There were slight increases in the early spring and early winter, and a decrease in the summer months all the way into September. No peak or increase in DIN was discernible for the month of June as was seen at station BCS-8, however a peak of chlorophyll in similar magnitude to the peak seen in the Mississippi Sound was present during this month. Chlorophyll concentrations followed NetPP patterns very closely for both stations, but the seasonal changes in biomass and rates showed no direct correlation to dissolved nutrient concentrations in the water at station NGI-5. From the beginning of the year and into May, ammonia was the dominant species. A shift occurred during the summer to a nitrate dominated system, which remained until August, when ammonia levels rose again and remained dominant for the rest of the year. Nitrite levels were fairly low throughout the year, but accounted for 10 – 20% of the DIN signal through the year.

Respiration and Organic Matter

Concentrations of DOC showed a poor relationship with measured community respiration (Figure 21 A, B, $r^2 = 0.05$, $p > 0.05$), but a negative correlation with salinity (Figure 20). Particulate organic matter concentrations showed a strong seasonality and a close relationship with community respiration through the year (Figure 21 C, D, $r^2 = 0.78$, $p < 0.01$). Between stations, the relative magnitudes of each organic matter

component were similar, with slightly elevated concentrations in the Mississippi Sound. However, the ratio of total POM/SPM was consistently higher in the Mississippi Bight (Figure 21 E, F).

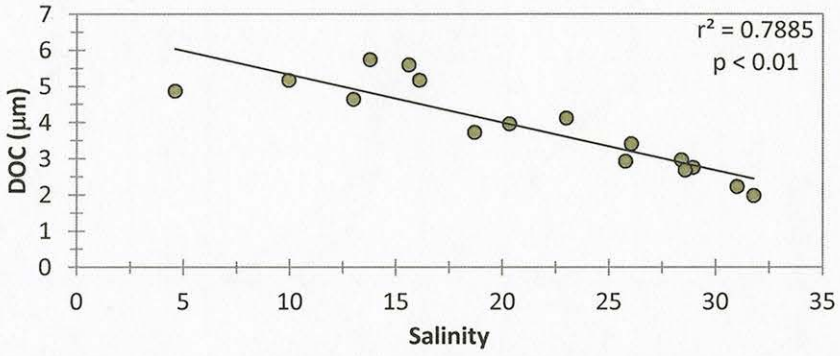

Figure 20. Dissolved organic carbon as a function of salinity for all stations sampled.

Particulate Elemental Stoichiometry

Figure 22 shows the concentrations of particulate organic carbon (POC), particulate organic nitrogen (PON), and particulate total phosphorous (PTP) throughout the year, as well as the elemental ratios of these particulate components. The POC, PON, and PTP values tended to be much higher at station BCS-8 compared to station NGI-5. The values for all parameters were highest in the summer months, and lower in the beginning and end of 2011.

The elemental ratio of the organic particulate fraction was variable throughout the year, and across stations. Generally, C:P, N:P, and C:N ratios were all elevated at station NGI-5 relative to station BCS-8 and Redfield ratios. A notable decrease in C:P and N:P values was apparent in May, followed by a shift to higher ratios in June and a high C:P peak in July. The N:P ratio decreased at both stations in May, and then increased in June and July, but did not peak high above Redfield ratios, as was apparent with C:P. The C:N

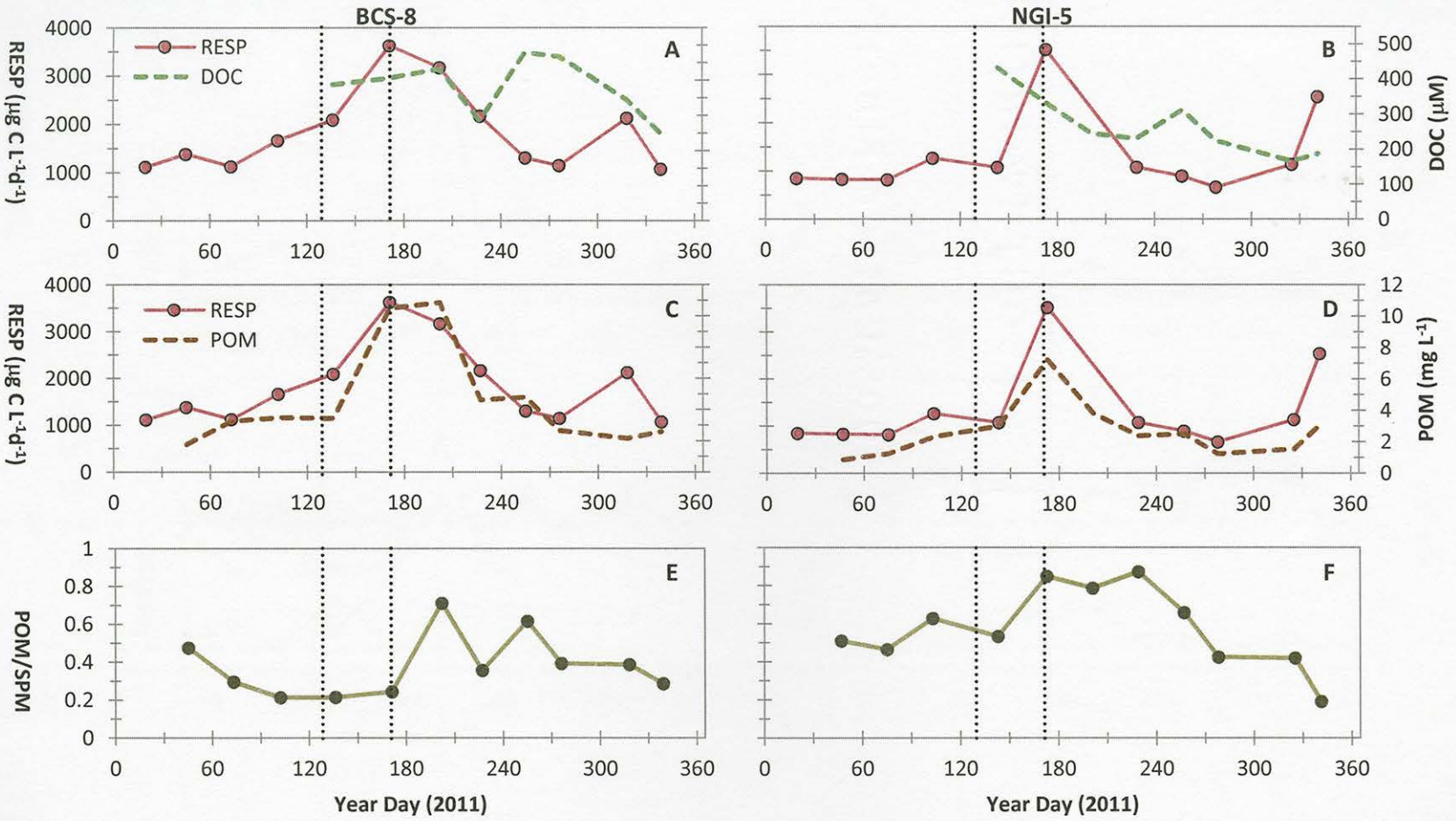

Figure 21. Time-series of daily surface respiration (RESP) and dissolved organic carbon (A, B) as well as particulate organic matter (C, D), and the particulate organic to suspended particulate matter ratio (E, F) collected from surface waters in the Mississippi Sound (BCS-8) and the Mississippi Bight (NGI-5). The dotted vertical lines represent the open period of the Bonnet Carré Spillway.

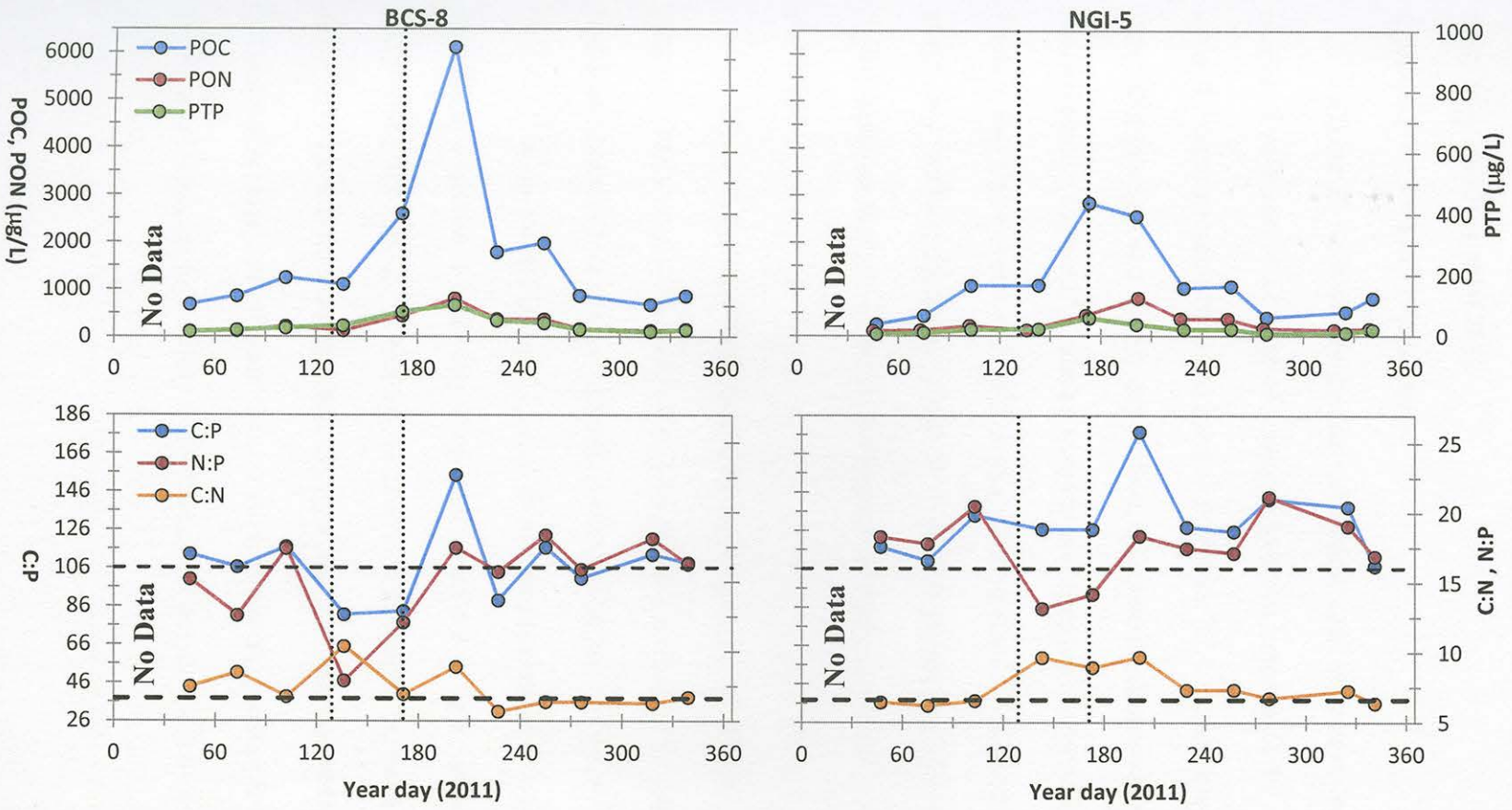

Figure 22. Concentrations of POC, PON, and PTP (top) and particulate C:P, N:P, and C:N ratios (bottom) collected in surface waters from the Mississippi Sound (BCS-8) and Mississippi Bight (NGI-5). The dashed horizontal lines represent the C:P, N:P, and C:N Redfield ratios (106, 16, and 6.6, respectively, Redfield 1934). The dotted vertical lines represent the period of time when the Bonnet Carré Spillway was open.

ratio remained relatively constant and close to Redfield values, but doubled in May – July (only May and July at BCS-8).

Light and Net Primary Productivity

Figure 23 A, B shows the changes in dissolved oxygen concentrations over the course of an *in situ* incubation of seawater, in conjunction with the subsurface light intensity measurements from the incubator. Figure 23 A shows irregular changes in the light field throughout a cloudy day in July, and concurrent short-term spikes in oxygen concentrations. Figure 23 B shows a steady and constant increase in the incident light field. In this figure, rates of NetPP continued to increase from morning until midday eventually reaching a plateau in activity even with increasing light. It is only these steady light conditions that allow for the subsequent analysis mentioned in the following paragraph.

In situ oxygen and light data from Figure 23 B were used to construct a photosynthesis versus irradiance (P v. E) curve, by averaging the incident light and biological rates in five minute intervals, and plotting them as a function of one another. The result is shown in Figure 23 C, and illustrates the manner in which photosynthesis changes in response to relatively short-term variations in light. Data from the photosynthetron (using ^{14}C techniques described in chapter II) from the same sampling day is also plotted for a comparison. Oxygen data has been converted into carbon units, but some discrepancies between the two exist. While P_{max} values are similar, the slope, α, shows some considerable differences between the *in situ* and lab-derived curves.

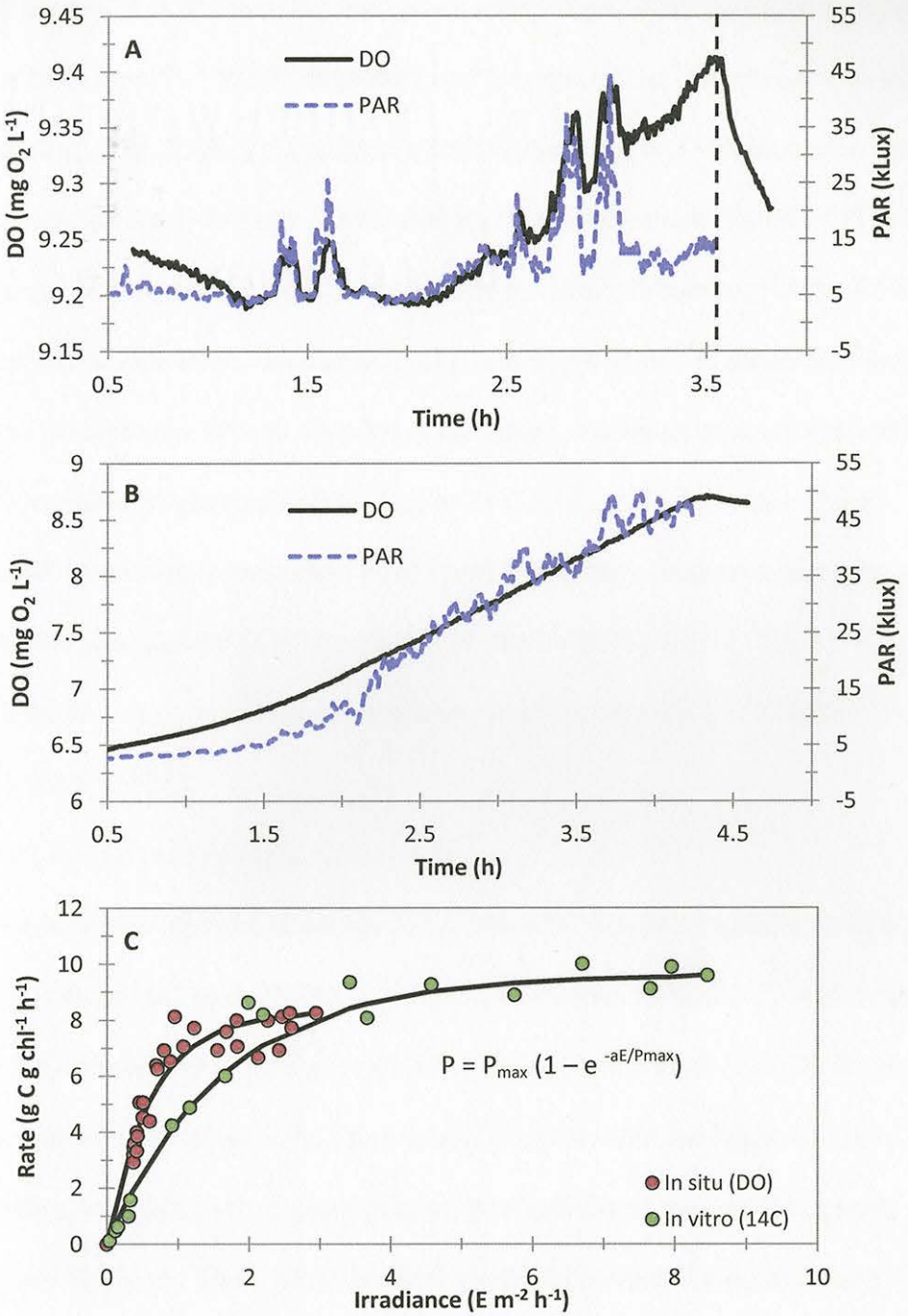

Figure 23. In situ monitoring of dissolved oxygen and downwelling irradiance. Data is shown for a cloudy day in July (A) and a sunny day in September (B). The vertical dotted lines represent the start of the dark period of the incubation. Also shown is primary production rates as a function of irradiance (C), comparing *in situ* (DO incubation) and *in vitro* (^{14}C incorporation 3 h after collection) methods at station BCS-8 (12Sep2011).

In Figure 24 A, the monthly maximum value of gross primary productivity (GPP, calculated from Net PP + RESP) is plotted as a function of the instantaneous PAR (IPAR) reading. The IPAR is taken from a stationary sensor and values correspond to the time of the maximum *in situ* max NetPP and RESP measurement. Figure 24 B compares the maximum photosynthetic rate (normalized to chlorophyll biomass) to the PAR level at photosynthetic saturation, calculated from a non-linear fit of ^{14}C incubation data in the laboratory. Both graphs showed a tendency for higher maximum primary productivity rates with increasing light availability. Figure 24 C looks at the ratio of surface NetPP/RESP in relation to individual NetPP and RESP rates taken over the year, and shows that the productivity term correlates with NetPP/RESP ($r^2 = 0.726$, $p < 0.01$, $n = 22$), while respiration term shows no consistent relationship with NetPP/RESP ($r^2 = 0.175$, $p > 0.05$, $n = 22$).

Biological Consequence of Light Attenuation

In addition to changes in surface light intensity, how incident light is distributed with depth is examined next. Figure 25 shows a time series of *in situ* derived surface gross primary productivity and K_d(PAR) for 2011. At station BCS-8, K_d(PAR) values showed a high amount of variability throughout the year, with the highest peak in June corresponding to a high peak in gross primary productivity as well as the opening of the Bonnet Carré Spillway. The K_d(PAR) values were considerably lower at station NGI-5 in comparison to BCS-8, and variability was reduced considerably. Further dynamics and patterns of K_d(PAR) distribution throughout the estuary are presented in the following section.

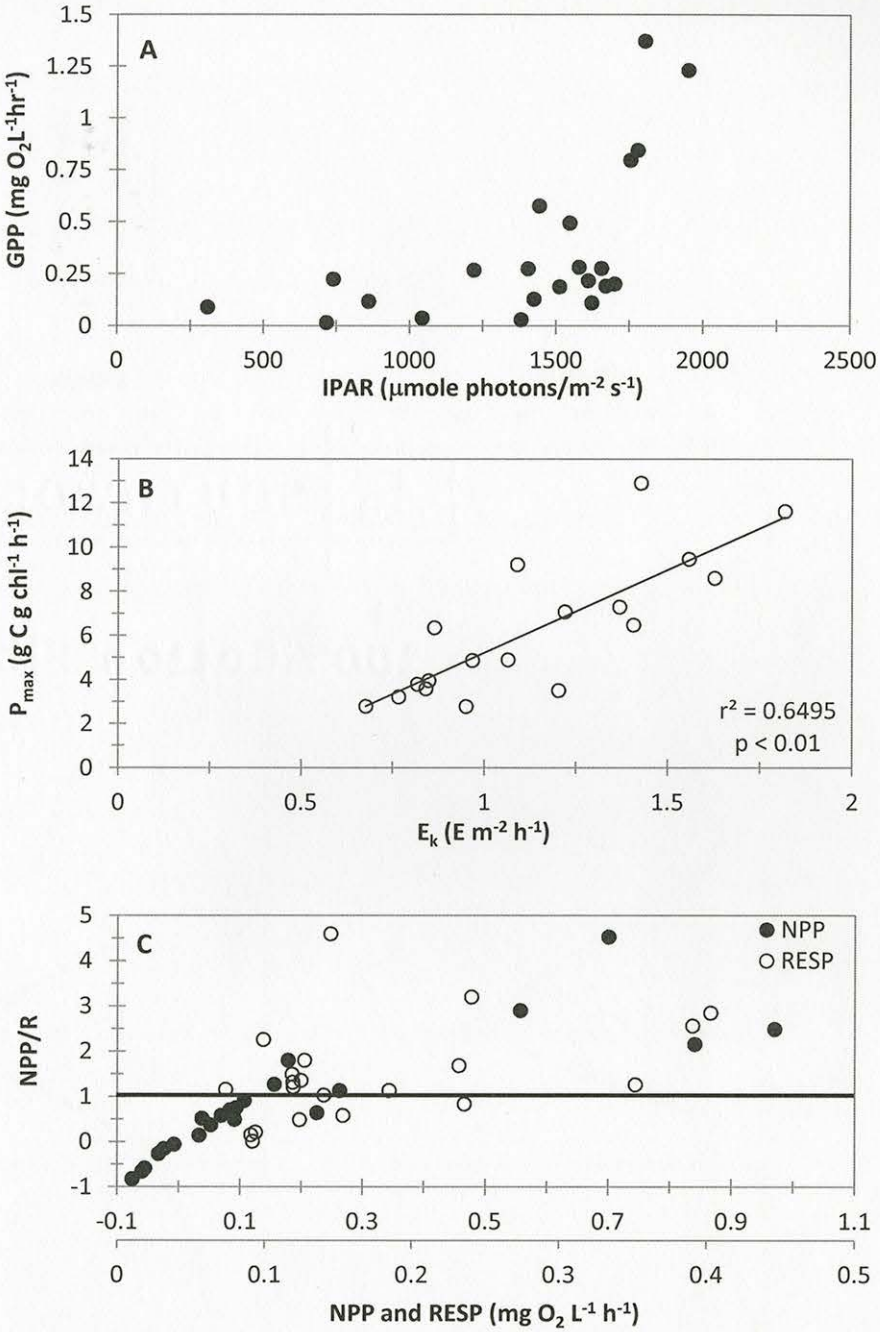

Figure 24. Maximum GrossPP rates as a function of irradiance. (A) *In situ* GrossPP rates (per volume) as a function of Instantaneous Photosynthetically Available Radiation (IPAR). (B) ^{14}C-derived P_{max} (per chlorophyll) as a function of light intensity at saturation (E_k). (C) Surface NetPP/RESP as a function of surface NetPP (filled dots) and RESP (open dots). The line in Figure C illustrates the boundary at which maximum NetPP rates equal RESP rates.

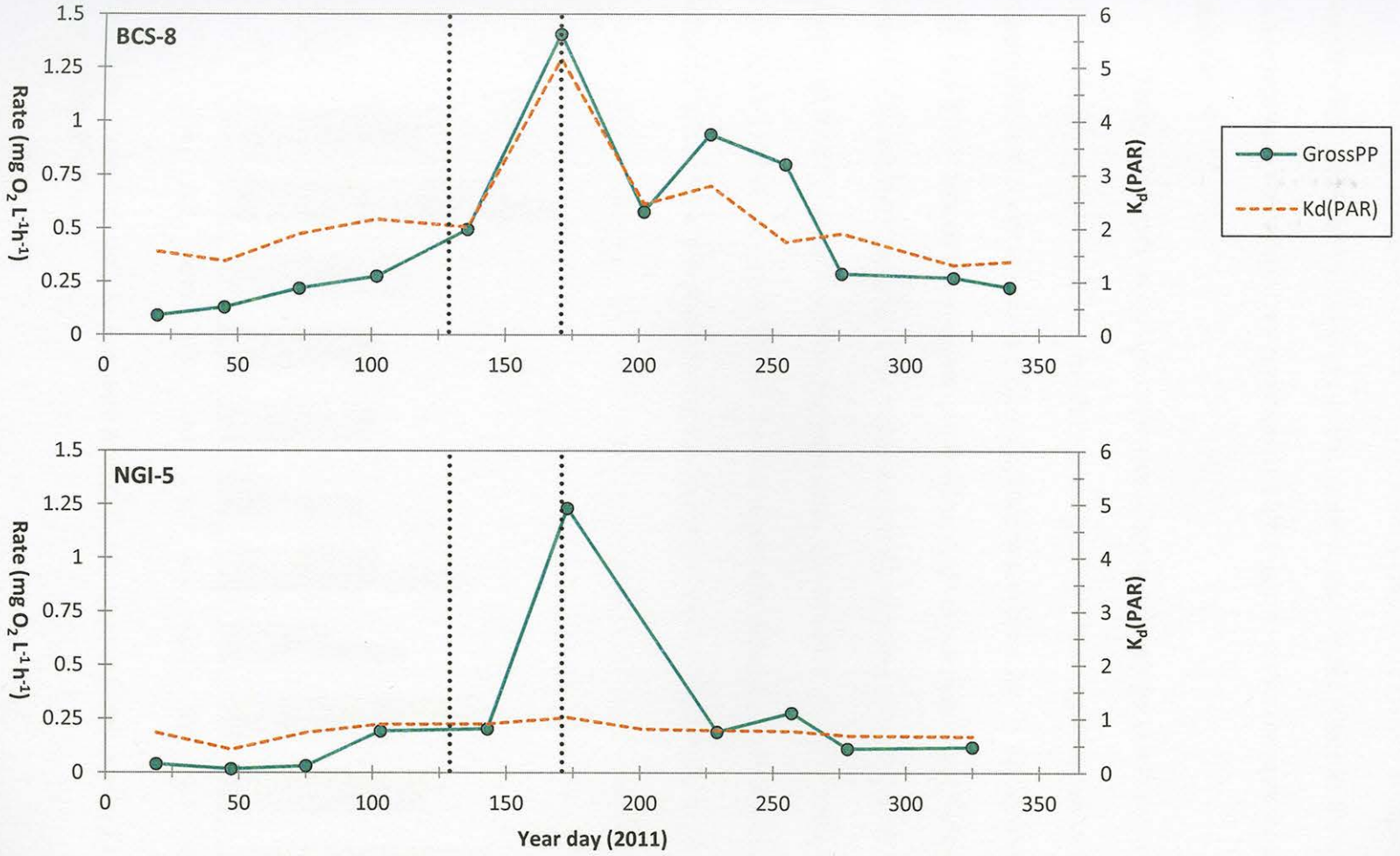

Figure 25. Time-series of surface GrossPP and K_d(PAR) measured in the Mississippi Sound (BCS-8) and the Mississippi Bight (NGI-5) from January to December 2011. The dotted vertical lines represent the period of time the Bonnet Carré Spillway was open.

Depth and Time Integrations of NEP (Net Ecosystem Productivity)

The ratio of euphotic depth (Z_{eu}) to water depth (Z) is shown in Figure 26. The lowest ratios (more turbidity) occur in the summer, and higher ratios in the winter. Comparatively, ratios were not consistently higher at one station or another throughout the year.

Daily and depth integrated estimates of gross primary productivity, respiration, and net ecosystem productivity are shown in Figure 27. Missing data makes the seasonality and trends at station NGI-5 difficult to decipher, but in the months shown, GPP and RESP tended to be higher in the Mississippi Bight than in the Mississippi Sound. Net ecosystem productivity was consistently negative (integrated NetPP < integrated RESP) through most of the year, and only becomes positive (integrated NetPP > integrated RESP) at station BCS-8 for two months in August and September. A table of integrated mean values is presented in the discussion with comparisons to other studies.

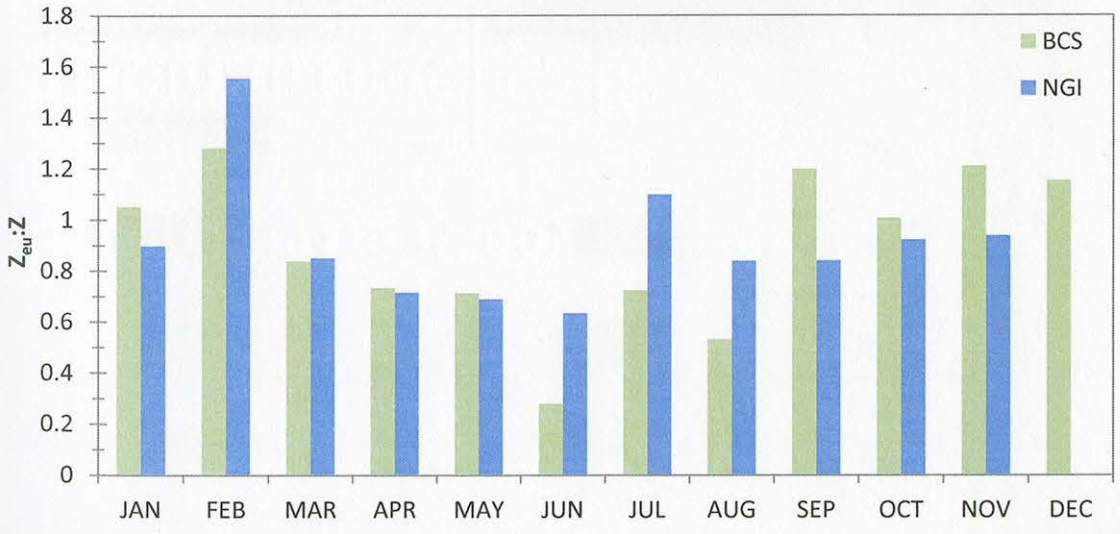

Figure 26. Time-series of the euphotic depth (Z_{eu}) to water column depth (Z) ratio for both sampled stations.

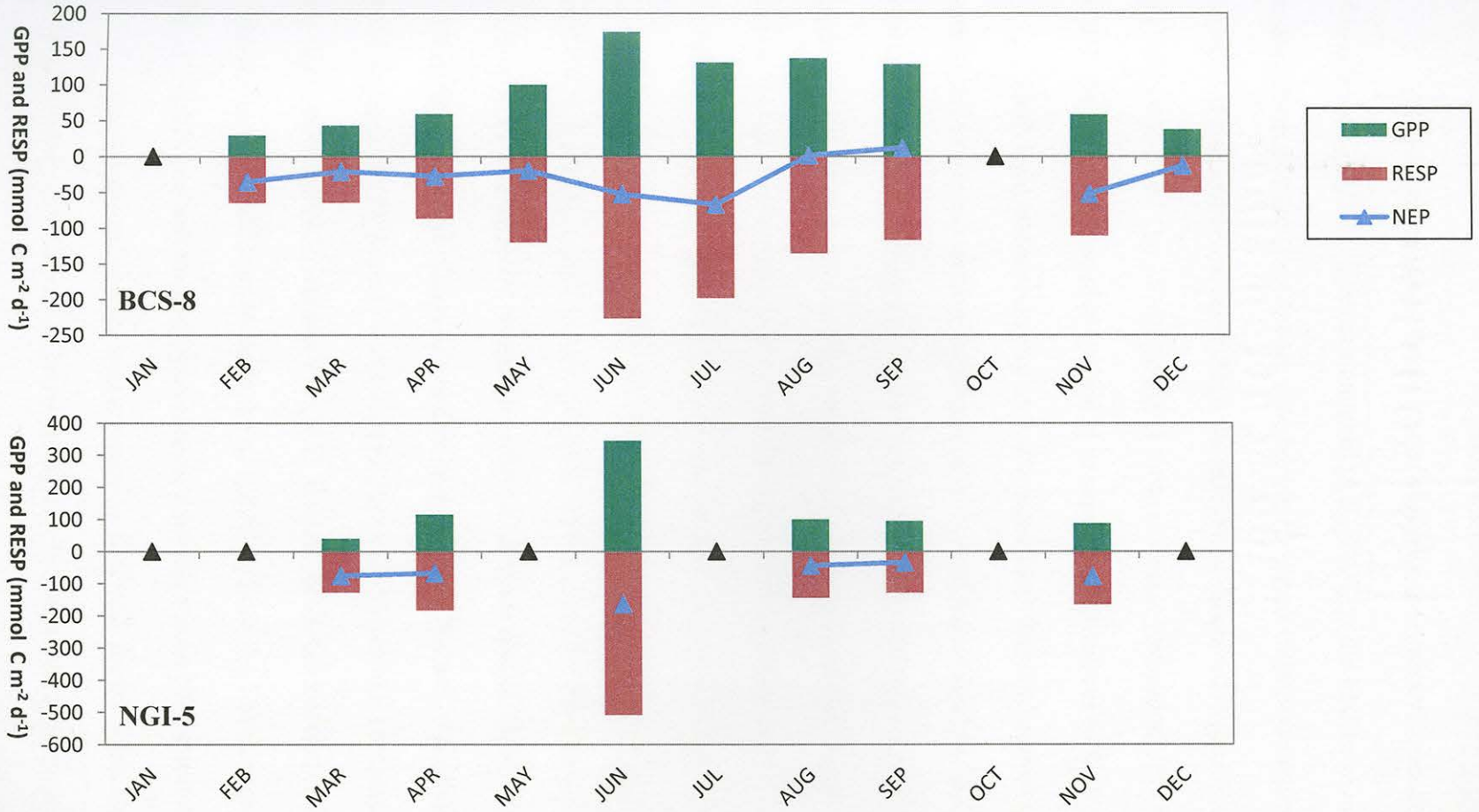

Figure 27. Time-series of daily and depth-integrated gross primary productivity and community respiration rates as well as the integrated NEP in the Mississippi Sound (BCS-8) and the Mississippi Bight (NGI-5) from January to December 2011. Note the difference in scales for the two stations. Black triangles represent missing data points where integrations were not possible.

Optical Variability

This section presents the results of variation in measured optical parameters through the year 2011. The measurement of K_d(PAR) is the backbone of this examination, but the contributing members to its signal were also monitored, including suspended particulate matter (SPM), chromophoric dissolved organic matter (CDOM), and chlorophyll-a. The SPM fraction is further divided into organic (POM) and inorganic (PIM) fractions, and are also examined as separate contributors to K_d(PAR).

Both light attenuation and optically significant biogeochemcial parameters are considered across all stations on both transects, enabling a high resolution spatial (within region) and temporal examination of their distribution. For this examination, it is assumed that these parameters are relatively well mixed and distributed evenly with depth, though this may not be the case throughout the entire estuary.

Temporal Variability of K_d(PAR) and Contributing Biogeochemical Parameters

The temporal variability of K_d(PAR) is examined in Figure 28 across different regions of the Mississippi estuarine region. Values from the Mississippi Sound were derived from two different sources in order to compare spatial variability in the Sound as well as the integrated effects of multiple sample dates. Values of K_d(PAR) from the entire BCS transect (BCS_Sound) was averaged for every month and compared to K_d(PAR) averages from the NGI stations 1-4 (NGI_Sound), both representing the Mississippi Sound waters. In addition, an estimate of K_d(PAR) from the Mississippi Bight (NGI_Bight) was determined by averaging the values from NGI stations 5-8.

Some seasonal change was apparent in K_d(PAR) for the Mississippi Sound throughout the year, as well as some variability between averaged stations on a daily

scale. The Mississippi Bight showed very little fluctuation in K_d(PAR) values throughout the year, and also showed a relatively constant amount of variability between stations. The relative magnitude of K_d(PAR) was also higher in the Mississippi Sound compared to the Mississippi Bight. Some differences in average K_d(PAR) are present between the two Mississippi Sound comparisons, though it should be noted that the NGI_Sound

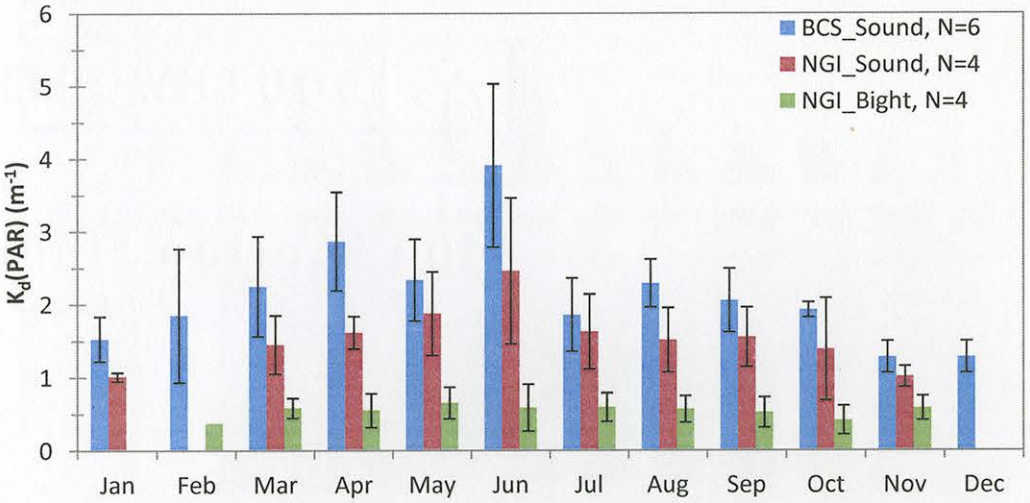

Figure 28. Time-series of K_d(PAR) averaged over three different subsections of the Mississippi estuarine region. Vertical bars represent the standard deviation between the averaged stations (within region variability).

estimate follows a transect away from shore, while the BCS_Sound stations parallel shore. Nevertheless, some seasonality can be distinguished in both estimates of the Mississippi Sound, with higher K_d(PAR) values in the summer months, lower values into the winter, and a notable peak in June, coinciding with several biogeochemical patterns as shown in Figure 29. The Mississippi Bight measurements of K_d(PAR) showed no seasonality and no significant change throughout the year.

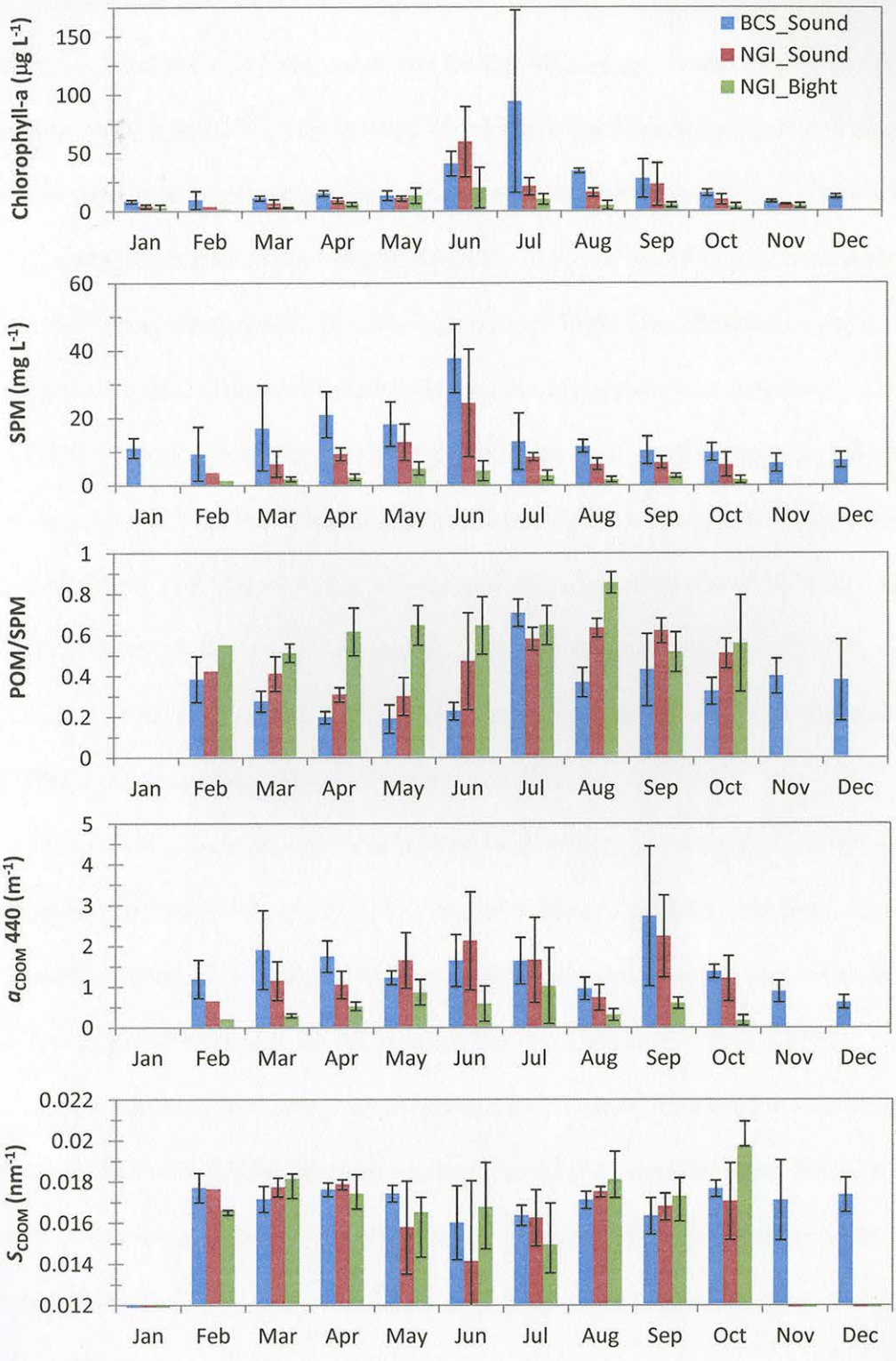

Figure 29. Time-series of chlorophyll-a, SPM, POM/SPM, CDOM absorption (a_{CDOM}_440), and CDOM slope (S_{CDOM}, 350 – 500 nm) averaged over three regions within the study area for 2011.

The various biogeochemical parameters displayed in Figure 29 showed a large amount of regional and temporal variability for the Mississippi Sound throughout the year. Chlorophyll-a and SPM values were very high in the Mississippi Sound during the summer months, with a concurrent increase in variability between stations. Chlorophyll-a values tended to be higher in the fall compared to spring, while SPM values tended to be higher in the spring compared to fall. The Mississippi Bight also showed the same seasonal patterns for chlorophyll-a and SPM, but the magnitude was decreased.

Of the SPM fraction, the Mississippi Bight was dominated by organic material through most of the year, but a near equal contribution of PIM and POM was observed during the beginning of the year. The Mississippi Sound stations tended to be dominated by inorganic material, however, averaged BCS_Sound stations reflected a higher contribution of PIM than averaged NGI_Sound stations. The highest contribution of POM/SPM was seen during the summer for all regions.

The contribution of CDOM was estimated from filtrate absorption at 440 nm. There was no clear seasonal pattern to be discerned through the year, and there was a large amount of variability between stations. The CDOM contribution was lower in the Mississippi Bight compared to the Mississippi Sound. The slope of the CDOM absorption spectra was also used as an indicator of the type of dissolved matter present. Values were relatively similar between regions throughout the entire year, but all regions experienced a relative decline in the slope in the summer, coinciding with the opening of the Bonnet Carré Spillway. These months also displayed the highest amount of variability between stations.

Spatial Distribution of K_d(PAR) and Contributing Biogeochemcial Parameters

The spatial variability of K_d(PAR) is examined in Figure 30 across all sampled stations. Data for each station was averaged over the entire year, in order to generalize which stations had the highest and lowest availability of subsurface light. The error bars illustrate the temporal variation of K_d(PAR) through the year for each station. The BCS stations are shown in a geographic order, from West to East, and the NGI stations are shown in order from North to South. The position of each station is shown in Figure 2.

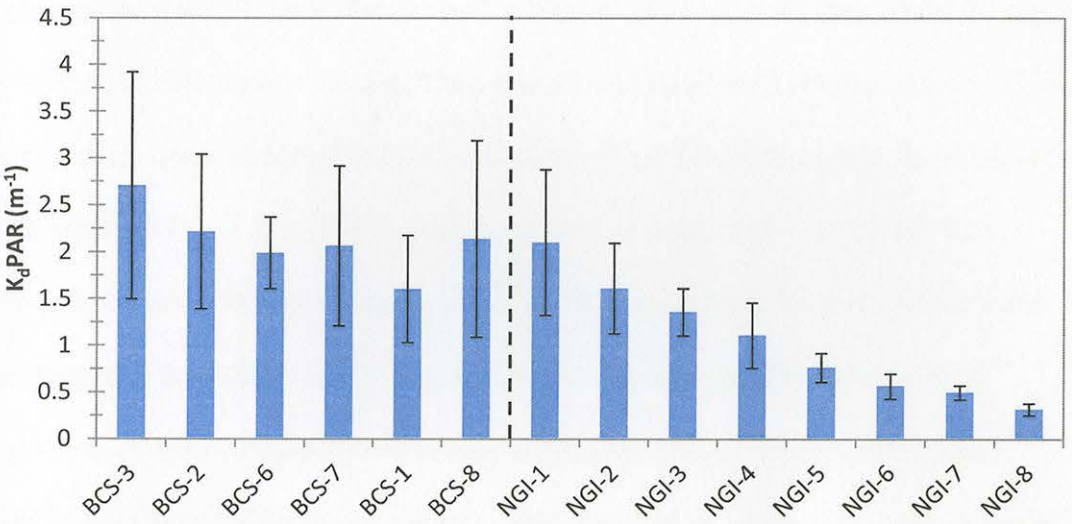

Figure 30. Annual mean and seasonal variation (standard deviation) of K_d(PAR) for each station sampled in 2011. The vertical dashed line separates the two sampling transects.

Figure 30 shows that mean values of K_d(PAR) tended to decrease as the sampling transect moves into the Mississippi Bight, as does the temporal variability. The highest mean values were found at the two stations closest to the Pearl River outflow, stations BCS-2 and BCS-3. Stations within the BCS transect all showed high amounts of temporal variability, but even the lowest values in the Mississippi Sound were consistently higher than any of the K_d(PAR) values seen in the Mississippi Bight stations through the year. Stations NGI-2 and BCS-1, as well as stations NGI-1 and BCS-7 reside in the same

geographic location, respectively, and are only distinguished by differing sampling dates. The similar magnitude and variability between these stations showed consistency, even with a temporal disconnect.

Figure 31 shows the spatial variability of various optical parameters by station. Many of the same patterns that are shown in Figure 29 can be distinguished here, such as a decreasing gradient of concentrations and variability in chlorophyll-a, SPM, and CDOM in the Mississippi Bight. This graphical representation differs in allowing for a careful look at some of these features in the Mississippi Sound. While variability was very high in the Mississippi Sound, there was a tendency towards higher mean CDOM concentrations over the entire year at the stations closer to riverine input. This can be seen at stations BCS-3 and BCS-2, which are in close proximity to the Pearl River outflow, and station BCS-7, located within Bay St. Louis. Stations closer to the Pearl River tended to be higher in SPM concentrations, however, and a higher relative contribution of PIM compared to stations closer to input from the Bay of St. Louis. Spatially, the CDOM slope did not vary greatly between all stations, averaging around 0.017 nm^{-1} throughout the year. Differences between the slopes can be seen but do not differ enough to distinguish from natural variability.

Also notable is the consistent and gradual increase in POM/SPM along the NGI transect, coinciding with the loss of the total SPM fraction. While variability remains high for all parameters, this figure shows that changes within biogeochemical factors (except S_{CDOM}) were to some degree a function of distance from the mainland.

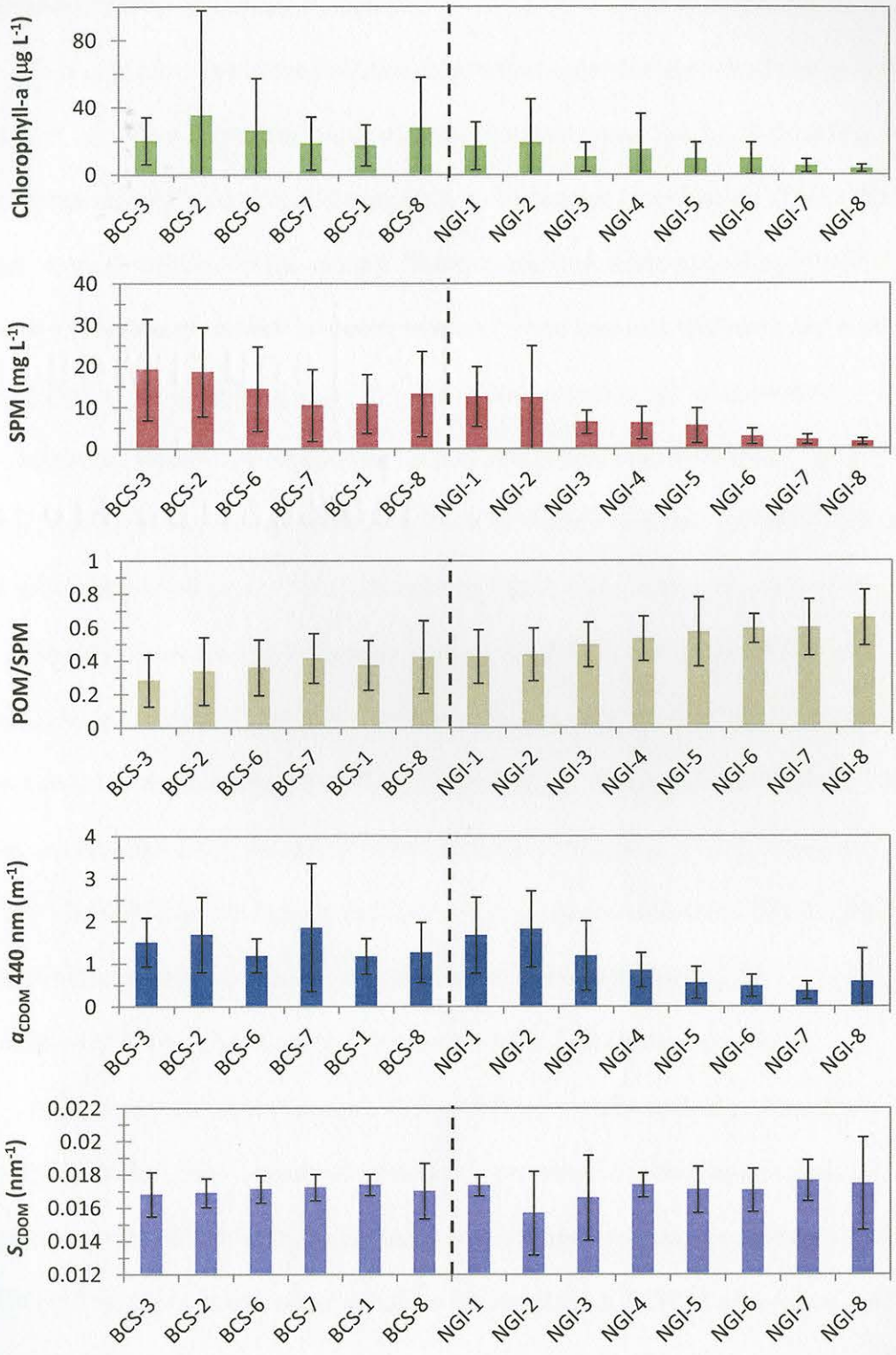

Figure 31. Annual mean and seasonal variation (standard deviation) of chlorophyll-a, SPM, POM/SPM, CDOM absorption (a_{CDOM}_440), and CDOM slope (S_{CDOM}, 350 – 500 nm) across all sampled stations. The dashed vertical line separates the sampling transects.

Conservative Mixing of Optical Parameters

Given the afore mentioned relationship, a first order description of the spatial distribution of optical parameters in coastal environments may also be obtained by observing the mixing behavior, allowing for a more concise examination of how these parameters are distributed in the estuary. Determining how these optical parameters behave as a function of salinity is useful, as each component acts to absorb and scatter light in different ways, depending on its relative concentration and composition.

Figure 32 shows that while these optical parameters tended to change as a function of salinity, they were not all distributed in a similar manner. In this figure, all station data was pooled and plotted individually, thereby preventing the variability between stations from biasing the results. Values of CDOM absorption, POM, and chlorophyll-*a* all tended to react conservatively, though there exists a fair amount of scattered data points above the mean that did not behave in a predictable fashion. Values of SPM, on the other hand, tended to mix non-linearly, with high extinction at low salinities. The particulate inorganic fraction also displayed a non-linear mixing pattern, and appeared to behave very differently above and below a salinity of 10.

Contribution of Biogeochemistry to Light Attenuation – Multiple Regressions

A first order direct comparison of K_d(PAR) to various optical parameters is shown in Figure 33. This comparison serves as a preface to the subsequent multiple regression analysis, which estimates a linear relationship between a dependent variable (K_dPAR) and multiple independent variables (chlorophyll-a, CDOM absorption, and suspended particulate matter).

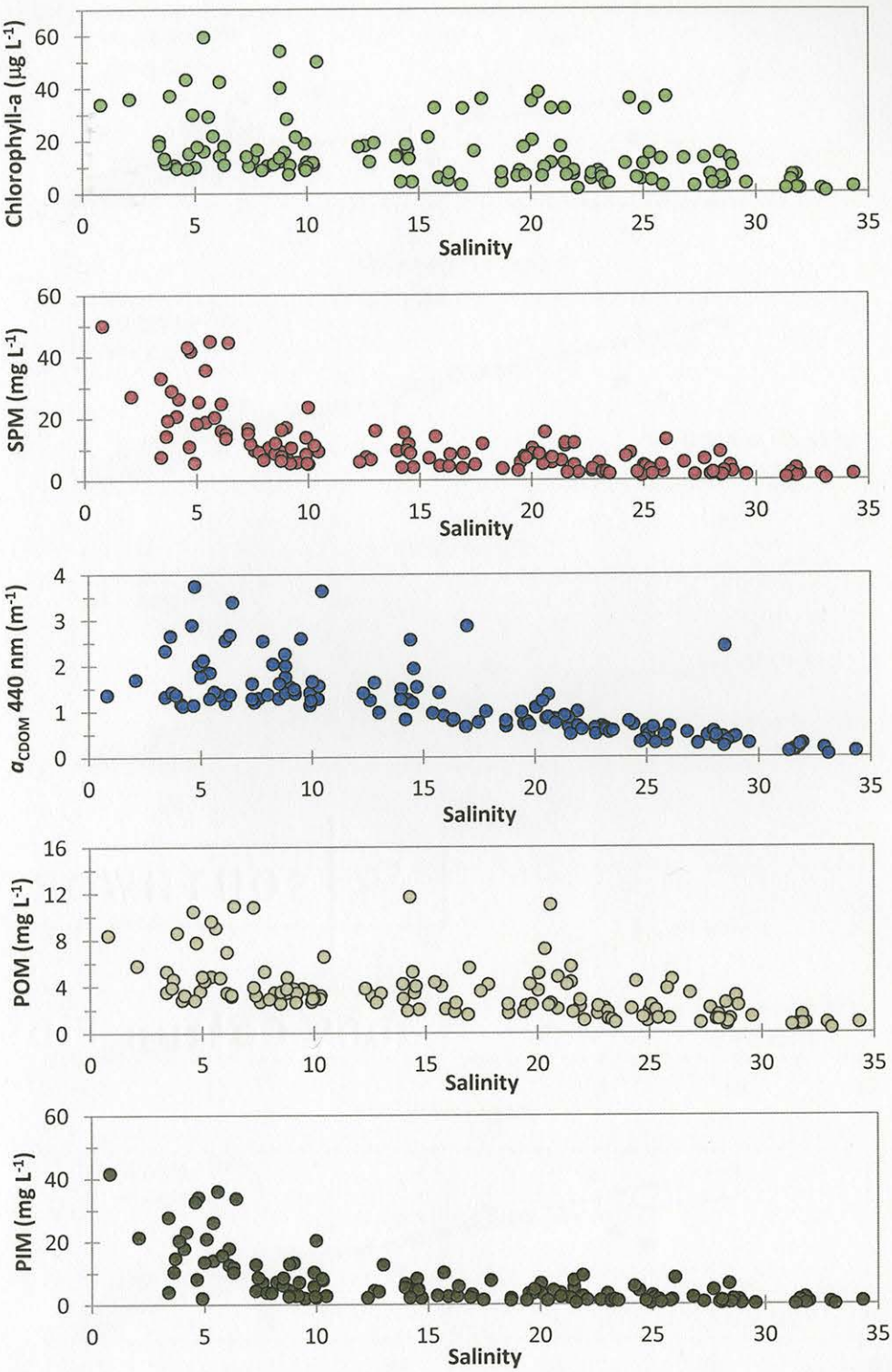

Figure 32. Chlorophyll-a, SPM, CDOM absorption (a_{CDOM}_440), particulate organic matter (POM), and particulate inorganic matter (PIM) for all sampled stations, plotted as a function of salinity.

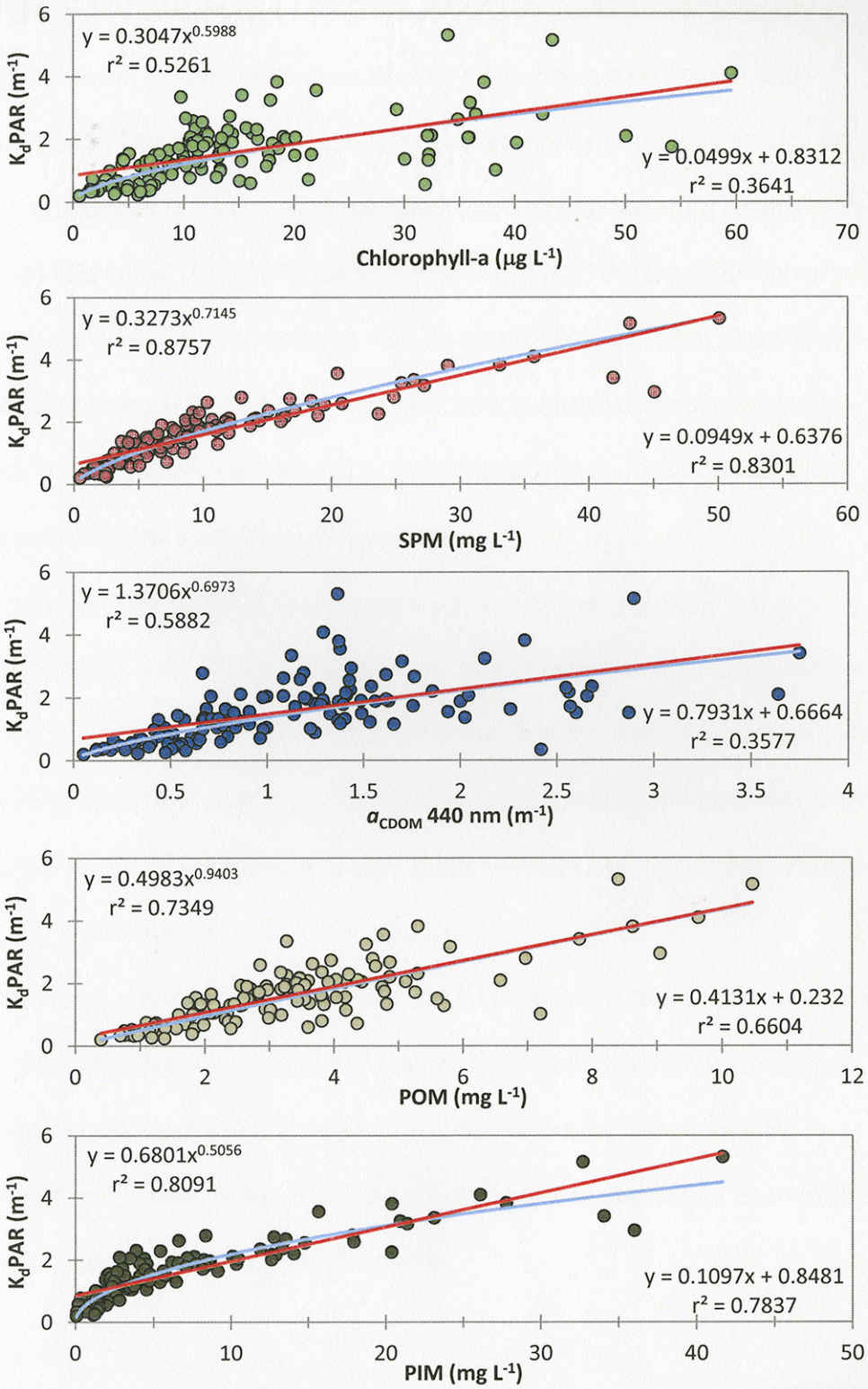

Figure 33. First order comparison between calculated K_dPAR and optical parameters: chlorophyll-a, SPM, CDOM absorption (a_{CDOM}_440), POM, and PIM for all sampled stations. Both power (blue line) and linear (red line) trends are shown.

Figure 33 shows that relationships between K_d(PAR) and optical parameters are not always strictly linear, and are better described by a power function (Morel and Maritorena, 2001). The comparison is shown as subsequent analysis can require an assumption of linearity. This first order comparison shows the strongest relation between K_d(PAR) and suspended particulate matter. Of the SPM fraction, the contribution of PIM to light attenuation tended to be stronger than the contribution of POM. Chlorophyll-a and CDOM absorption both showed a relatively low, but similar correlation to light attenuation. Overall, correlations tended to be tighter at lower concentrations, with increasing variability as concentration increases.

Results from the multiple linear regression analysis are shown in Table 6. A model of predicted K_d(PAR) was constructed by multiplying the coefficients derived from the analysis by each respective independent variable for every sample point, and adding the slope intercept value to this sum total. The regression of the predictive model with measured K_d(PAR) is shown in Figure 34. As with the first order regressions in Figure 33, the uncertainty increased as K_d increased.

This analysis enables one to weigh the relative contribution of each parameter to K_d(PAR), if the assumption is maintained that the derived coefficients remain constant and linear across time and space. In order to do this, each independent variable (x, representing chlorophyll-a, SPM, or CDOM absorption) is multiplied by its respective coefficient (m), and normalized to the sum total:

$$\% \, x_1 \text{ to } y = \frac{m_1 * x_1}{\Sigma \, (m * x)_{total}} \qquad \text{Equation 3-1}$$

Table 6

Statistical Summary Output for Multiple Regression Analysis

Regression Statistics	
Multiple R	0.929
R Square	0.863
Adjusted R Square	0.860
Standard Error	0.369
Observations	127

ANOVA

	df	*SS*	*MS*	*F*	*Significance F*
Regression	3	105.431	35.144	258.287	0.000
Residual	123	16.736	0.136		
Total	126	122.167			

	Coefficients	*SE*	*t Stat*	*P-value*	*Lower 95%*	*Upper 95%*
Intercept	0.410	0.064	6.437	0.000	0.284	0.536
Chlorophyll	0.011	0.003	3.334	0.001	0.005	0.018
SPM	0.080	0.004	18.004	0.000	0.071	0.089
CDOM a440	0.184	0.053	3.450	0.001	0.078	0.289

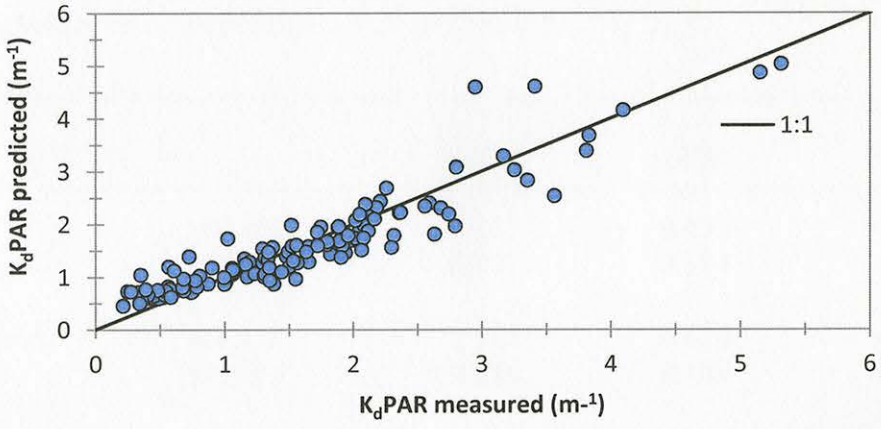

Figure 34. Comparison of the predicted K_d(PAR) values to the measured K_d(PAR) values.

A spatial and temporal description of the percent contribution each optical parameter imparts on K_d(PAR) is shown in Figure 35. This figure shows that the SPM fraction dominated the signal for K_d(PAR) at all stations throughout the entire year. This contribution of SPM to total light attenuation was generally greater in the Mississippi Sound than in the Mississippi Bight, and was highest at the stations closest to the Pearl River outflow. Overall, CDOM and chlorophyll imparted similar magnitudes of influence on light attenuation. In the Mississippi Sound, the relative weight of CDOM absorption to total light attenuation was high in the Bay St. Louis stations, but also increased slightly into the Mississippi Bight, as the weight of SPM diminished. The highest contribution of chlorophyll-a to total light attenuation appeared in the Mississippi Bight at station NGI-6. Temporally, SPM had a higher contribution in the winter and spring months, while the proportion of the CDOM and chlorophyll signal increased in the summer. Spatially-averaged values of the percent contribution of each optical parameter to K_d(PAR) for different regions within the Mississippi estuarine region are shown in Table 7.

Table 7

Spatially-averaged Values of the Percent Contribution of each Biogeochemical Parameter to K_d(PAR) for all Stations (Total, BCS+NGI), the Mississippi Sound (BCS-transect), and the Mississippi Bight (NGI stations 5-8).

		CHL	SPM	CDOM
TOTAL	MEAN	0.157	0.632	0.210
	STDEV	0.077	0.114	0.092
BCS_Sound	MEAN	0.141	0.679	0.180
	STDEV	0.074	0.109	0.080
NGI_Bight	MEAN	0.193	0.574	0.233
	STDEV	0.080	0.100	0.101

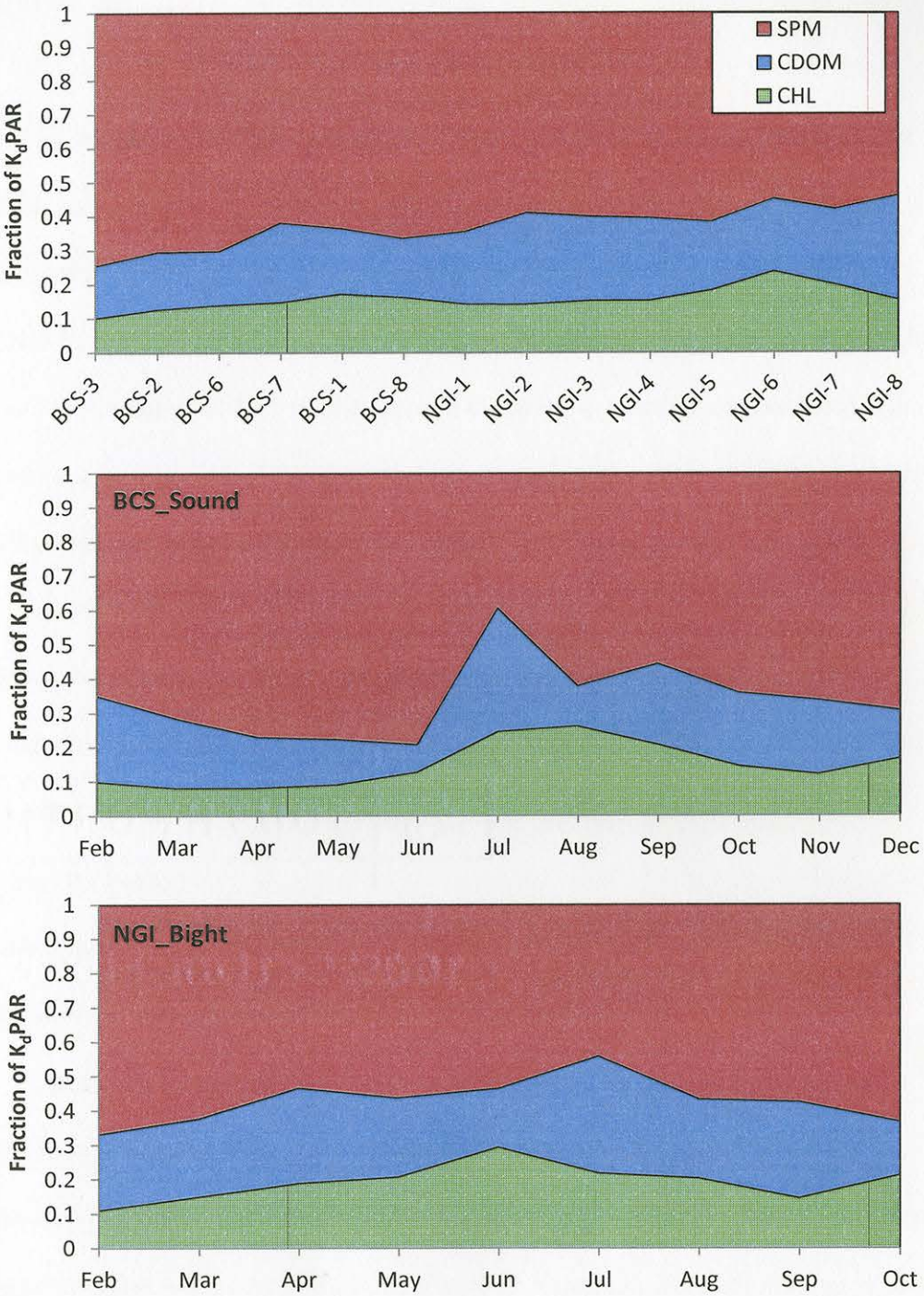

Figure 35. The relative contribution of SPM, CDOM, and chlorophyll-a to K_d(PAR). Data shown at each station for the entire year (top), or spatially distinguished and plotted per month (BCS_Sound, NGI_Bight). Months not shown lacked sufficient data for the analysis.

Remote Sensing Variability

The focus of this section relates to the variability of remotely sensed data retrieved in the estuary for the study period. Ground measured biogeochemical and optical parameters are compared to quality controlled MODIS Aqua data, including remote sensing reflectance, band ratios, and algorithms. These comparisons are performed in order to establish a relationship with biologically significant parameters and examine the potential for high quality spatial mapping in a turbid environment. The parameters of interest to be examined include chlorophyll-a, SPM, CDOM absorption, K_d(PAR), euphotic zone depth (Z_{eu}), and daily PAR.

The MODIS Aqua data is only examined for the dates and coordinates (at 1 km resolution) that correspond to ground sample collection. No spatial or temporal averaging was conducted for the ground truth comparison. All data that did not meet quality control criteria was removed before performing the following comparisons. A Pearson's correlation test was run on all parameters, and included all possible combinations of two band ratios in the visible and near-IR wavelengths available from MODIS bands.

Biogeochemical parameters – Chlorophyll, SPM, and CDOM

A comparison of laboratory measured chlorophyll-a to MODIS-derived chlorophyll-a products (chlor_a) and proxies (fluorescence line height [flh], Rrs_748/Rrs_667 [Dall'Olmo et al. 2005], and aph_qaa_531 [phytoplankton absorption]) was found to show weak correlations, as shown in Figure 36. Remote sensing reflectance at the MODIS high resolution band (645 nm) as well as the 1 km resolution 667 nm and 748 nm wavelengths showed a strong correlation to SPM (Figure 37).

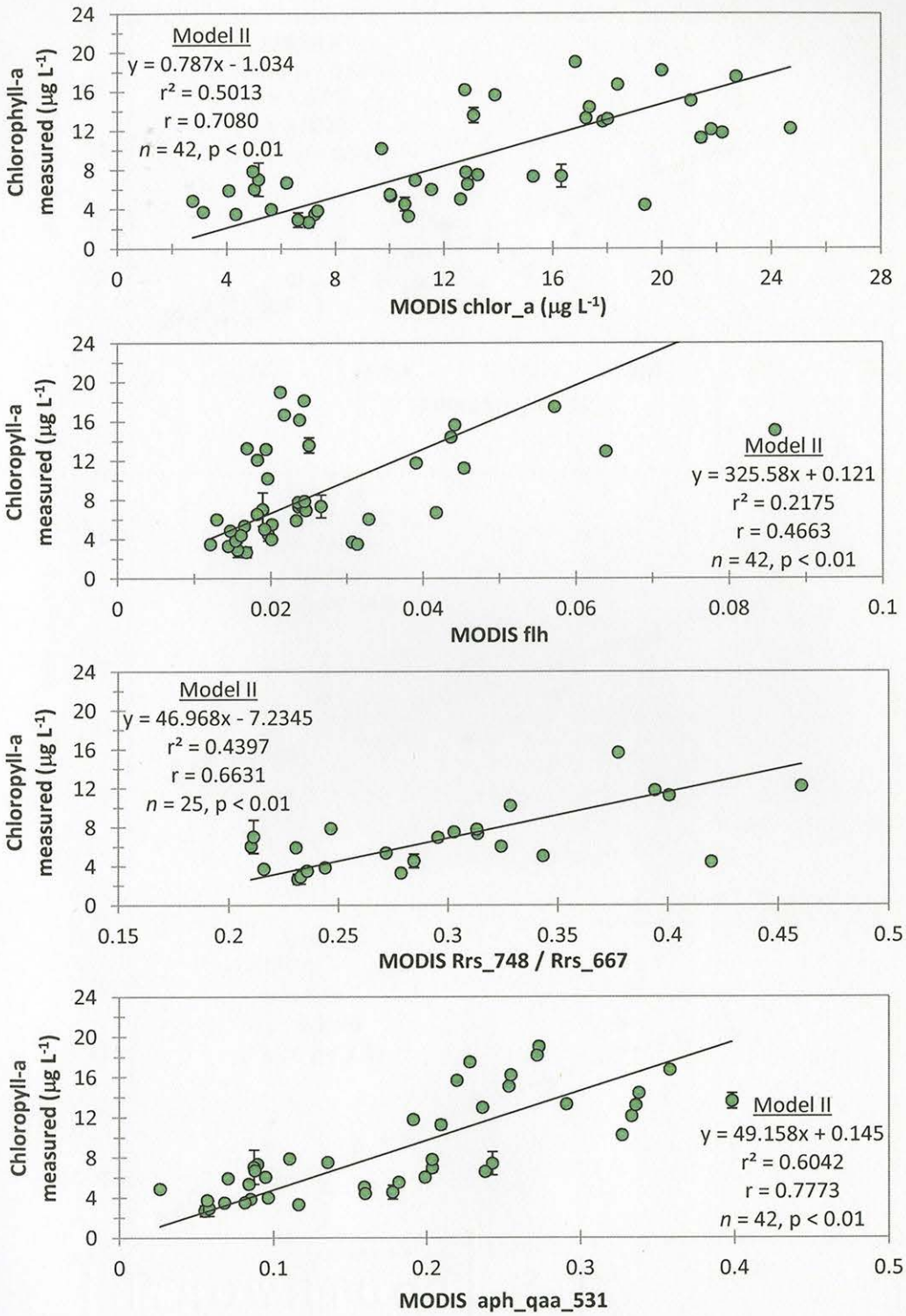

Figure 36. Comparison of MODIS-derived algorithms to ground measurements of chlorophyll-a. Chlorophyll-a (chlor_a), Fluorescence Line height (flh), band ratios (Rrs_748/Rrs_647), and phytoplankton absorption (aph_531_qaa) products are shown.

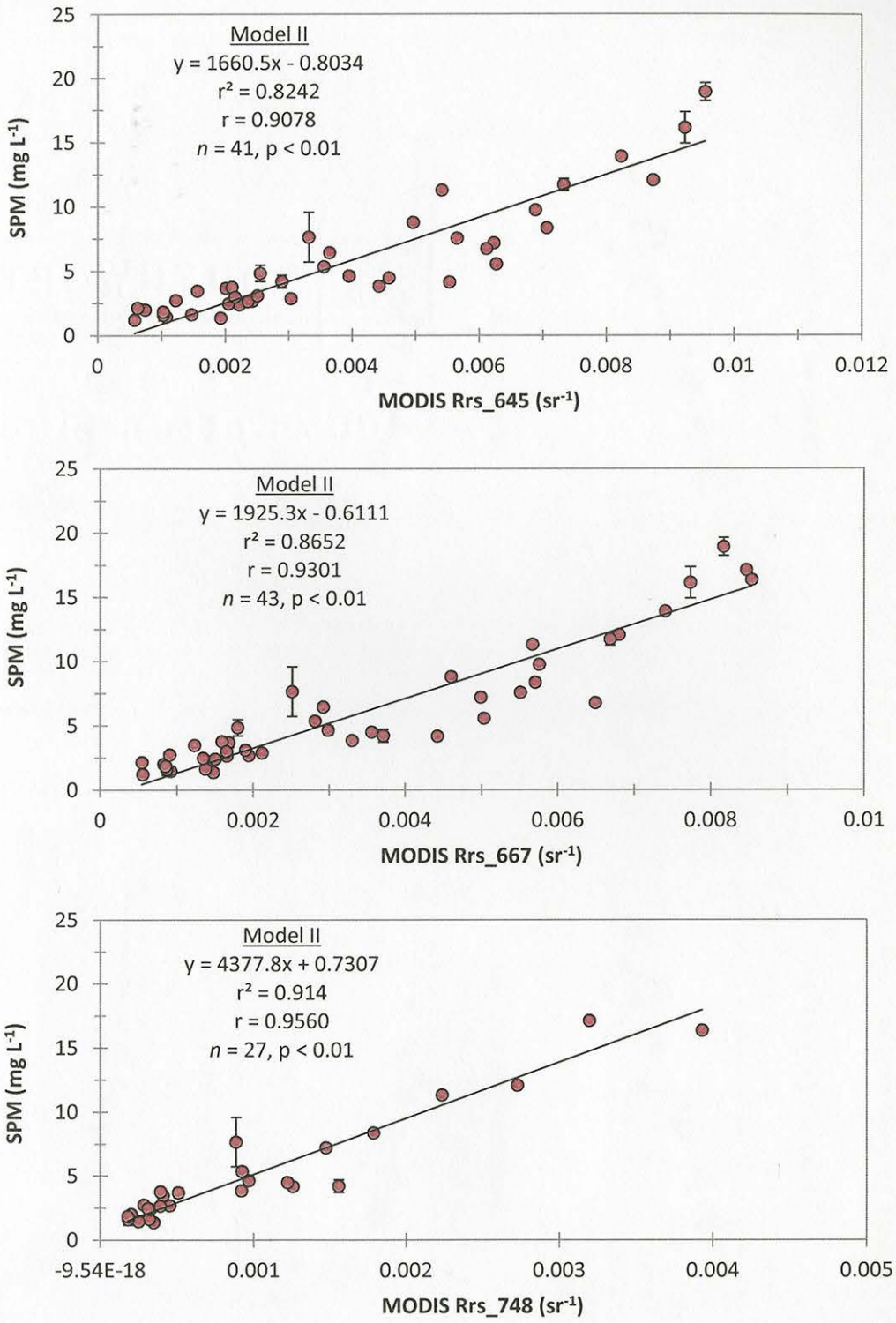

Figure 37. Comparison of MODIS-derived Remote Sensing Reflectance Bands to Ground Measurements of Suspended Particulate Matter. The R_{rs} at 645 nm (250 m resolution), 667 nm (1 km resolution), and 748 nm (1 km resolution) is shown.

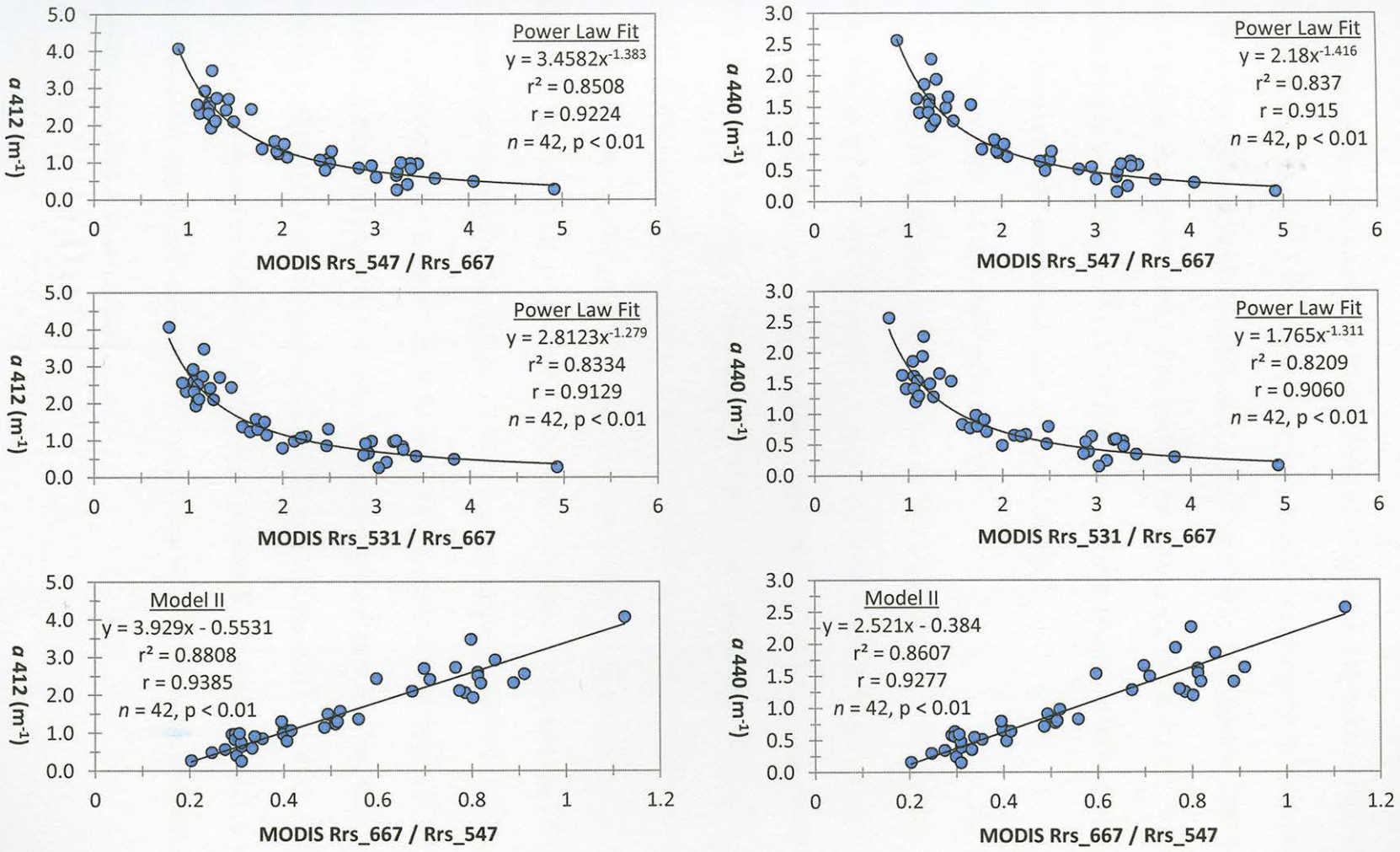

Figure 38. Comparisons between various MODIS band ratios and *a*412 (left), and *a*440 (right).

Figure 38 shows that CDOM absorption at 412 nm and 440 nm had strong non-linear (power) correlations to the Rrs547/Rrs667 band ratio. The relationship between Rrs531/Rrs667 and *a*412 was also examined as the closest comparison between the relationship between Rrs510/Rrs670 and *a*412 described by Del Castillo (2005). This was also found to be a power relationship, and the band ratio showed a slightly lower correlation to *a*412 than the Rrs547/Rrs667 ratio. The strongest correlation was linear and found between *a*412 and a band ratio of Rrs667/Rrs547.

Light Parameters- K_dPAR and Euphotic Depth

Three MODIS algorithms that exist for deriving light attenuation values are compared to ground measurements in Figure 39. There exists a strong correlation between the Kd_PAR_lee quasi-analytical algorithm (QAA) and K_d measured (r^2 = 0.9079, $p < 0.01$), however, there was slight offset between the two values (slope = 1.469). A similar offset was observed in comparing K_d measured to the MODIS Kd_490 algorithm (slope = 1.394), but, a much lower correlation was observed here (r^2 = 0.4994, $p < 0.01$). The Kd_PAR_morel algorithm appeared to have the highest disparity with K_d measured, with a large offset (slope = 4.943) and low correlation (r^2 = 0.5227, $p < 0.01$).

The euphotic depth, or 1% light level, can be derived from two MODIS algorithms that are compared to *in situ* derived values in Figure 40. The Zeu_lee algorithm showed a good correlation to ground measurements (r^2 = 0.8083, $p < 0.01$), however, the algorithm tended to slightly overestimate K_d measured. The Zeu_morel algorithm was not as well correlated (r^2 = 0.6032, $p < 0.01$) and overestimated the euphotic depth to a larger degree.

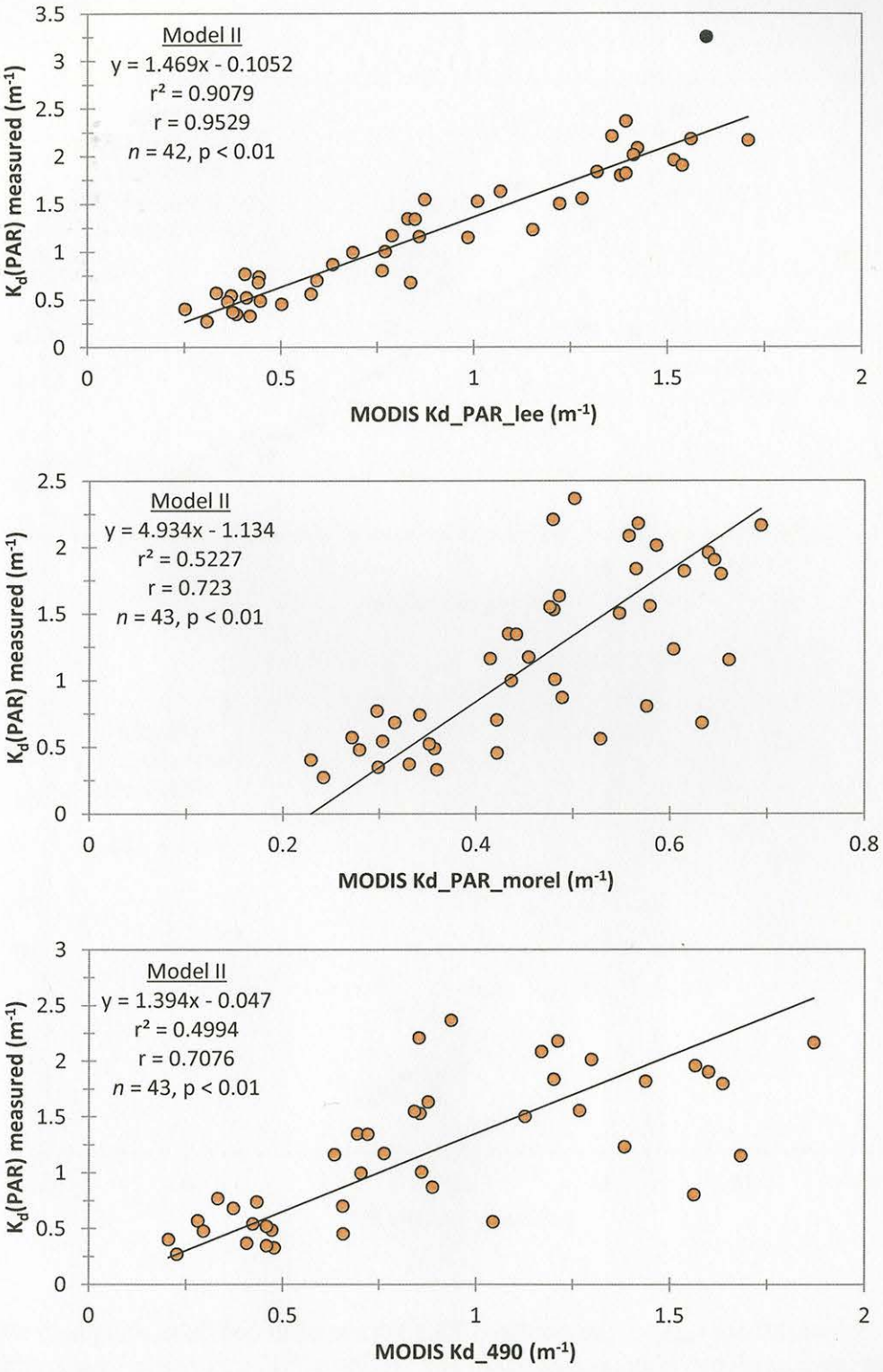

Figure 39. Comparison of three MODIS K_d products to ground derivation of K_d from *in situ* light profiles. The black data point is considered an outlier and is excluded from the regression.

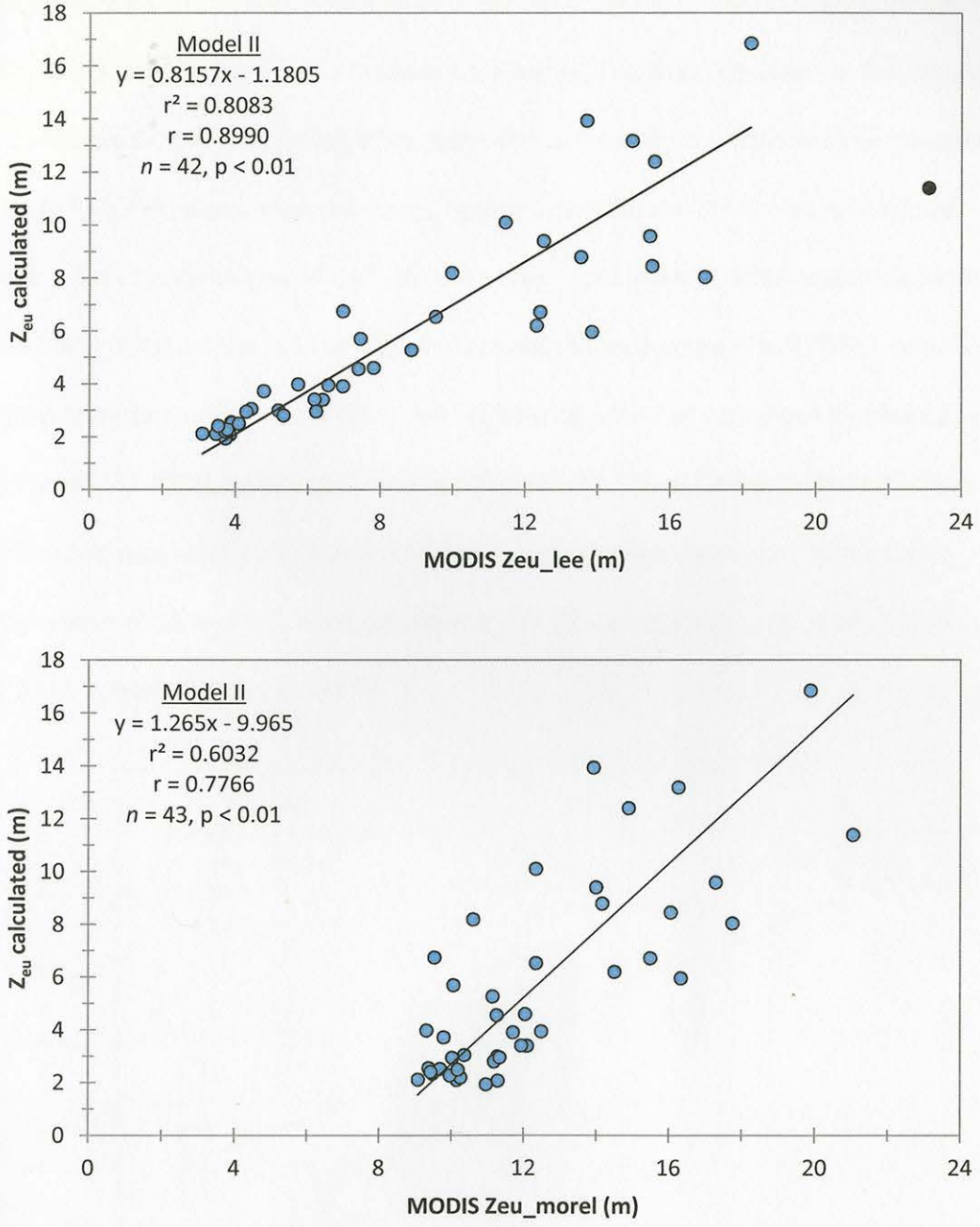

Figure 40. Comparison of two different MODIS euphotic depth (Z_{eu}) products with calculated values from *in situ* light profiles. The black data point is considered an outlier and is excluded from the regression.

PAR Time series

Figure 41 shows a comparison between daily MODIS PAR and daily integrated PAR calculated from the LI-COR sensor time series. The data presented in this figure only corresponds to the sampling dates that were covered by a viable satellite overpass. Since the LI-COR sensor was stationary, spatial variability of PAR was determined through a direct comparison of the LI-COR sensor data to the HOBO sensor measuring downwelling PAR on the boat as it moves around the study area. The HOBO data was analyzed from two cruises (one NGI, one BCS) with no cloud cover and compared to thestationary LI-COR output as shown in Appendix C. The error bars represent the deviation between the LI-COR and HOBO sensors for each equivalent time period. The average value of all spatial deviation measured in this comparison was applied to the daily PAR output from the LI-COR.

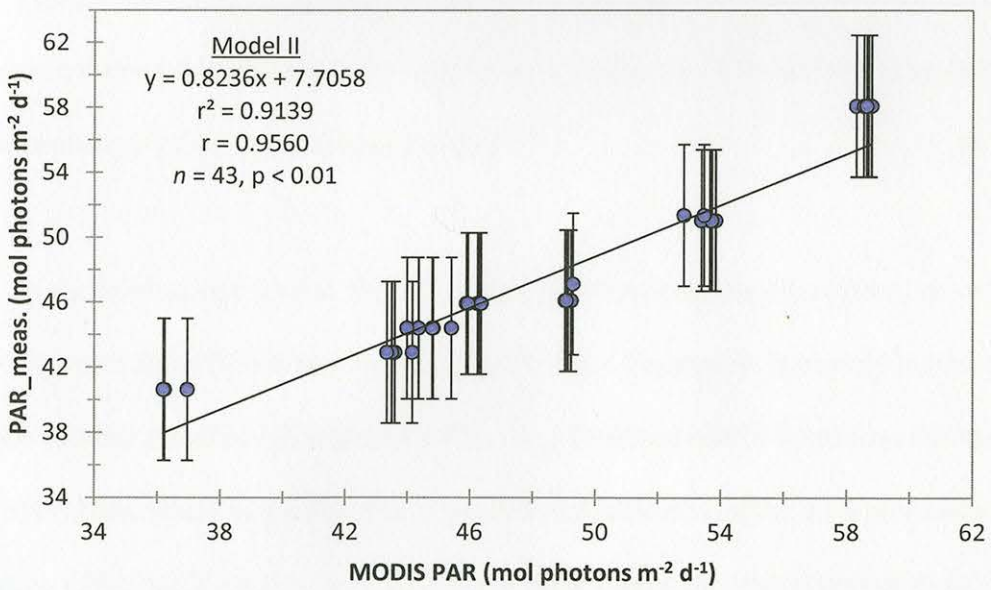

Figure 41. Comparison of MODIS daily PAR to LI-COR time series. The error bars represent the average spatial variability in the Mississippi Sound and Bight.

CHAPTER IV

DISCUSSION

The Mississippi coastal estuarine region exhibits a high measure of optical and biogeochemical variability, thus driving similar patterns of primary productivity and respiration. The results of this study demonstrate that the drivers of this variability are not always obvious, and that a multitude of factors may simultaneously contribute to whether the system is a net source or sink of carbon. The objective in this study was to resolve the variability of ecosystem metabolism and biogeochemistry on relevant temporal and spatial scales, while assessing the possibility of large-scale extrapolations of biologically significant parameters. The following chapter is a critical evaluation of the study results as they relate to the proposed hypotheses.

Analysis of Hypothesis I

Measurements of net primary productivity and respiration will vary on seasonal scales and between stations, showing significant correlations with salinity, temperature, biogeochemistry, light attenuation (K_d), and PAR.

Salinity

In the Mississippi Sound, the delivery of nutrients (nitrate, phosphate, silica) primarily comes from freshwater input, indicating that the system is heavily influenced by allochthonous materials (Eleutarius 1976). It is therefore useful to discuss the spatial and temporal distribution of salinity as a generalized indicator of the allochthonous parameters affecting biological activity. While the ambient concentrations of most nutrients did not correlate highly with salinity for this study (Figure 16), this was likely due to environmental interactions across the estuary, such as variable mixing behaviors,

benthic resuspension, and biological uptake/remineralization. Even with this disparity, however, changes in salinity due to localized rainfall and river output remain important to providing nutrients and carbon to the system and subsequently driving biological activity in estuarine environments (Mallin et al. 1993).

Historically, the distribution of chlorophyll along the northern Gulf of Mexico has been shown to decrease with increasing salinity (Atwell 1973, Qian et al. 2003). Over the course of 2011, there existed a substantial amount of variability in chlorophyll-a along a salinity gradient in the Mississippi Sound and Mississippi Bight (Figure 32 A), and concentrations were generally higher at station BCS-8 compared to station NGI-5 on similar temporal scales (Figure 29 A). *In situ* derived maximum primary productivity rates (NetPP) tended to follow the concentration of chlorophyll-a very closely in surface waters for the sampled dates (Figure 18 E), but had the potential to fall out of phase with one another as a result of either nutrient limitation or light limitation due to high turbidity (Sampou and Kemp 1994, Iriarte et al. 1996). Both chlorophyll and NetPP showed very little consistent temporal correlation to changes in salinity. However, some isolated events of decreasing salinity coincided with elevated rates of primary productivity, especially with the opening of the Bonnet Carré Spillway in May/June, and the riverine outflow from Tropical Storm Lee in September (Figure 17).

While historical respiration data is lacking for Mississippi waters, rates are usually elevated in lower salinity estuarine regions due to the high amount of organic loading from both allochthonous and autochthonous sources (Hopkinson and Smith 2005). In this study, DOC was one organic substrate that showed a relatively conservative distribution throughout the estuary (Figure 20). Overall, DOC has been

shown to be a strong driver of bacterial respiration, which can be a substantial portion of total respiration in estuarine environments (Fuhrman 1985, Griffith et al. 1990). However, Figure 21 demonstrates that respiration showed a much better relationship with the particulate organic matter (POM) than it did the dissolved organic fraction. It is important to note here that the production and consumption of DOC can be tightly coupled, and that the relative amount of DOC in the water column may not reflect biological response (Carlson 2002). While POM does include the pool of detrital matter and fresh photosynthetic material available for oxidation, respiration is common to all organisms, therefore covariance may not necessarily be a direct indicator of causation, but simply a function of particulate biomass that is capable of respiration.

The contribution of DOC to fuel respiration should not be discounted based on these data. Smith and Kemp (2003) show that the relationship between DOC and bacterial production may not be straightforward in estuarine environments, as there can be substantial bacterial resource limitation along salinity gradients (either DOC or nutrients). In addition, the relative lability of DOC can change spatially and temporally based on its origin, with autochthonous DOC having a higher rate of uptake in the community (Carlson 2002). Assuming that POM was the dominant contributor to the respiration signal over the Mississippi estuary, Figure 32 D indicates that its distribution was also nearly as highly variable along a salinity gradient as chlorophyll-a. It follows then, that respiration also showed very little correlation to salinity changes over longer temporal scales (Figure 18 B), and that there are other factors besides delivery of allochthonous materials determining its temporal distribution.

Figure 18 F suggests that respiration was coupled to chlorophyll biomass to some extent, but it is important to note that the regulation of primary productivity and respiration can potentially have one or more common variables (del Giorgio and Cole 1998). Other estuarine studies have shown that when primary productivity is low, respiration tends to be more influenced by the availability of allochthonous materials, while periods of high primary productivity shows a higher dependence of respiration on autochthonous materials (Iriarte et al. 1996, Hopkinson and Smith 2005). Thus, given the clear seasonal patterns of primary productivity and respiration, and the sporadic influence of high allochthonous flux indicated by salinity changes, it appears that salinity provides no direct indication of biological activity in this area. However, the delivery of nutrients and organic matter in the freshwater certainly act to influence biological activity, but this relationship is variable in time and space, suggesting covariance with other regulating factors.

Temperature

Eppley (1972) discussed the importance of temperature effects on photosynthetic rates, and demonstrated that the upper limits of growth can be mediated by temperature. Both light-dependent and light-independent reactions involved in photosynthesis have some degree of temperature dependence, whether it be due to enzymatic processes, or in the case of light-dependent reactions, due to changes in membrane viscosity or intermolecular collision processes affecting electron transport (Falkowski and Raven 2007, Raven and Geider 1988). Certainly, the reduction or increase of photosynthetic efficiency at various temperatures is important enough to have warranted the incorporation of temperature as an input into photosynthetic models (Behrenfield and

Falkowski 1997). Numerical respiration models also incorporate temperature terms as respiration has been shown to vary linearly, or exponentially as a function of temperature in several estuaries (Bartleson and Kemp 1991, Sampou and Kemp 1994, Smith and Kemp 1995).

Figure 18 C, D shows a significant change ($p < 0.01$) in both maximum primary productivity and respiration rates as a function of temperature over the course of the year. The mathematical description of this pattern is not strictly linear, as there is an apparent non-linear increase in primary productivity and respiration at higher temperatures. An exponential fit poorly describes this pattern, likely as a result of a few data points in the higher temperature range exhibiting low rate measurements. This may be a result of some substrate limitation (light, carbon, nutrients), which is more likely in the warmer months, when competition for resources is high. Similar patterns of variable biomass distribution at higher temperatures have been observed in other turbid estuaries (Irigoien and Castel 1997).

There is evidence of temperature acclimation mechanisms in natural assemblages that may reduce the apparent seasonal effects of temperature on NetPP and RESP rates. For phytoplankton, there can be a reduction in the amount of chlorophyll per cell and an increase in carboxylation activity in colder temperatures. As a result, primary productivity per unit chlorophyll can be similar across several temperature regimes (Falkowski and Raven 2007). Without adaptation mechanisms, the chlorophyll content per cell tends to elevate when temperatures are increased and light is held constantly at a saturation level (Geider 1987). However, in low light conditions, such as the bottom of the euphotic zone, variation in temperature has little effect on photosynthetic rates,

suggesting that even a relatively shallow water column may experience different limiting factors from surface to bottom (Kirk 1994).

For microheterotrophs, there has been evidence of temperature-selection among estuarine bacterial populations (i.e. regime shift) as well as smaller scale physiological adaptations (Sieburth 1967, Sampou and Kemp 1994). This adaptation does not always hold true, especially for larger species of zooplankton with longer turnover rates, whose metabolic rates and feeding patterns have shown a significant relationship to changes in temperature (Burns and Rigler 1967, Heinle 1969, Hernandez-Leon and Ikeda 2005).

It is reasonable to assume, however, that there are other factors which covary with increases in temperature in natural waters (Hopkinson and Smith 2005). For the case of the phytoplankton community, seasonal patterns of downwelling irradiance followed a similar pattern to the temperature distribution over the year (Figure 14), showing a summer maximum and winter minimum. Elevated levels of organic matter were also present in the warmer months (Figure 21), and while temperature has been shown to have a pronounced effect on metabolic rates in some estuaries, it is ultimately the supply of organic matter that seems to have a heavier control on rates of respiration (Pomeroy and Johannes 1968, Hopkinson and Smith 2005). Still, estuaries are dynamic ecosystems and natural biological assemblages have shown a sensitivity to sudden changes in natural water temperatures over the course of a few days (Iriarte 1996).

Biogeochemistry

The previous subsection on salinity broadly discussed the potential for allochthonous sources of carbon and nutrients to influence biological activity. As discussed, salinity is not always an accurate indicator of a specific nutrient regime, due to

multiple interactions of chemical species within the environment. In addition, even though estuaries are heavily influenced by fluvial nutrient input, there are several possible fates of this material, as well as other sources in Mississippi waters.

While phytoplankton support the heterotrophic community with autochthonous carbon and organic nutrients, heterotrophic respiration can be an important source of ammonia and phosphorous for photosynthesis through remineralization processes, particularly in times of nutrient limitation (Williams 1984). Nitrification, though a light-inhibited process, is an important microbial contributor to total pelagic respiration as well, and can serve as a source of regenerated nitrate (Iriarte 1996). Possible sources of ammonia into the Mississippi Sound include inputs from autochthonous sources, such as nitrogen fixation, as well as another allochthonous source of atmospheric deposition, which may provide as much as 14 – 18% of the total nitrogen input into the area (Castro et al. 2003, Ren 2010). Conversely, processes of anammox and denitrification can ultimately be an important sink for nitrogen in the northern Gulf of Mexico at the sediment-water interface (Gardner et al. 2010).

These nitrogen cycling processes are particularly important for Mississippi waters. Based on the relatively low DIN, high anthropogenic DIP, and low dissolved inorganic N:P ratio within the Mississippi Sound and Bight (Figure 16), the system appears to be largely nitrogen deficient (Sawant 2009, Cai et al. 2012). This potential for nitrogen limitation is ubiquitous in estuaries, but can vary over time and space (Howarth 1988). The opening of the Bonnet Carré Spillway appears to have been an event characterized by increased allochthonous input of nutrients into the coastal system, as evident from the concurrent spike in DIN and other nutrients at station BCS-8 (Figure

16). This particular event is a good case to examine as it shows how the community reacts to surges in limiting nutrients.

The increase in nutrients seemed to prompt a significant biological response at both stations, though ambient concentrations of DIN were very low at station NGI-5 and very high at station BCS-8 during this time (Figure 19). This may suggest that nitrogen uptake at station NGI-5 proceeded until there was very little substrate left, while another limiting factor may have prevented complete nitrogen uptake at station BCS-8 at the time of sampling. Phosphorous concentrations at station BCS-8 still remained relatively high during this period, with dissolved N:P ratio of 6.5, therefore phosphorous limitation was not a likely cause for the high nitrogen levels.

Light attenuation (K_d) for this sampling point, however, was elevated by a factor of 5 at station BCS-8 compared to NGI-5 (Figure 25), translating to a euphotic depth of slightly less than 1 meter at BCS-8, and approximately 5 meters at NGI-5. For the month of June, the amount of light available to facilitate the photosynthetic uptake of nutrients throughout the water column may be the limiting factor at station BCS-8. The subsequent decrease in surface primary productivity rates per unit volume, chlorophyll, DIN, and K_d(PAR) in July suggest a return to nitrogen limitation over time. Patterns of alternating light and nutrient limitation of photosynthesis has been documented in other turbid estuaries and coastal waters as well (Cloern 1987, Pennock and Sharp 1994, Smith and DeMaster 1996, Caffrey et al. 1998, Lohrenz et al. 1999).

It is also important to note that while some quantity of limiting nutrients is essential, the quality may also be important in determining ecosystem metabolism, as not all materials are utilized with equal efficiency. For example, in autotrophs, the amount of

carbon fixation per oxygen evolution (photosynthetic quotient) can be enhanced by up to 30% when utilizing ammonia as a nitrogen source as opposed to nitrate (Falkowski and Raven 2007). As mentioned previously, this is not always a straightforward assessment as the standing stock of nutrient concentrations may not reflect the supply of nutrients to the water mass due to high turnover rates and environmental interactions. Also, the very nature of estuarine variability opens up the possibility of nutrient micropatches disrupting what is assumed to be a representative sample.

Nevertheless, Figure 19 shows that at station BCS-8, ammonia dominated the DIN signal throughout the year, which may indicate high amounts of nutrient regeneration through heterotrophic activity in excess of the amount that can be taken up by phytoplankton (Williams 1984). Ammonia is taken up preferentially by phytoplankton as it does not need to be reduced before assimilation, unlike nitrate (Miller 2004). Historically, ammonia uptake dominates other forms of nitrogen assimilation at station BCS-8 (Ren 2010). Ammonia tended to dominate the DIN signal at station NGI-5 for the beginning of the year as well, but a chemical species shift to nitrate domination began to occur in June, until ammonia levels dropped to very small fraction of the DIN signal in July. This may be further evidence of nitrogen limitation at this station, as the phytoplankton utilize the ambient supply of readily assimilated nitrogen.

By July, not only did nitrate dominate, but nitrite levels were also elevated, possibly indicating the presence of nitrifying bacteria (Cauwet 2002). As a phytoplankton bloom declines (as indicated by the lower chlorophyll concentrations), and especially under nutrient limitation, extracellular release of dissolved organic nitrogen can quickly stimulate bacterial activity (Bronk 2002). After this material is remineralized into

ammonia, there can be a subsequent stimulation of nitrification (Iriarte et al. 1996). Given the already depleted supply, any new ammonia coming into the system is likely incorporated very quickly during these months, keeping ambient levels of nitrate high. Even the ammonia-dominated conditions at station BCS-8 were drawn down slightly during this month, corresponding to a decline in primary productivity possibly associated with nutrient limitation.

The specific nutritional status and physiology of organisms can be difficult to qualitatively assess on large scales, but elemental stoichiometry of phytoplankton is useful in that it essentially reflects the assimilation of nutrients into cellular material such as proteins, carbohydrates, and lipids (Beardall et al. 2001). When analyzing the elemental ratios of natural waters (Figure 22), there is likely interference with heterotrophic organisms and detritial material that may not reflect similar nutrient histories. However, analyzing how these ratios deviate from Redfield ratios can still provide useful information about community structure.

For instance, July has been proposed as a month in which some nutrient limitation occurred at both stations, and Figure 22 shows high C:P and C:N ratios, which tend to indicate growth limitation by nutrients as carbon fixation exceeds incorporation of N and P into cellular materials (Bronk 2002). The high C:N ratios persisted from May to July, further suggesting nitrogen limitation during this period. Lower C:P ratios and increasing primary productivity rates at both stations during May suggest a rapid community growth rate, as P-rich ribosomal DNA accumulates during reproduction or perhaps simply luxury P-uptake under low nitrogen conditions (Sterner and Elsner 2002). These ratios are not always predictable, and can experience some interference, such as from the presence of

large copepods, that have high C:P and N:P ratios, and are often present during bloom collapses (Sterner and Elsner 2002). In addition, C:N and N:P ratios may shift in response to limitation by other materials, including silicate, inorganic carbon, and light (Bronk 2002). Though exceptions exist in natural populations, as a general rule, it stands that growth limitation by nitrogen or phosphorous will be manifested by a high C:N or C:P ratio.

The supply of nutrients is primarily associated with influencing autotrophic activity. However, this relationship is not as clear when it comes to community respiration. Phytoplankton respiration can be elevated during times of nutrient limitation as the cell utilizes carbohydrate reserves (Geider 1992), but ultimately heterotrophic respiration is related to the total supply of organic matter (Pomeroy and Johannes 1968, Howarth 1988, Hopkinson and Smith 2005). In fact, Revilla et al. (2002) suggests that total net ecosystem production in estuaries is determined by three main factors: (1) The ratio of inorganic to organic matter, (2) the water residence time, and (3) the overall lability of the allochthonous organic matter. Caffrey (2003) observes that over several estuaries, a general trend can be deciphered in which organic rich runoff tends to favor a net heterotrophic system, while nutrient rich runoff supports net autotrophy. This is a reasonable assumption given that the terrestrial organic matter from runoff is generally carbon rich, therefore the release of nutrients associated with respiration doesn't support a proportional amount of productivity compared to the amount of carbon consumed (Kemp et al. 1997). In this way, respiration may have some periodic control on the balance determining NEP.

The passing of Tropical Storm Lee prior to the September sampling event is another good case study for how this system reacts to organic and nutrient loading that may help resolve potential biogeochemical drivers within this system. Initially, the high winds (Figure 11) from the passing of this storm likely caused some initial sediment resuspension. This organic-rich sediment re-entering the water column was essentially increasing the residence time of organics, and this has been shown to elevate heterotrophic activity in coastal zones after the passing of storms (Jensen et al. 1990, Dickey et al. 1998). On the other hand, the rain event associated with the storm (Figure 10) and the subsequent delivery of nutrients via a large volume of river water into the system (Figure 12), may be a factor driving the observed increase in surface primary productivity rates at both stations (Figure 17) and a shift to total water column net autotrophy at station BCS-8 during this month (Figure 27).

Heterotrophic-autotrophic processes are not always coupled on short temporal scales, and there may be a lag phase associated with these shifts (Blight et al. 1995). This may help explain why September is the only month in which station BCS-8 shows bottom water hypoxia (Figure 15) in spite of the net autotrophy indicated by Figure 27. The nature of an intermittent sampling regime creates some degree of uncertainty when discussing short term temporal patterns. However, other studies have shown that hypoxia can intrude into shallow waters via tides and wind patterns (Breitburg 1990, Sanford et al. 1990) and may only persist for several hours at a time (Engle et al. 1999). A moderate (5 - 6 m s^{-1}) southerly wind (Figure 11) and an incoming tide (Figure 13) may be conducive to this transport, and some small level of stratification (Δ salinity = 7.26) may suggest very different biological patterns occurring within a relatively shallow water column.

Appendix E shows that near-benthic respiration in April exceeded surface respiration by a factor of 7, indicating that the assumption of constant respiration with depth used to calculate NEP for this study may not always be valid. Clearly, while the synthesis of cellular material is ultimately dependent on carbon and nutrients, the controls on biological activity are not a strict function of biogeochemistry and may include physical factors in the system.

Photosynthetically Available Radiation

Unlike community respiration, primary productivity is driven by photons as a sole energy source. Light has no potential for storage in photosynthetic systems, and it is a highly variable constituent within the water, given its natural propensity for absorption (del Giorgio and Williams 2005). While discussions on occasional respiratory control of NEP carry some merit, Figure 24 C suggests that, primary productivity tended to have a higher control on the balance between P and R in surface waters. Light, therefore may be an important control on the autotrophic term of the NEP equation, and varies significantly with time (diel to seasonal) and space (between stations and with depth).

Relationships between primary productivity and light are not completely straightforward. While daytime production has been shown to correlate well with daily irradiance in turbid estuaries (D'Avanzo et al. 1996), the response is not linear as shown in Figure 23. On daily scales, as irradiance changes, physiological adaptations occur causing alterations of photosynthetic rates (Kirk 1994). Geider (1987) showed that in constant temperature conditions, changes in photosynthetic pigment abundance can change by a factor of 2 – 5 as a result of the daily change in irradiance. The density of these pigments, in turn, can affect electron flow associated with photosynthesis and

modify rates of production (Falkowski and Raven 2007). Given a high photon flux and minimal interference with clouds or other light absorbing properties, at some point during the day, there is usually enough light available for photosynthesis to be saturated (E_k) and changes in photosynthetic rates (α) reach some maximal peak (P_{max}).

On sunny days (Figure 23 B), when this saturation level was attained, rates reached a steady state, suggesting limitation by some other factor (D'Avanzo et al. 1996). At times, this limitation may also be a function of photoinhibition, though this is less of a problem in coastal waters where high concentrations of CDOM absorb heavily in the photosystem-damaging UV wavelengths (Kirk 1994). Figure 23 A suggests that when a photosynthetic community is adapted to higher light intensities experienced in the summer, reductions in irradiance due to cloud cover are such that maximum potential photosynthetic rates may not be attained. The changes in the light regime experienced on a day to day basis can be as high as the seasonal variability (Figure 14), and this is potential weakness in assessing ecosystem metabolism on larger time scales from single *in situ* measurements.

Nevertheless, the derived maximum photosynthetic rates appeared to elevate in response to higher light intensities throughout the year, regardless of whether or not biomass was taken into account (Figure 24 A, B). While physiological adaptation may be at work here as well, changes in seasonal community composition also have the potential to change observed rates, as some species may absorb light more efficiently than others (Falkowski and Raven 2007). However, as has been cautioned for other comparisons, many other factors have the potential to covary with light in the natural environment. Lohrenz et al. (1994) showed that for northern Gulf of Mexico waters, changes in P_{max},

E_k, and α showed some correlation to several environmental factors (temperature, salinity, nutrients, mixed layer depth, light attenuation, and PAR) that were highly variable between stations and could not be generalized.

While heterotrophic respiration has no direct dependency on light, some aspects of phytoplankton respiration do (Falkowski and Raven 2007). Given that an estimated 10 to 50% of gross photosynthesis can be remineralized as a result of phytoplankton respiration, it really should not be ignored (Geider 1992). Since respiration measurements are taken in dark bottles, a portion of light-dependent respiration, including Mehler reaction, RuBisCO reactions (photorespiration) and mitochondrial respiration, are often neglected (Weger et al. 1989, Williams and del Giogio 2005). Light-dependent respiration rates have been observed to change in response to a forced variable light regime (Falkowski and Owens 1978, Beardall et al. 1994). In these studies, a hysteresis is observed when cells are moved from increasing to decreasing light, and is described as enhanced post-illumination respiration (EPIR). Falkowski et al. (1985) postulated that the effects of EPIR are likely due to light creating an increased pool of photosynthate, which leads to an increase in availability of respiratory substrates. The presence of EPIR may help explain the immediate drop in oxygen concentrations seen with *in situ* incubations following periodic perturbations of natural light on cloudy days (Figure 23 A).

However, the described patterns of hysteresis (3 – 4 minutes of enhanced respiration) are also observed immediately following the removal of light from *in situ* and lab incubations under a slow-changing or constant light field (Figure 1, Appendix E, F). In other words, unlike the EPIR experiments, the incubator was not pulsed with a high photon flux prior to the respiration measurement. Weger et al. (1989) monitored gas

exchange for a *Thalassiosira weisflogii* culture using mass spectrometry and also found some enhanced respiration for five minutes following the removal of a *constant* light source from incubations. As an added test, Weger et al. (1989) added DCMU to inhibit non-cyclic electron flow, and thereby negating any contribution of the Mehler reaction or photorespiration to oxygen consumption processes. They concluded that neither of these light-dependent reactions were responsible, and that the hysteresis was a direct result of mitochondrial respiration. As mitochondrial respiration is an enzymatic reaction, this may explain why *in situ* enhanced respiration is primarily observed in warmer months (Appendix F). Furthermore, Weger et al. (1989) suggested that the short-term nature of P-E measurements would not likely account for some of these respiratory losses, leading to possible overestimates of net productivity if extrapolated over the course of a photoperiod. This may account for the difference in observed P_{max} between the ^{14}C and *in situ* derived P-E curves (Figure 23 C).

Light Attenuation (K_d)

Thus far, it has been shown that many factors have the potential to affect the balance between primary productivity and respiration in natural environments. Of all these factors, none shows more of an extreme variation with depth than light. Several factors induce the diffuse attenuation of light including chlorophyll, CDOM, minerals, living cell bodies, and detrital material (Kirk 1994). While the spatial and temporal variation of K_d is discussed in the following section, it is adequate to say that its distribution varies in response to the type of material present in the water, which may in turn, affect the potential for transfer of photons into the biota through photosynthesis.

Respiration occurs throughout the entire water column and primary productivity is only confined to the euphotic depth, leading some to conclude that estuaries are generally net sources carbon as the high turbidity causes integrated heterotrophic processes to exceed autotrophic ones (Revilla et al 2002, Caffrey 2003). While this generally stands true, the type of material present can make this relationship less clear. For instance, chlorophyll absorption can lead to high levels of light attenuation, and while biomass can accumulate to levels of self-shading, high concentrations of living cells may also increase the amount of autotrophic activity in the water. High levels of suspended particulate matter, which is a large component of the K_d signal in the study area (Figure 35), act to scatter light instead of absorb it, which effectively increases its total path length and increases the probability of light absorption by phytoplankton (Kirk 1992).

As light continues to attenuate with depth, its spectral composition is also modified. While the shorter wavelengths of blue light tend to penetrate deepest in open ocean waters, high concentrations of CDOM close to shore tend to absorb blue light. In addition, SPM backscatters and phytoplankton absorb the red wavelengths, potentially leaving bottom waters to dominate in green light (Kirk 1992). The phytoplankton community may adapt to changes in spectral quality by utilizing pigments such as carotenoids that can absorb the available quality of light (Kirk 1992). When little light is present, such as the case in highly turbid waters, cells may also adapt and achieve a higher photosynthetic rate per unit biomass by increasing pigment concentrations, accompanied by a reduction in respiration rates (Kirk 1994, Falkowski and Raven 2007). While changes in chlorophyll throughout the water column were accounted for in the

depth-integrated estimates of NEP, many of the afore mentioned adaptations are more difficult to quantify, and can change based on species composition and nutritional status.

Regardless of the amount of biomass present however, the depth of the euphotic zone can still play an important role in determining NEP. Cloern (1987) suggests that phytoplankton dynamics are heavily controlled by light availability in estuaries and that whenever the euphotic depth is less than 20% of the total water column depth, the water will be net heterotrophic. Figure 26 shows that the ratio of Z_{eu}:Z never reached this threshold even in the highly turbid summer. However, Figure 27 shows the dominance of net heterotrophy at both stations for most of the year. The degree of net heterotrophy does appear to be loosely linked to Z_{eu}:Z during the warmer months, with more turbid months equating to less autotrophy in the water column.

At station BCS-8, the deepening of the euphotic zone to the benthic layer in September may have pushed the balance towards a net autotrophic system. In August, however, the shift towards slight autotrophy may have had more to do with a spike in ambient nutrient concentrations, as light attenuation remained relatively high. While depth-integrated gross primary productivity rates at station NGI-5 exceeded those at station BCS-8, likely due to the presence of a deeper euphotic zone, light attenuation was such that the photons never reached the benthic layer in warmer months, and primary productivity was not high enough to surpass the amount of water column respiration in any month that was calculated. This relationship between light attenuation and K_d is not as clear in all months, especially during colder periods, and may suggest a seasonal shift in the trophic mechanism determining NEP.

Model and Regional Comparisons

Cole and Cloern (1987) showed that, among several estuaries, the daily productivity could be defined as a proportional function of:

$$B_c E_d^{0+}/K_d(PAR),$$

where B_c = chlorophyll concentration, E_d^{0+} is daily integrated irradiance, and $K_d(PAR)$ is the light attenuation coefficient over PAR. Put simply, the equation takes the ratio of phytoplankton absorption (assumed to be proportional to chlorophyll concentration) to total absorption (assumed to be proportional to $K_d PAR$) in order to estimate the amount of light absorbed by phytoplankton over the course of a photoperiod, E_d^{0+} (Kirk 1994). A comparison between the computed and measured rates shown in Figure 42 demonstrates that these assumptions hold some merit across different estuaries, however the model is not intended to compute absolute values of primary productivity.

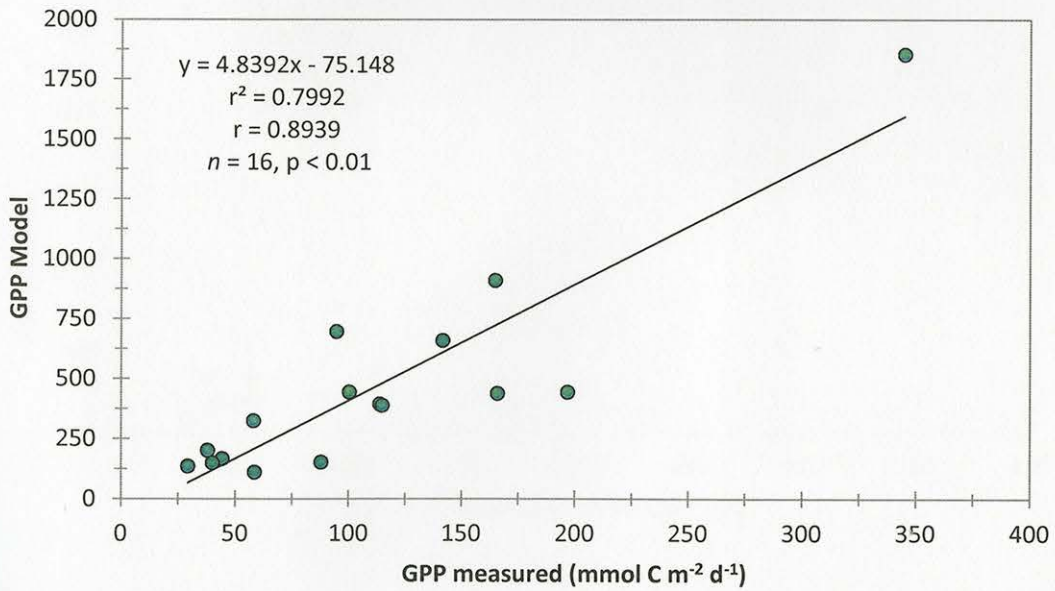

Figure 42. Comparison between depth- and time-integrated gross primary productivity calculated from *in situ* derived rates and the equation of Cole and Cloern (1987).

Behrenfeld and Falkowski (1997) propose a complete depth-integrated model of primary productivity:

$$\Sigma PP = C_{surf} \times Z_{eu} \times P^{b}_{opt} \times DL \times f(E_0)$$

where C_{surf} = surface chlorophyll concentration (mg Chl-a m^{-3}), Z_{eu} = euphotic depth (m), P^{b}_{opt} = maximum chlorophyll specific C-fixation rate (mg C [mg chl]$^{-1}$ h^{-1}), DL = daylength (h d^{-1}), and $f(E_0)$ = irradiance dependent function (unitless). The parameters C_{surf}, Z_{eu}, and DL were put into the model using collected data, while P^{b}_{opt} and $f(E_0)$ were derived from observed empirical relationships to temperature and light, respectively. A comparison between the computed and measured rates shown in Figure 43 demonstrates that this model correlates well to observed rates, but is slightly overestimated, likely due to the lack of variables accounting for light and nutrient limitation.

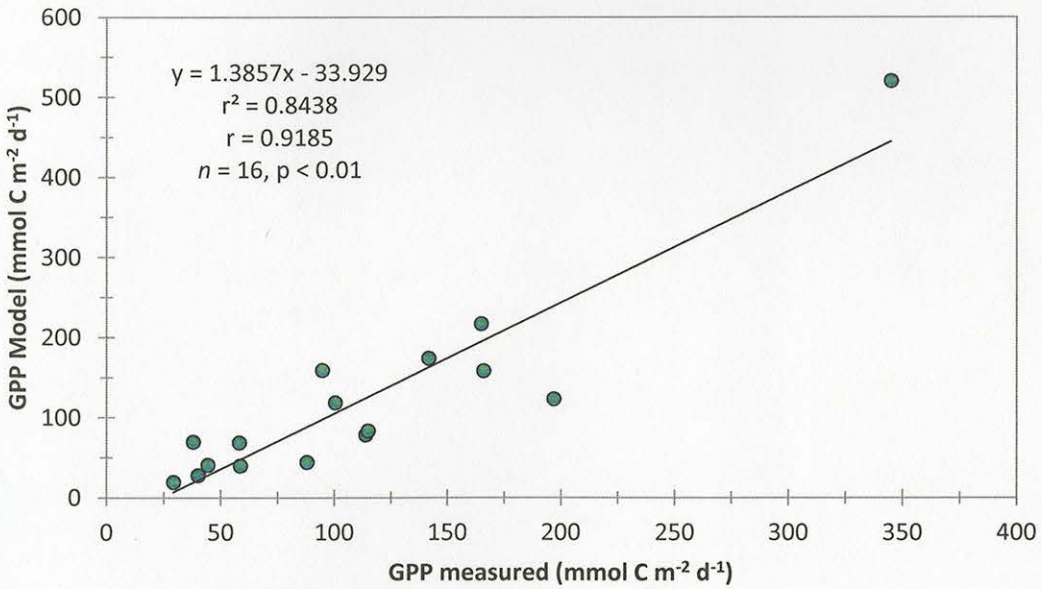

Figure 43. Comparison between depth- and time-integrated gross primary productivity calculated from *in situ* derived rates and the equation of Behrenfeld and Falkowski (1997).

Many of the assumptions made in order to calculate NEP may not be accurate, such as the assumption of constant respiration with depth and time, as well as the assumptions of predictable changes in P_b with depth. Nevertheless, these estimates enable some assessment of trophic status for a particular body of water, and comparisons across several study areas can help characterize regional trends. Table 8 demonstrates the variability in primary productivity and respiration estimates across the Northern Gulf.

Table 8

Daily Estimates of Water Column Primary Productivity and Respiration for Several Northern Gulf of Mexico Estuaries.

Author	Region	PP (mmol C m^{-2} d^{-1})	RESP (mmol C m^{-2} d^{-1})
Lohrenz et al. (1990)	MS River Plume	75	N/A
Redalje et al. (1994)	LA Continental Shelf	10 – 725	N/A
Biddanda et al. (1994)	LA Continental Shelf	N/A	60.3 – 120
Caffrey (2004)	Apalachicola Bay, FL	87 ± 6	137 ± 9
Kiene et al. (unpub.)	Mobile Bay, AL	65 ± 40*	64 ± 37*
Mortazavi et al. (2012)	Weeks Bay, AL	146	206
Vandermeulen (2012)	MS Sound	101 ± 62	117 ± 57
Vandermeulen (2012)	MS Bight	130 ± 108	209 ± 148

*Values estimated from presentation figure.

Table 8 demonstrates that the determining factors of NEP in the Northern Gulf are variable, and are as heterogeneous in time and space as the biogeochemistry of estuaries. It is important to consider that a negative NEP value (NetPP < RESP) does not indicate that no organic matter is available for higher trophic levels, as evidenced by estuaries being highly productive fishery areas. The system is open, and exchange of products originating from primary productivity have potential for storage in the sediment, or export to other water bodies before it is ultimately utilized (del Giorgio and Williams 2005).

Analysis of Hypothesis II

The spatial-temporal variability of light attenuation (K_d) measurements can be correlated and partitioned to laboratory-derived measurements of CDOM, SPM, and chlorophyll.

As previously mentioned, the attenuation of light with depth can be modeled as a function of the Beer-Lambert Law, whereby the exponential decay of light can be described by the term K_d. This assumption of exponential decay was designed for monochromatic light and holds true under such conditions. Figure 44 shows that different wavelengths have varying attenuation coefficients (i.e. red light attenuates faster than blue light). Therefore, integrations over PAR can potentially show a change in the value of K_d with depth due to the uneven absorption spectra. In other words, K_d(PAR) is not monochromatic and may not obey the Beer-Lambert Law.

Figure 44 would indicate that integrating across several wavelengths would make K_d(PAR) decrease with depth, as the red wavelengths are attenuated more quickly and become impoverished compared to other wavelengths (Kirk 1994). However, scattering

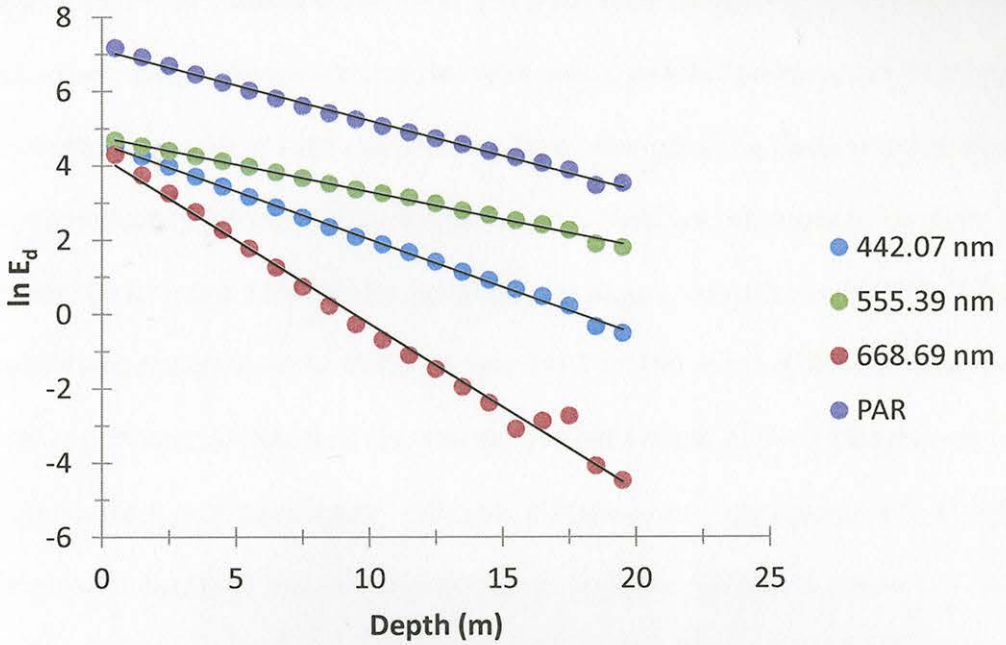

Figure 44. Natural log transformation of downwelling irradiance as a function of depth for three wavelengths of light, and integrated PAR. Measured *in situ* with a hyperspectral LI-COR downwelling irradiance sensor in the Gulf of Maine, July 19, 2011 (Arellano et al. 2011).

causes the downward flux of light to become more diffuse (less vertical), thereby increasing attenuation with depth and counteracting the effects of integrating over a wide spectral bandwidth (Kirk 1994). While the assumption of K_d(PAR) obeying the Beer-Lambert Law has come under criticism, Figure 44 shows that it generally conforms well to a constant exponential decrease so long as there are not any major discontinuities in the water, such as nepheloid layers, subsurface chlorophyll-a maxima, or humic-stained surface layers (Gallegos and Moore 2000). However, both chlorophyll-a maxima and CDOM-rich stratified layers are a common feature of estuarine environments.

Other optical challenges can potentially bias measurements of K_d(PAR) in the natural environment. Wave focusing and de-focusing near the surface can create an oscillation between high and low pulses of radiation which can intensify variability in

readings (Kirk 1994). Sudden cloud cover can also create changes in underwater light field, however, these changes are constant with depth, and this problem can be overcome by monitoring the incident light above the surface when profiling. Some error is also possibly introduced by sampling in proximity to the boat, but this tends to be more problematic on overcast days and for upwelling irradiance measurements (Kirk 1994). The wavelength response of the HOBO sensor (450 – 1100 nm at >50% response level) is also of importance, as absorption/scattering of light outside of the PAR range by optical parameters may significantly influence the perceived light attenuation. Therefore, it is not actually K_d(PAR) that is being measured, though a significant amount of the near IR wavelengths should not penetrate very deeply into the water column and will likely have a negligible influence on attenuation with depth. It is important to realize the limitations of field measurements of K_d(PAR), but it still remains a useful parameter for optically characterizing a given area. Certainly, from a water management perspective, *in situ* profiles of light are much more practical than Monte Carlo simulations of the Radiative Transfer Equation for those who are not well versed in applied mathematics.

Besides existing as a practical parameter in calculating primary productivity with depth, the diffuse attenuation coefficient is also useful when partitioned into its respective components:

$$K_d(PAR) = K_w[Water] + K_p[Phyto] + K_s[SPM] + K_o[CDOM]$$

The partitioning of K_d(PAR) enables the relative weight of each fraction to be examined, and can help resolve the controlling factors of light attenuation. This often requires some assumptions that do not always hold true, but are justified given the natural variability of the contributing optical properties in natural waters as well as the variability in

measurements of these properties (Gallegos and Moore 2000). One of these assumptions is that phytoplankton, SPM, and CDOM are a linear expression of K_d(PAR), but Figure 33 demonstrates that this is not necessarily the case. The possible reasons for this non-linearity will be discussed on an individual basis (below), but overall may be a large function of the integration over a wide range of wavelengths (Gallegos 2001).

The calculated multiple regression model (Figure 34) showed a relatively linear trend, and a moderately high correlation coefficient ($r^2 = 0.863$). This model tended to slightly underestimate higher values of K_d(PAR), and slightly overestimate the lower values. This same trend was apparent in other studies that performed linear interpolations of K_d(PAR) partitioning (Gallegos 2001, Christian and Sheng 2003). Gallegos (2001) suggests that this deviation is likely the result of the failure for K_d(PAR) to obey the Beer-Lambert Law, but noted that the good agreement with more mechanistic simulations of the radiative transfer theory offers some validity to the relative accuracy of the simplified methodology. While they are only estimations, what follows is a discussion of the contribution of each individual component to K_d(PAR).

Pure water is an absorbing component that contributes to the natural attenuation of light and it is usually regarded as a constant across several bodies of water (Kirk 1994). A commonly accepted value of K_w is that measured by Lorenzen (1972), who estimated the pure seawater attenuation coefficient to be 0.038 m^{-1}. Water absorption is generally considered negligible at wavelengths below 500 nm, but can become very significant in the red region. Kirk (1994) reports that in a theoretical pure water bath, about 35% of the incident light at 685 nm will be absorbed within the first meter. Thus, the attenuation due to water varies with the depth of the water column (Morel 1988).

Gallegos (1994) uses a model to predict K_w, and finds attenuation to be more significant at the surface, with values of 0.16 to 0.13 m^{-1} at 1 and 3 meters, respectively. As a general rule, the attenuation of water should be represented by the intercept of the regression between K_d(PAR) and the concentrations of the contributing water quality parameters (Gallegos and Moore 2000). The intercept values shown in Figure 33 range from 0.2 – 0.8 m^{-1}, and do not likely reflect realistic values of K_w, but instead are an artifact of variance and using a linear regression to describe a non-linear relationship. Values of K_w are considered constant for this study, and were not included in the partitioning.

Phytoplankton contribute to both the scattering and absorption of light. The absorption spectra from chlorophyll-a, which is common to all phytoplankton, has two peaks at approximately 430 nm and 675 nm (Miller 2004). The spectral signature of a phytoplankton population will vary with pigment composition, which in turn, varies with species diversity, light intensity (i.e. depth), spectral distribution, and nutrient concentrations (Kirk 1994). Since K_d is integrated over PAR, however, the relative weight of K_p to K_d(PAR) becomes dependent on more than just total concentration of pigments as other materials in the water may also absorb at similar wavelengths (Gallegos and Moore 2000).

It may be little surprise then that on average, chlorophyll concentrations contributed the smallest amount to K_d(PAR) in Mississippi waters as shown in Table 7. Figure 35 shows that K_p tended to increase as the sampling transect moved further into the Mississippi Bight, which was likely a result of the reduced contribution of K_s, as chlorophyll concentrations (Figure 30) and K_d(PAR) (Figure 31) generally decreased in

the Bight. Temporally, K_p tended to increase (Figure 35) in accordance with observed chlorophyll concentrations (Figure 29) in the Mississippi Bight. This was again, likely due to the reduced influence of K_s, because the Mississippi Sound shows some disconnect between ambient chlorophyll concentrations and K_p. The Mississippi Sound is dominated by PIM from spring to June, and it isn't until July, when SPM concentrations decline and shifts to POM dominance that K_p increases. This disparity shows the difference between two environments, and demonstrates the greater significance of fluvial inputs to biogeochemistry in the Mississippi Sound compared to the Mississippi Bight.

Figure 33 shows an extremely variable relationship between K_d(PAR) and higher chlorophyll-a concentrations. Xu et al. (2005) suggests that in very turbid waters, higher values of K_d(PAR) may give rise to some limitation of primary productivity, and in some cases, a negative slope between K_d(PAR) and chlorophyll-a may arise. It is difficult to assess this from Figure 33, but it is notable that the station with highest light attenuation (BCS-3, Figure 30) also has reduced chlorophyll-a concentrations (Figure 31) in comparison to many other stations in the Mississippi Sound. However, this may also be a function of dilution as station BCS-3 is just outside of the Pearl River outflow. Wofsy (1983) showed that this inverse correlation that inhibits primary productivity generally occurs at concentrations of SPM greater than 50 mg/L, but this was seldom reached in this study (Figure 33). Peterson and Festa (1984) on the other hand, showed decreases in primary productivity associated with SPM loads between 10 – 100 mg/L, illustrating the truly unique nature of biological responses within different estuaries.

Suspended particulate matter consists of an organic (POM) and inorganic (PIM) fraction that are optically distinct. The PIM fraction is made up of inorganic mineral particles either resuspended or delivered through rivers, and tends to scatter light much more strongly than it absorbs. As previously mentioned, this can increase the pathlength of a photon in water, and contribute to a more diffuse underwater light regime and increasing the chance of absorption (Kirk 1992). The POM fraction can be a substantial portion of total SPM, and is made up of detritus, humic materials bound to mineral particles, zooplankton biomass, or living phytoplankton cells (Kirk 1994). The sum total of SPM absorbs strongly in the blue region, with a negative exponential decay into the red wavelengths.

The model used to predict K_d(PAR) in this study uses the total SPM fraction. Though the presence of phytoplankton cells is redundant, the contribution of detrital matter and colored humic particulates should not be neglected in estuarine regions. This study shows that K_s consistently contributed the largest amount to K_d(PAR) in Mississippi waters over the duration of the study period (Table 7). Concentrations of SPM decreased with increasing salinity (Figure 32) in a slightly non-linear trend, as does the PIM fraction, while the POM fraction decreases more linearly. The PIM fraction is composed of clay-like minerals emerging from the rivers, and is likely flocculating and settling as it mixes with salt water, leading to the non-linear decay. The higher correlation between the PIM and K_d(PAR) suggests that the highly scattering PIM fraction tends to contribute more to K_s than POM (Figure 33). Thus, with an increasing fraction of POM dominating K_s into the Mississippi Bight (Figure 31), there is a concurrent increase in the relative attenuation by both K_p and K_o (Figure 35).

Xu et al. (2005) suggest that the disparity between modeled and measured K_d(PAR) may be a function of substrate variability in SPM dominated estuaries. The size, composition, and geometric shape of SPM all potentially modify its optical properties, and these properties are likely as highly variable in time and space as the concentration itself. In an estuary influenced by several different sources of allochthonous input, such as the Mississippi coastal region, it can be expected that no two samples of SPM look alike. Gallegos and Moore (2000) found that for a SPM dominated estuary, the highest attenuation was found at the times and locations of highest river flow. The K_d(PAR) and SPM values in this study were highest at the stations closest to fluvial inputs (BCS-3, BCS-2, Figures 3.21, 3.22), but the temporal variability is not as straightforward. Input from various unquantified sources (i.e. Bonnet Carré Spillway) and the possible dilution effect of heavy outflow associated with Tropical Storm Lee may have created a divergence from such a predicted outcome.

The CDOM fraction can be a substantial contributor to light absorption, and does not contribute to much scattering of light (Bricaud et al. 1981). But CDOM is a rather complicated combination of substances, consisting of high-molecular weight compounds including humic and fulvic acids, respiration byproducts, and many uncharacterized compounds (del Castillo 2005). The absorption spectra follows a similar pattern to that of SPM, with negligible amount of absorption present at red wavelengths, and an exponential increase in absorption into the blue/UV wavelengths (Kirk 1994). The CDOM distribution is influenced by several environmental factors, including freshwater input, mixing, flocculation/particle aggregation, photodegradation, bacterial degradation, resuspension, and biological production (Branco and Kremer 2005, del Castillo 2005).

These factors all have the potential to not only introduce or remove CDOM from the environment, but to modify its optical properties (i.e. K_o) as well (del Castillo 2005). Thus, a substance commonly described as conservative within estuaries has the potential to display a highly variable distribution.

For this data set, a high degree of variability in concentration was apparent in the lower salinity ranges (Figure 32), where the majority of mixing was taking place, but tended to converge along a linear trend of decreasing concentrations with increasing salinity. The data shows that the stations with the highest average concentration of CDOM tended to have the highest amount of variability as well (Figure 31). Del Castillo (2005) notes that a significant amount of the removal processes occur as CDOM is introduced to salt water, though processes like photodegradation may not be as important for removal until more light is available throughout the entire water column. Even with this removal, however, the temporal changes in CDOM concentrations tend to correlate with changes in salinity. A comparison of Figures 3.6 and 3.20 reveals concurrent CDOM spikes/salinity lows throughout the year, but these events are also characterized by a high degree of spatial variability, likely due to uneven mixing during heavy rain and river discharge periods.

Besides the concentration of CDOM, information about its optical properties can be examined using the slope of the exponential line from the absorption spectra (del Castillo 2005). Carder et al. (1989) found that changes in the spectral slope (*S*) of absorption curves were related to changes in the chemical properties of CDOM, more specifically the proportion of Humic to Fulvic acids. These changes in the spectral slope affect K_o, as a steeper slope is equated to more absorption of blue light at similar

concentrations. For this study, a non-linear fit method was compared to the least square regression of λ vs. ln $a(\lambda)$ over several wavelength ranges, and the greatest agreement between the two methods was found in the 350 – 500 nm range. The spectral slope remained relatively consistent throughout the year, however some deviation was experienced in May/June, which is likely due to the impact of the Bonnet Carré Spillway opening (Figure 29). The drop in *S* indicates a higher concentration of humic acids in the water, which are of higher molecular weight (i.e. more complex), and this would be expected from a large river system (Carder et al. 1989, Blough and del Vecchio 2002).

The contribution of K_o to K_d(PAR) was intermediate throughout the year compared to K_p and K_s (Table 7). As is the case for K_p, the increasing contribution of K_o to K_d(PAR) in the Mississippi Bight is likely a function of K_s removal. Often, even with increasing inputs of CDOM, there were concurrent increases of SPM, which dominated the signal (Figure 29). Some significant rain/flushing events, however, may essentially dilute out particulates and retain the dissolved portion, as indicated by the increase of K_o during July and September at both stations (Figure 35).

As with the other constituents contributing to K_d(PAR), both the ambient concentration and the spectral quality of CDOM play a role in determining K_o. Given this trend among all contributing parameters to K_d(PAR), it holds that some of the differences between the modeled and measured K_d is due to the variable distribution of input parameters in time and space. This variability is not unique to Mississippi estuaries, so the derived model in this study should not be applied to other estuaries.

Analysis of Hypothesis III

Satellite (MODIS) derived estimates of biologically significant parameters (chlorophyll, SPM, CDOM, K_d(PAR), Z_{eu}, and PAR) can be validated with ground measurements and used to calculate regional primary productivity.

The large variation of these optically active water constituents and the potential effect on ecosystem dynamics has been discussed in previous sections. However, in addition to affecting biology, these parameters add a layer of complexity to satellite ocean color monitoring. Though they are sometimes considered a nuisance to biologists, these and other parameters are still useful in monitoring biogeochemical processes and water quality in coastal areas. This section examines the relationships between some common established algorithms used for Case 2 waters, and assesses the possibility of extrapolating rudimentary primary productivity models over a larger geographic area.

As is often the case for turbid waters, none of the chlorophyll-a products available through MODIS processing produced very promising results for this study (Figure 36). The standard chlor_a product empirically derives chlorophyll-a using the band ratio between 443, 488, and 551 nm (O'Reilly et al. 2000). This derivation works well in open ocean waters but usually breaks down in coastal regions due to the elevated absorption influence of riverine CDOM that does not covary with chlorophyll (del Castillo 2005). Fluorescence line height (flh) essentially measures the relative increase of water leaving radiance at the chlorophyll fluorescence band (678 nm) in comparison to the two bands (667 nm, 748 nm) around it (Abbott and Letelier 1999). However, in coastal waters characterized by high turbidity, scattering from suspended solids dominates the red portion of the reflectance spectra (Miller and McKee 2004), which may essentially dilute

the already weak signal from fluorescence. In addition, the relationship between chlorophyll and fluorescence is not always linear, and can change with species composition, nutrient concentrations, light intensity, and any other factor that influences phytoplankton physiology (Behrenfeld et al. 2009).

Since band-ratios in the blue reflectance spectra do not work in turbid waters, Dall'Olmo et al. (2005) suggested the use of the red and near-infrared (NIR) bands to predict chlorophyll. He found that the band ratio of $R_{rs}748/R_{rs}667$ showed a good correlation to observed chlorophyll measurements ($r^2 = 0.96$) in several turbid sandpit lakes and reservoirs. The results were promising, but were based on simulations of remote sensing reflectance based on *in situ* hyperspectral data, and not actual MODIS data. In addition, this operates on the assumption that absorption in the red to NIR is dominated by phytoplankton only. As previously mentioned, the low signal to noise ratio caused by the reflectance of red from suspended particulates could be the cause of some deviation from this relationship. It should also be noted that the number of pixels passing the quality control standards was dramatically decreased when using the NIR band.

The absorption property of water at various wavelengths is another proxy for chlorophyll-a, and potentially other pigments as well. Lee et al. (2002) developed a quasi analytical algorithm (QAA), which uses the relationship between R_{rs} and IOPs (from radiative transfer equations) to derive total absorption (a) and backscattering (b_b) coefficients in the visible wavelengths. This can be further partitioned to derive phytoplankton (a_{ph}) absorption coefficients by essentially subtracting the amount of absorption by water (a_w) and detritus/gelbstoff (a_g) from the total a. In order to accomplish this, a_g must first be semi-analytically derived, which requires some

information about the absorption characteristics of phytoplankton, more specifically the ratio of $a_{ph}(410)/a_{ph}(440)$ as an input parameter. This ratio is empirically derived from remote sensing reflectance at 440 and 555 nm, which in Mississippi waters, is likely influenced by very high CDOM and detrital absorption. This may be the primary source of error, as these QAA algorithms tend to work very well for coastal waters (Lee and Carder 2004). While the QAA-derived values compared better to chlorophyll-a measurements than any other approach, there was still no robust correlation (Figure 36). In addition, there was little relation between a_{ph} and chlorophyll in the red or blue bands, where phytoplankton absorption dominates. For Mississippi waters, the highest correlation was in the wavelength (531 nm) with less interference from other optically active constituents.

Measurements of suspended particulate matter (SPM) concentrations correlated well with remote sensing reflectance at several wavelengths (Figure 37). Miller and McKee (2004) found a high correlation ($r^2 = 0.89$) between SPM and the MODIS high resolution 250-m band 1 (620 – 670 nm) in northern Gulf of Mexico waters, using data from the Terra satellite. This study used only Aqua data, and found a correlation of $r^2 = 0.82$. A comparison between SPM and the lower resolution 1 km band 13 (662 – 672 nm) showed a higher correlation ($r^2 = 0.86$). Figure 45 demonstrates the advantage of using high resolution bands, even if the correlation is slightly lower. However, the higher spatial resolution (250 m) also has a lower spectral resolution (i.e. larger bandwidth), which may account for the increased variability. The highest correlation was present in the NIR 1 km band 15 (743 – 753 nm, $r^2 = 0.914$, Figure 37), but the data return was minimized significantly compared to visible bands, and may not be as useful.

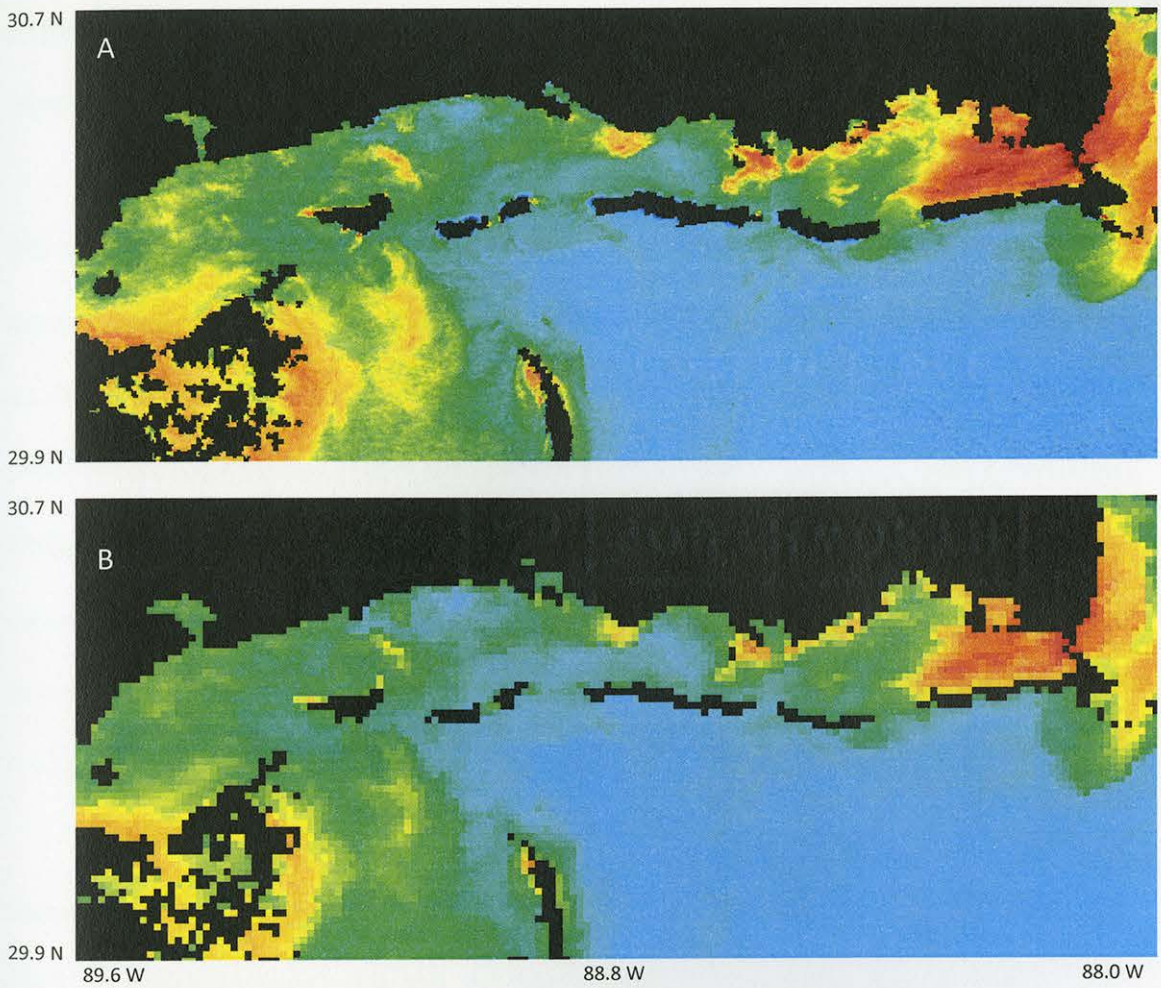

Figure 45. Comparison between MODIS Aqua (A) high resolution 250 m band 1 (620 – 670 nm) and (B) lower resolution 1 km band 13 (662 – 772 nm) from October 3, 2011.

The presence of suspended particulate matter essentially increases the backscattering coefficient relative to the absorption coefficient, and this effect is amplified in regions of the spectrum where there is lower absorption (Kirk 1994). As discussed previously, organic detrital particles absorb mostly in the blue region, and therefore backscatter more in the red regions, explaining the high correlation between SPM and R_{rs} in these regions (Miller and McKee 2004). Unfortunately, SPM algorithms and relationships are most likely to be locality specific, as the scattering efficiency of

suspended particles per unit weight is a function of size, which can be extremely variable from estuary to estuary (Kirk 1994).

The CDOM absorption varied over a wide range ($a_{CDOM}412 = 0.25 – 4\ m^{-1}$) for this study area (Figure 38). In other nearby studies, different band ratios of remote sensing reflectance have been suggested to correlate with varying ranges of absorption coefficients. Del Castillo (2005) measured $a_{CDOM}412$ in the Mississippi River plume (absorption range [$a_{CDOM}412$] = $0.8 – 1.4\ m^{-1}$) and found an empirical linear relationship to $R_{rs}510/R_{rs}670$ ($R^2 = 0.93$). D'Sa and Miller (2003) also looked at $a_{CDOM}412$ (absorption range [$a_{CDOM}440$] = $0.01 – 0.4\ m^{-1}$) in the Mississippi River plume during low flow conditions and found an empirical power law relationship to $R_{rs}412/R_{rs}510$ ($r^2 = 0.83$), $R_{rs}443/R_{rs}510$ ($r^2 = 0.86$), and $R_{rs}510/R_{rs}555$ ($r^2 = 0.80$).

The blue-green band ratios (not shown) did not correlate well for Mississippi estuarine waters, possibly due to the influence of pigments contributing to the signal in the blue, which do not covary with CDOM in estuaries. The green to red ratios (R_{rs}_531/R_{rs}_667 and R_{rs}_547/R_{rs}_667) tended to work better over the wide range of a_{CDOM} in the Mississippi Sound and Mississippi Bight, showing a power law relationship and a fairly robust correlation ($r^2 = 0.82 – 0.85$, Figure 38). Using this ratio, the green portion of the spectrum still shows some significant absorption by CDOM but a reduced contribution of chlorophyll and accessory pigments (Del Castillo 2005). Some of the observed variability may be explained by the effect of longer wavelengths also exhibiting absorption by particles. However, these particles likely covary better with CDOM in near coastal and estuarine regions. Taking the inverse of the green to red ratio produced a linear relationship with a_{CDOM}, and a slightly higher correlation ($r^2 = 0.86 – 0.88$, Figure

38). The QAA model for detrital/gelbstoff absorption (Lee et al. 2002) was also compared at all visible bands (not shown) and found to display no useful correlation to CDOM, likely as a result of the model not partitioning the absorption by non-algal particles and assuming a S_{CDOM} of 0.015 nm^{-1}(average in MS waters = 0.017 nm^{-1}).

Comparisons between satellite and ground measurements of K_d(PAR) showed mixed results for the turbid Mississippi waters (Figure 39). The empirical model of Morel (1988) shows a weak correlation ($r^2 = 0.5227$). This model essentially estimates chlorophyll-a concentrations from the blue/green ratio of R_{rs}, and uses the relationship between K_d and chlorophyll-a to estimate $K_d(\lambda)$. This algorithm is more appropriate for Case 1 waters, where chlorophyll is the largest contributor to the K_d signal. As shown before, the blue/green ratio approach to detecting chlorophyll breaks down in Case 2 waters due to CDOM and detrital influence. The Kd_490 algorithm works in a similar manner, but derives $K_d(\lambda)$ from an direct empirical relationship with the blue/green ratio of R_{rs} (Austin and Petzold 1986). This suffers from the same problems in case 2 waters as the Morel model, as shown from the low correlation ($r^2 = 0.4994$, Figure 39).

The QAA model of Lee et al. (2005a) showed a remarkable correlation ($r^2 = 0.9079$, Figure 39). This model uses reliably derived values of a and b_b from remote sensing reflectance, and relationships based on applications of the radiative transfer equation to derive information about the downwelling light field (i.e. changes in model input parameters as a function of solar altitude and depth), and subsequently calculate K_d. The reason for the success of this model in turbid waters is likely due to the fact that the algorithm is not directly dependent on the variable and uncertain estimation of biogeochemistry over discreet wavelengths, which contain little information about optical

behavior in water. Instead, the sum influence of these parameters on IOPs (a and b_b) is used, which have a predictable contribution to K_d so long as the underwater light field is characterized properly (Sathyendranath and Platt 1988). This model works well, but is also dependent on accurate retrievals of R_{rs} (Lee et al. 2005b).

Realistically, a and b_b, and thus K_d, have potential to change with depth in stratified systems. The majority (90%) of the water leaving radiance detected by satellite comes from the first optical depth, which is the 37% light level, or $1/K_d$ (Kirk 1994). In a heavily stratified coastal system, the depth of the mixed layer in relation to the optical depth may potentially influence the satellite signal and thus make any direct water column measurement of K_d(PAR) uncertain at times. Another possible source of uncertainty is in the initial estimation of a and b_b from R_{rs}. Total absorption and backscattering were not considered as part of this study for comparison, therefore the assessment of this uncertainty is purely speculative. Some uncertainty is also present in the field measurement from the derivation of K_d(PAR) from a sensor that integrates beyond the PAR wavelengths. While the correlation between the HOBO and LI-COR PAR sensor is substantial (Appendix B), it has been discussed previously that the nature of the underwater light attenuation over differing wavelengths can vary considerably. Finally, the amplified effect of wave focusing near the surface may produce erroneously higher K_d(PAR) values. These factors may account for the apparent offset between the ground measured and satellite-derived values seen in Figure 39.

The QAA model of K_d is subsequently used to estimate the euphotic depth (Z_{eu}) as described by Lee et al. (2007). While there is a good correlation between the *in situ* K_d and that derived from R_{rs}, the apparent satellite algorithm overestimation of Z_{eu} is

difficult to assess (Figure 40). Figure 39 shows a slight underestimation of measured K_d(PAR) from the QAA, which may be further perpetuated upon input into the Z_{eu} model. In addition, the Z_{eu} model inputs a(490) and b_b(490) to derive K_d, will also lead to a lower K_d value compared to K_d(PAR) due to the uneven spectral attenuation (Kirk 1994). Figure 40 also shows a comparison between measured Z_{eu} and that derived by the Z_{eu} model of Morel (Morel and Berthon 1989). Much like the corresponding K_d model, this derivation is based on an empirical relationship with chlorophyll, which breaks down in turbid Case 2 waters.

Daily PAR corresponded well with measured PAR readings from the stationary LI-COR sensor (Figure 41). Estimations and associated uncertainties of PAR have less to do with ocean color, and more to do with proper atmospheric correction (Van Laake and Sanchez-Azofeifa 2005). The components that induce the scattering and absorption of light in the atmosphere include Rayleigh scattering, ozone, gases, water vapor, and aerosols (Gregg and Carder 1990). For a given area, the instantaneous PAR reading is obtained after the atmospheric component correction, and subsequently extrapolated over the course of the day using an adjusted sinusoidal interpolation method or a look up table (Wang et al. 2010). Given the variability of PAR measured in the Mississippi Sound and Mississippi Bight (Appendix C), the satellite derivation of PAR and subsequent mapping to a localized coordinate system works well for the area. While this study presents a relatively small sample of data points for comparison, other studies have shown an average absolute error of 5-15% between satellite and *in situ* derived PAR (Gregg and Carder 1990, Van Laake and Sanchez-Azofeifa 2005, Wang et al. 2010).

Summary

This study describes the spatial and temporal distribution of Net Ecosystem Productivity in relation to the optical and biogeochemical variability for the study area. For this data set, there is some evidence of seasonal variability in autotrophic activity through changes in the light regime and nitrogen dynamics, while the stimulation of heterotrophy can be linked to external biogeochemical influences as well as from within the system. Physical factors such as temperature may play an important role in regulating metabolic processes on longer time scales while the water column stability and external environmental forces can act to uncouple the surface biology from waters below on shorter time scales. In addition, the control of NEP appears to be closely linked to changes in autotrophic activity in many cases, but not exclusively. Future research focusing on benthic incubations on longer time scales (diel) could fill in some gaps of knowledge about NEP in the area.

This study proposes an empirical model for predicting K_d(PAR) in Mississippi waters and partitioning the contributing biogeochemical factors. While the correlation between measured values and the model is high overall, some required assumptions of linearity cause the model to overestimate K_d(PAR) in the lower range, and underestimate in the higher range. The analysis shows that K_d(PAR) is primarily controlled by the concentration of suspended particulate matter, and some evidence exists that the PIM fraction has a higher control on light attenuation than POM. Knowledge of how absorption and backscattering change in relation to biogeochemistry is needed for this area, and may be a more direct method for relating to K_d(PAR) as an apparent optical property.

Though chlorophyll-based models reasonably predicted GPP in this study, ultimately, the possibility of extrapolating GPP to larger scales is limited by the inefficiencies of satellites to derive chlorophyll measurements in turbid waters. While all other biogeochemical/optical parameters analyzed tend to show some significant correlations and may be used to assess biogeochemical cycling in this estuary, chlorophyll does not seem to covary with any of these parameters, as it is a dynamic and constantly adapting biological variable. However, given the reasonable estimates of PAR and euphotic depth, some GPP estimates may be derived by simply collecting ground chlorophyll measurements and supplementing the rest of the input parameters with satellite-derived data. Comparisons of measured phytoplankton absorption to satellite QAA models in the area could also be useful.

APPENDIX A

COSINE (2π) TO SCALAR (4π) PAR SENSOR COMPARISON

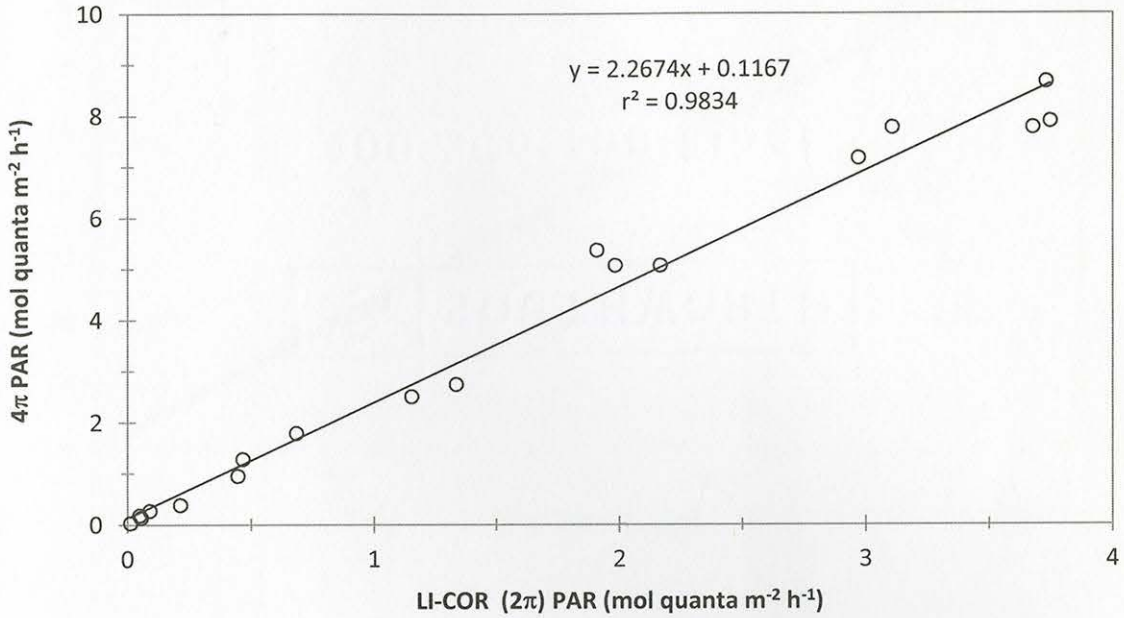

Comparison between LI-COR (2π) PAR sensor and Photosynthetron (4π) PAR sensor. Both sensors were exposed to variable light from the photosynthetron. $n = 17$.

APPENDIX B

COSINE (2π) PAR SENSOR COMPARISONS

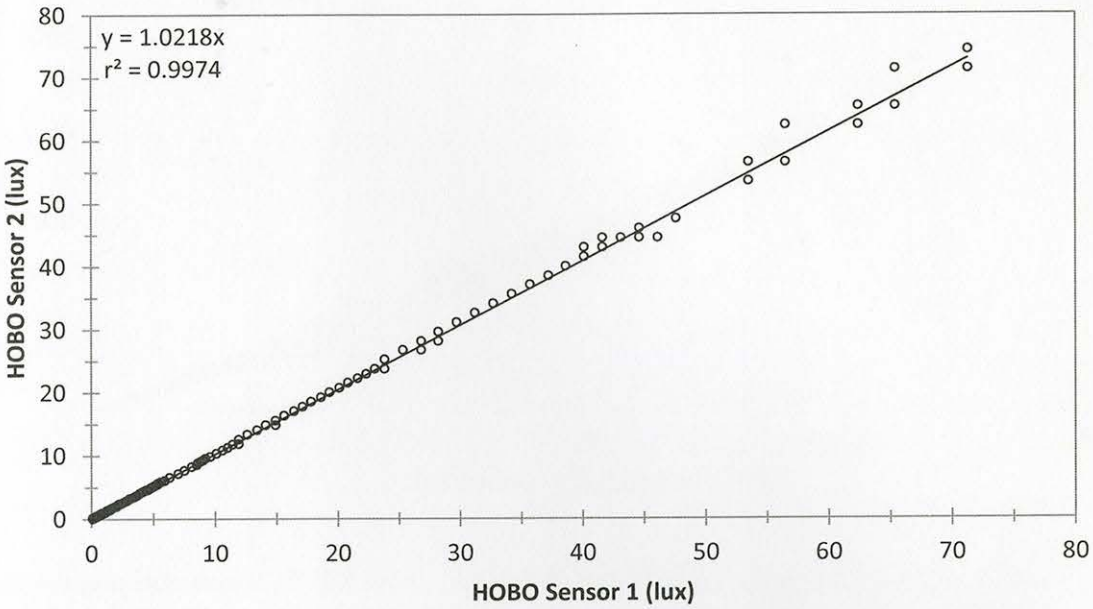

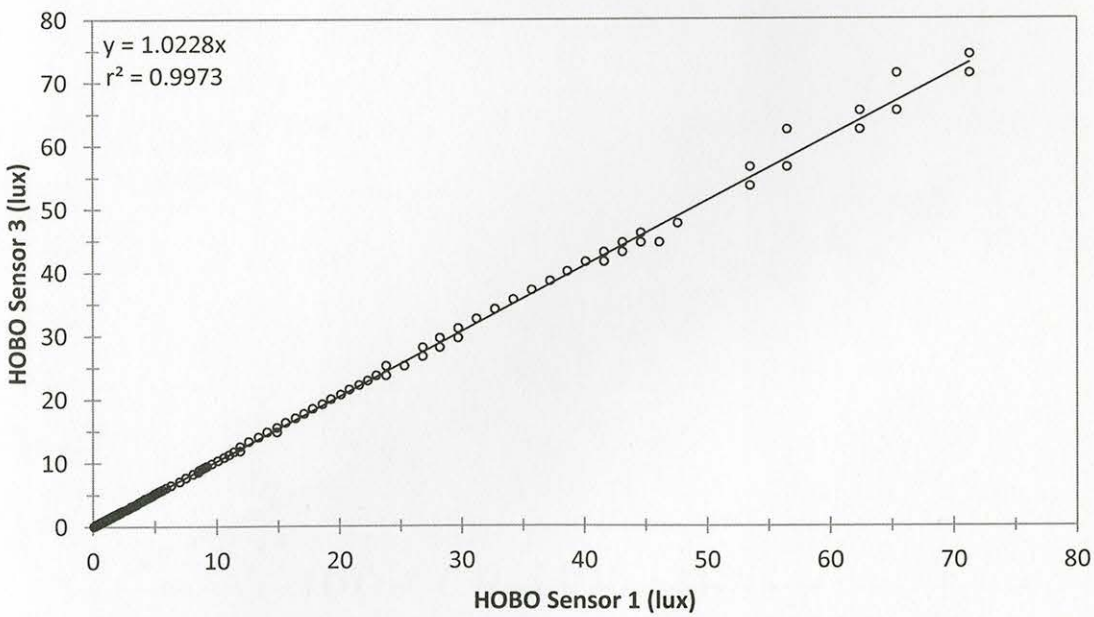

Comparison between three HOBO PAR sensors used in this study. Data taken from morning to midday. $n = 221$.

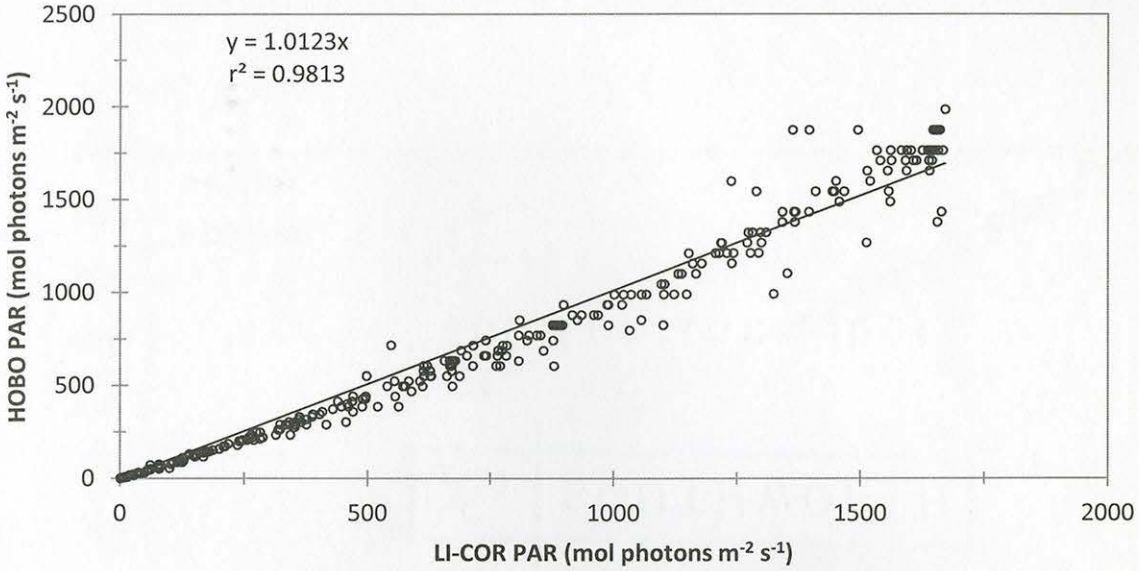

Comparison between LI-COR PAR and HOBO PAR (converted from lux) from St. Stanislaus PAR time series. Data taken over the course of one week (22Feb2011 – 27Feb2011). $n = 581$.

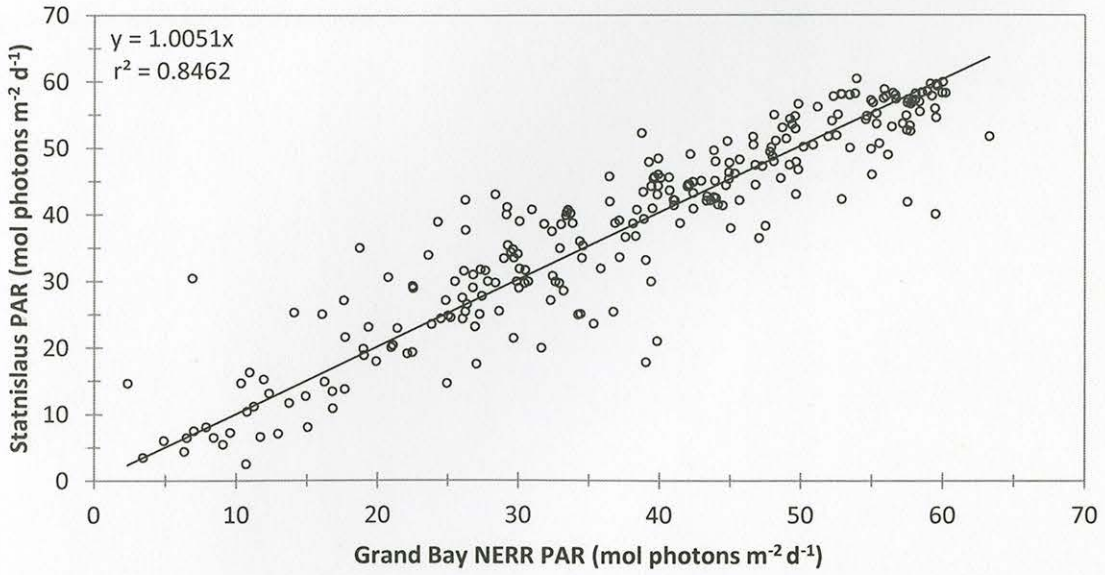

Comparison between Grand Bay NERR and St. Stanislaus PAR time series. Grand Bay NERR time series was incomplete, but includes approximately 10 months of comparable data. $n = 310$.

APPENDIX C

SPATIAL VARIABILITY OF PAR IN MISSISSIPPI WATERS

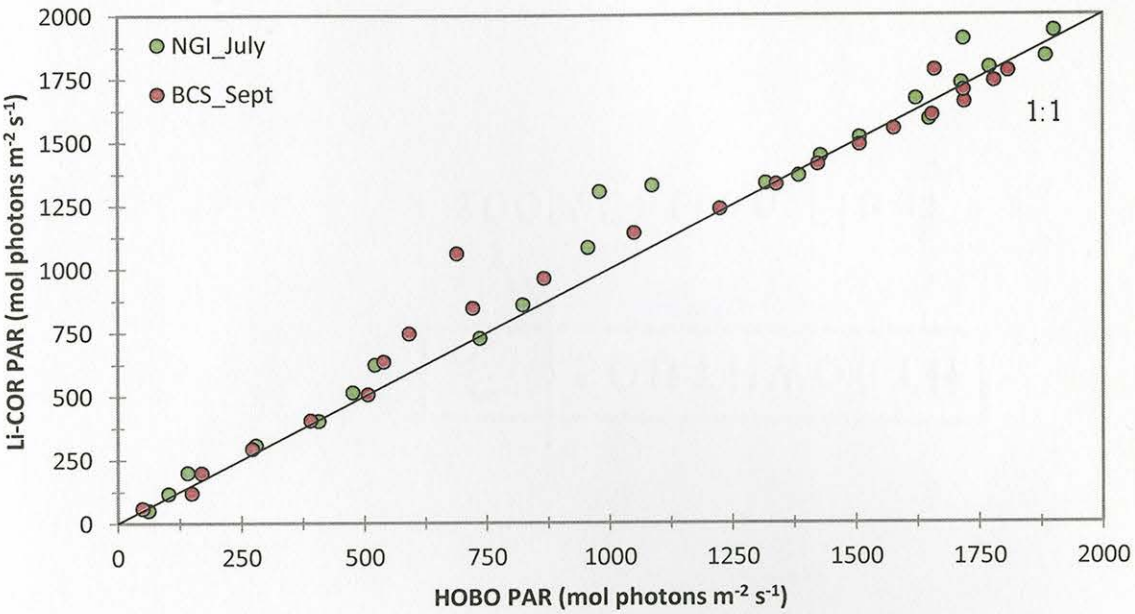

Spatial variability of PAR in the Mississippi Sound and Mississippi Bight. The HOBO sensor was attached to the boat, the LI-COR sensor was stationary.

APPENDIX D

PHOTOSYNTHESIS-IRRADIANCE (P-E) CURVES

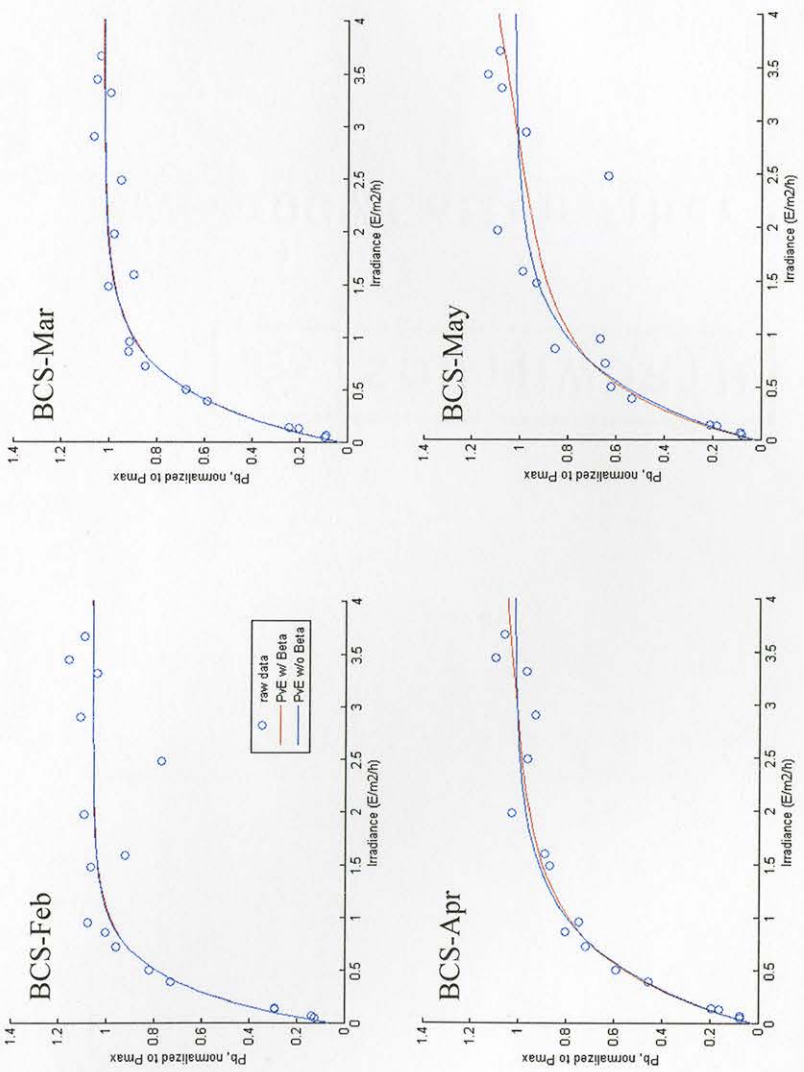

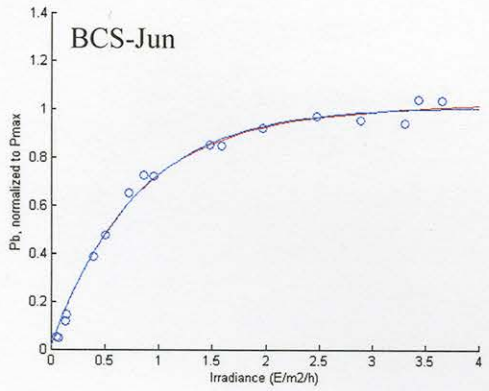
BCS-Jun
Pb, normalized to Pmax
Irradiance (E/m2/h)

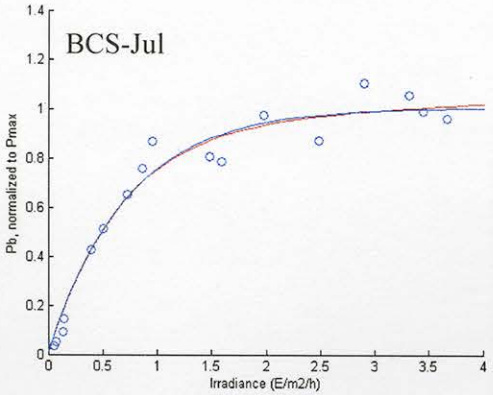
BCS-Jul
Pb, normalized to Pmax
Irradiance (E/m2/h)

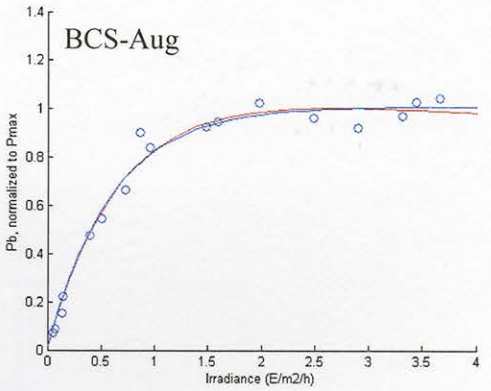
BCS-Aug
Pb, normalized to Pmax
Irradiance (E/m2/h)

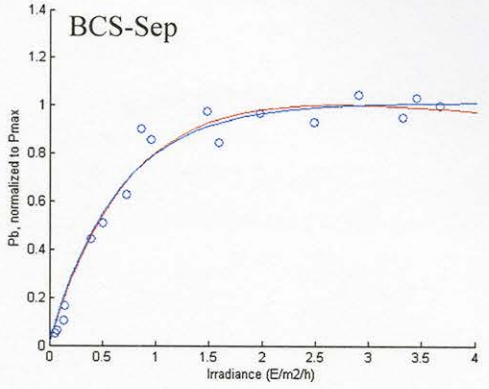
BCS-Sep
Pb, normalized to Pmax
Irradiance (E/m2/h)

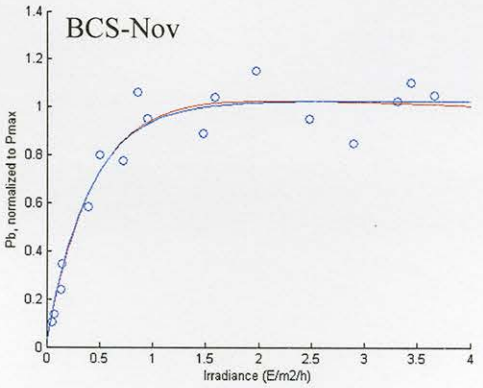
BCS-Nov
Pb, normalized to Pmax
Irradiance (E/m2/h)

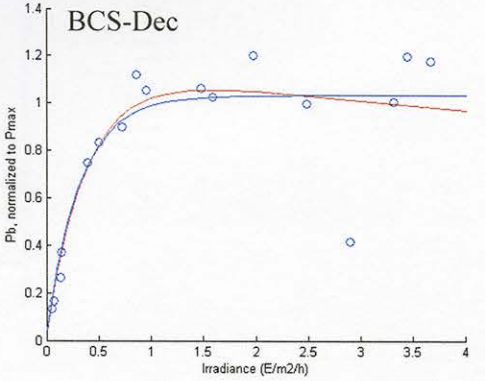
BCS-Dec
Pb, normalized to Pmax
Irradiance (E/m2/h)

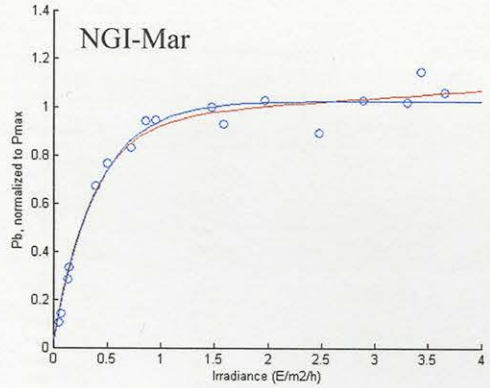
NGI-Mar
Pb, normalized to Pmax
Irradiance (E/m2/h)

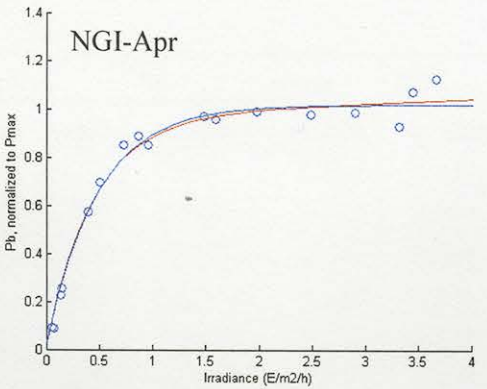
NGI-Apr
Pb, normalized to Pmax
Irradiance (E/m2/h)

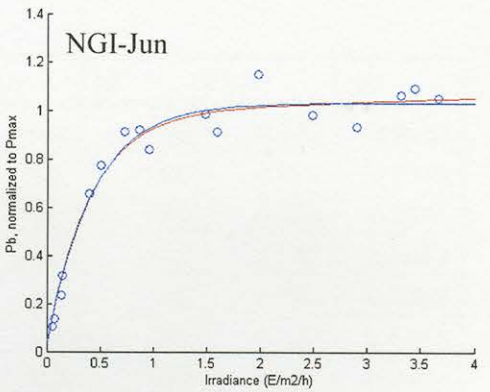
NGI-Jun
Pb, normalized to Pmax
Irradiance (E/m2/h)

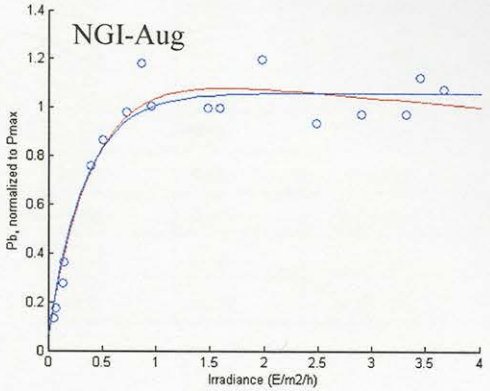
NGI-Aug
Pb, normalized to Pmax
Irradiance (E/m2/h)

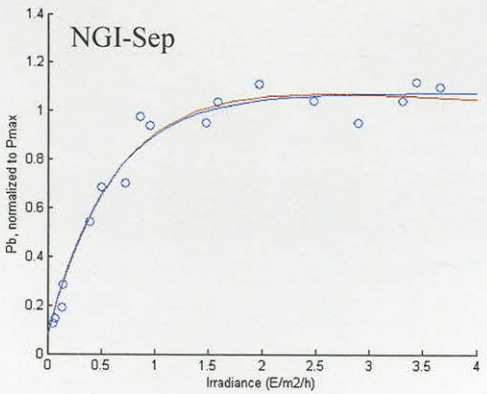
NGI-Sep
Pb, normalized to Pmax
Irradiance (E/m2/h)

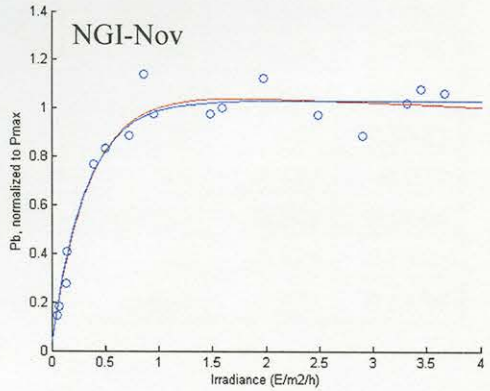
NGI-Nov
Pb, normalized to Pmax
Irradiance (E/m2/h)

Transect	Month	r^2	P_0	P_{max}	SE	Alpha	SE	Beta	SE	E_k	SE
BCS	Feb	0.9357	0.057	1.000	0.0359	2.668	0.3706	ND	ND	0.375	0.0538
BCS	Mar	0.9862	0.022	1.000	0.0187	2.111	0.1352	ND	ND	0.474	0.0316
BCS	Apr	0.9833	0.019	1.000	0.0222	1.520	0.0950	ND	ND	0.658	0.0437
BCS	May	0.9041	0.022	1.000	0.0527	1.559	0.2347	ND	ND	0.642	0.1023
BCS	Jun	0.9929	0.013	1.000	0.0180	1.264	0.0565	ND	ND	0.791	0.0381
BCS	Jul	0.9669	0.01	1.000	0.0349	1.385	0.1281	ND	ND	0.722	0.0713
BCS	Aug	0.9832	0.012	1.000	0.0216	1.690	0.1095	ND	ND	0.592	0.0404
BCS	Sep	0.9734	0.014	1.000	0.0305	1.468	0.1729	0.045	0.0879	0.674	0.1761
BCS	Nov	0.9407	0.026	1.000	0.0332	2.387	0.3644	0.015	0.0512	0.419	0.0853
BCS	Dec	0.7844	0.032	1.000	0.0633	3.086	0.8130	ND	ND	0.325	0.0878
NGI	Mar	0.9763	0.026	1.000	0.020	2.495	0.189	ND	ND	0.401	0.0314
NGI	Apr	0.9831	0.021	1.000	0.0196	2.083	0.1382	ND	ND	0.48	0.0332
NGI	Jun	0.969	0.034	1.000	0.0244	2.344	0.2068	ND	ND	0.427	0.039
NGI	Aug	0.9484	0.06	1.000	0.117	2.802	0.398	0.044	0.0512	0.364	0.0664
NGI	Sep	0.9734	0.075	1.000	0.0272	1.738	0.1447	ND	ND	0.575	0.0504
NGI	Nov	0.9556	0.032	1.000	0.0863	3.031	0.3797	0.019	0.035	0.332	0.0504

APPENDIX E

MONTHLY DATA PLOTS FOR DO INCUBATIONS

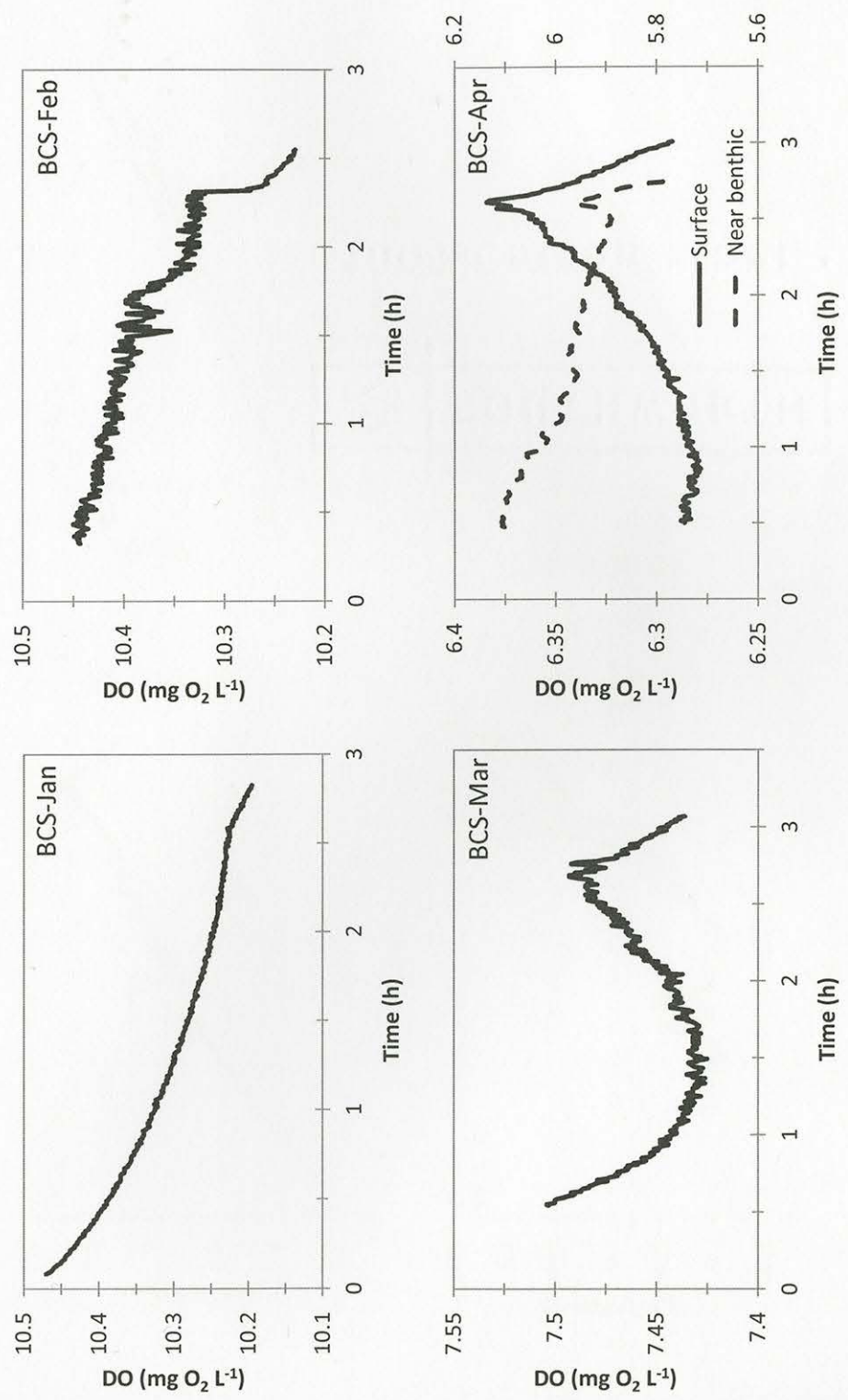

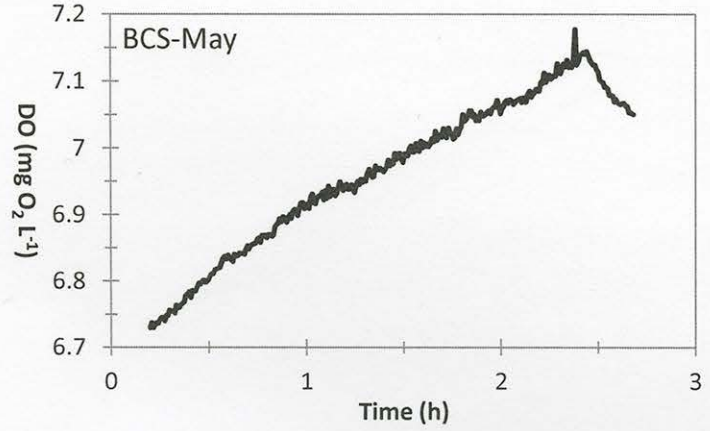
BCS-May
DO (mg O_2 L^{-1})
7.2
7.1
7
6.9
6.8
6.7
0
1
2
3
Time (h)

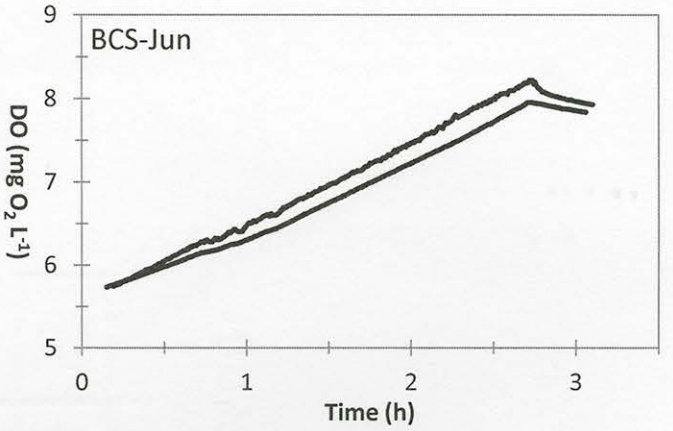
BCS-Jun
DO (mg O_2 L^{-1})
9
8
7
6
5
0
1
2
3
Time (h)

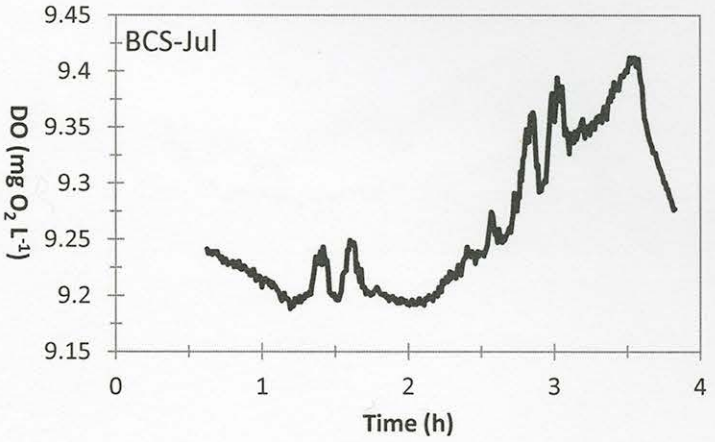
BCS-Jul
DO (mg O_2 L^{-1})
9.45
9.4
9.35
9.3
9.25
9.2
9.15
0
1
2
3
4
Time (h)

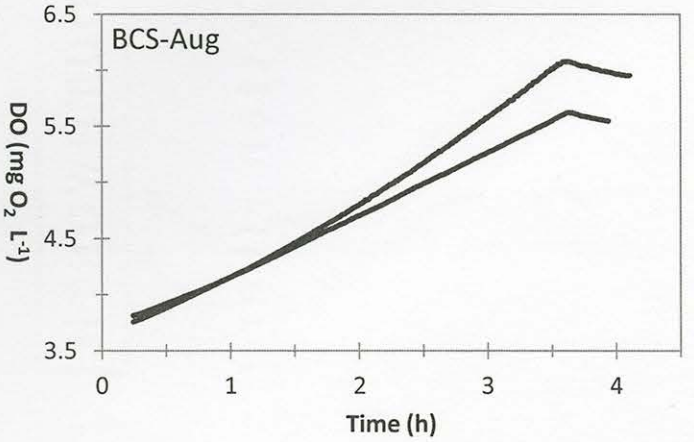
BCS-Aug
DO (mg O_2 L^{-1})
6.5
5.5
4.5
3.5
0
1
2
3
4
Time (h)

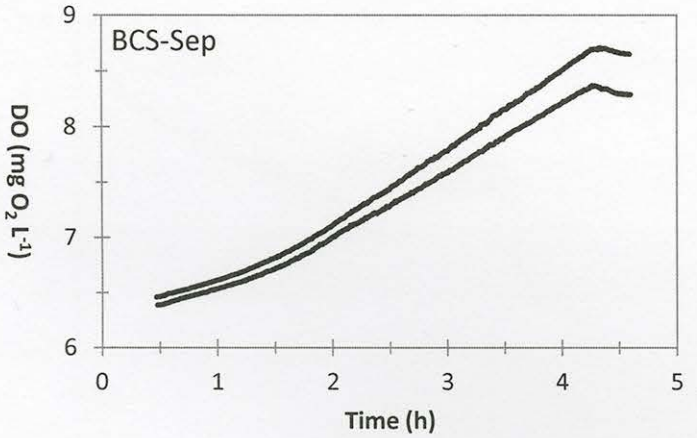
BCS-Sep
DO (mg O_2 L^{-1})
9
8
7
6
0
1
2
3
4
5
Time (h)

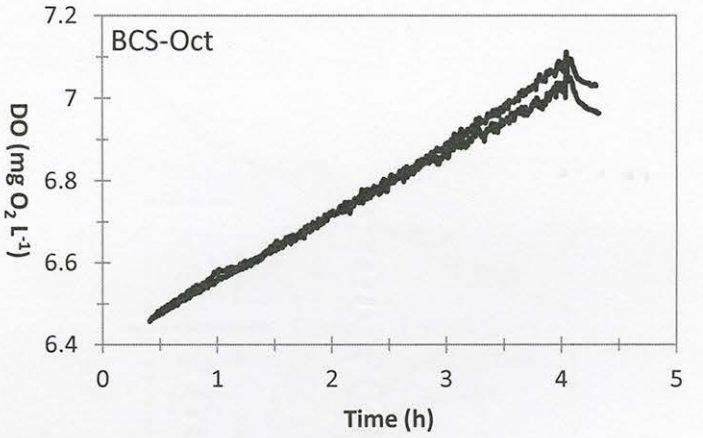
BCS-Oct
DO (mg O_2 L^{-1})
7.2
7
6.8
6.6
6.4
0
1
2
3
4
5
Time (h)

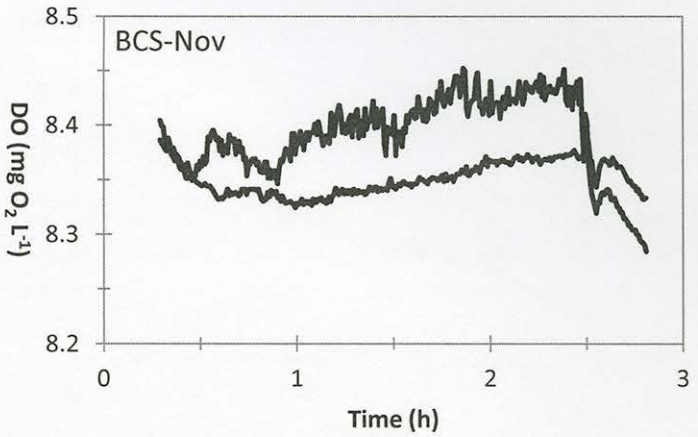
BCS-Nov
DO (mg O_2 L^{-1})
8.5
8.4
8.3
8.2
0
1
2
3
Time (h)

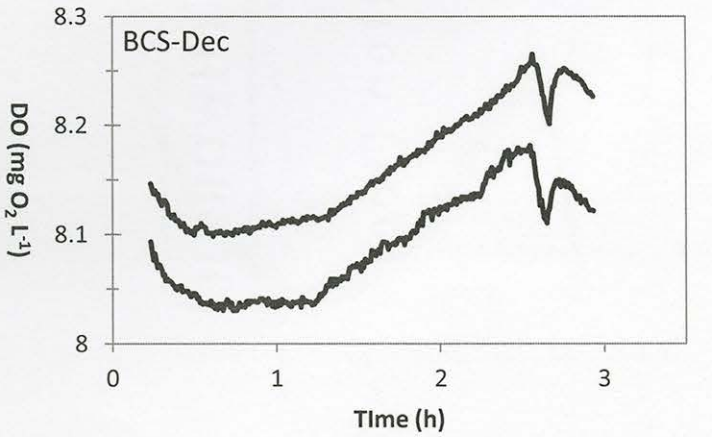
BCS-Dec
DO (mg O_2 L^{-1})
8.3
8.2
8.1
8
0
1
2
3
TIme (h)

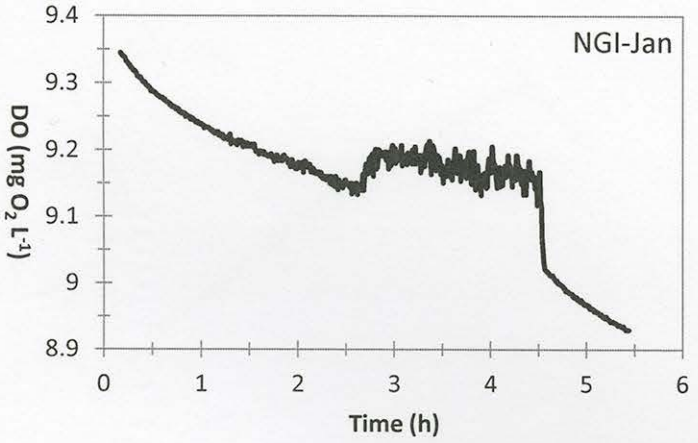
NGI-Jan
DO (mg O_2 L^{-1})
9.4
9.3
9.2
9.1
9
8.9
0 1 2 3 4 5 6
Time (h)

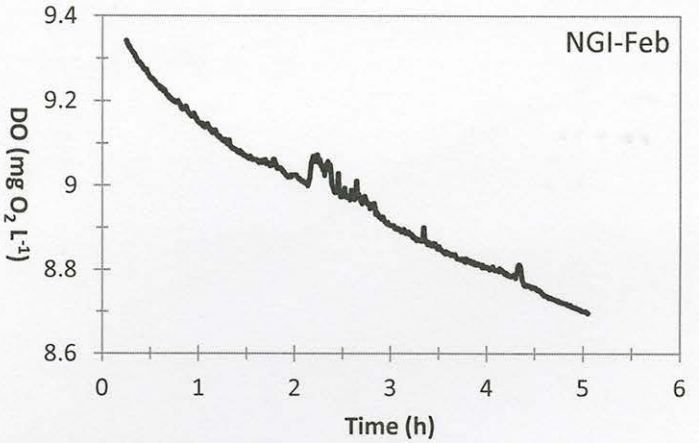
NGI-Feb
DO (mg O_2 L^{-1})
9.4
9.2
9
8.8
8.6
0 1 2 3 4 5 6
Time (h)

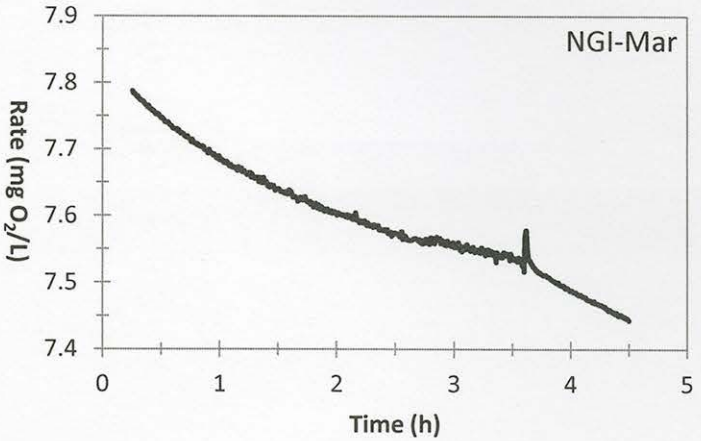
NGI-Mar
Rate (mg O_2/L)
7.9
7.8
7.7
7.6
7.5
7.4
0 1 2 3 4 5
Time (h)

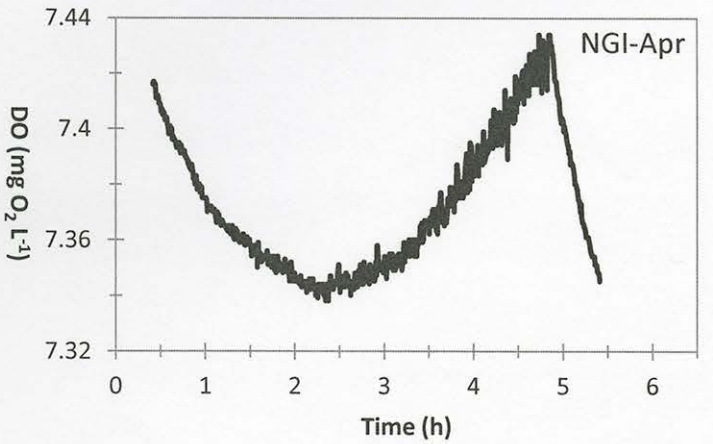
NGI-Apr
DO (mg O_2 L^{-1})
7.44
7.4
7.36
7.32
0 1 2 3 4 5 6
Time (h)

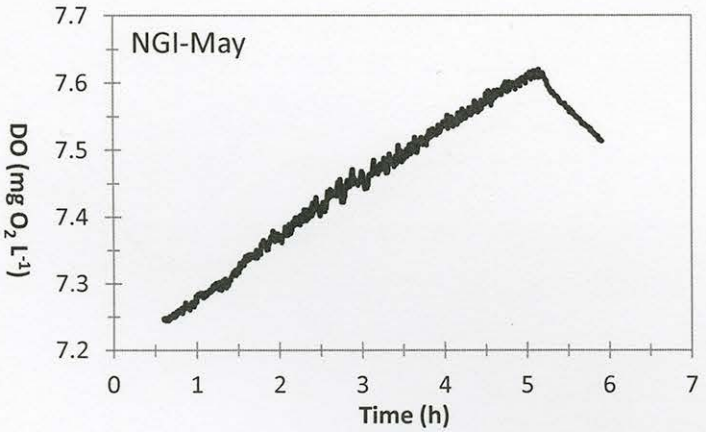

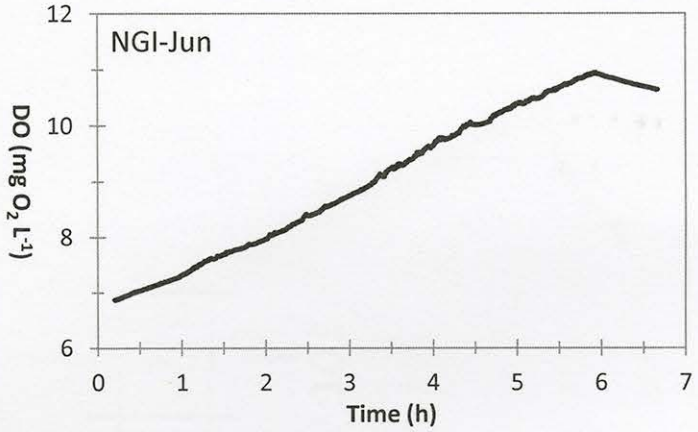

NO DATA FOR NGI JULY

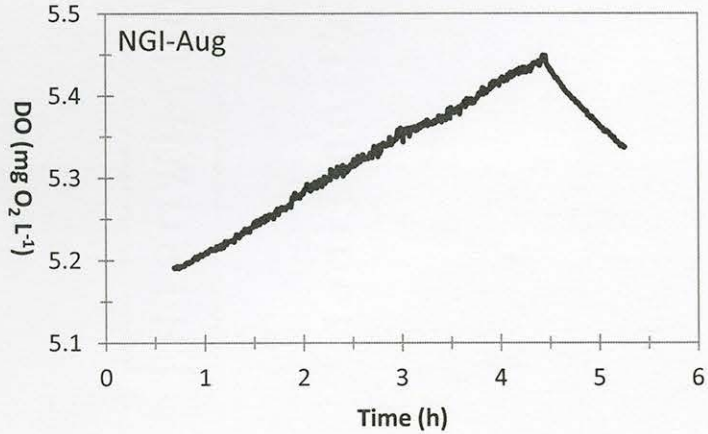

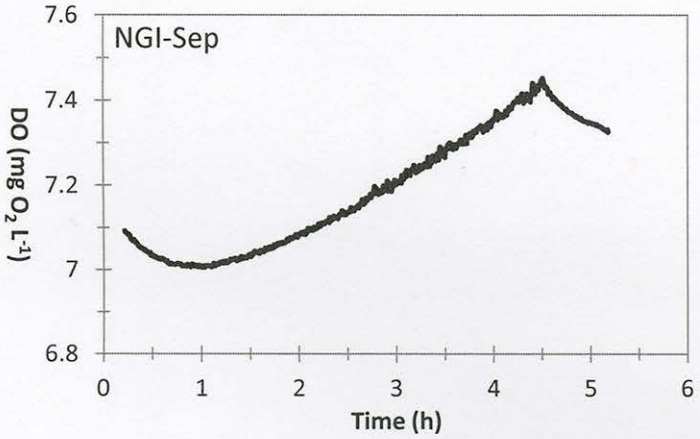
NGI-Sep
DO (mg O2 L-1)
7.6
7.4
7.2
7
6.8
0
1
2
3
4
5
6
Time (h)

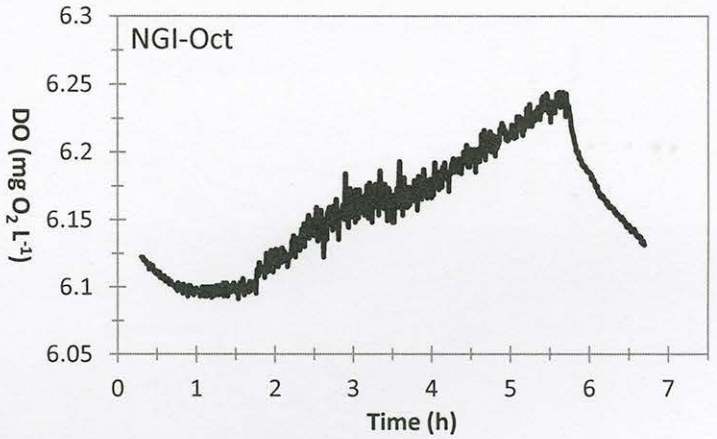
NGI-Oct
DO (mg O2 L-1)
6.3
6.25
6.2
6.15
6.1
6.05
0
1
2
3
4
5
6
7
Time (h)

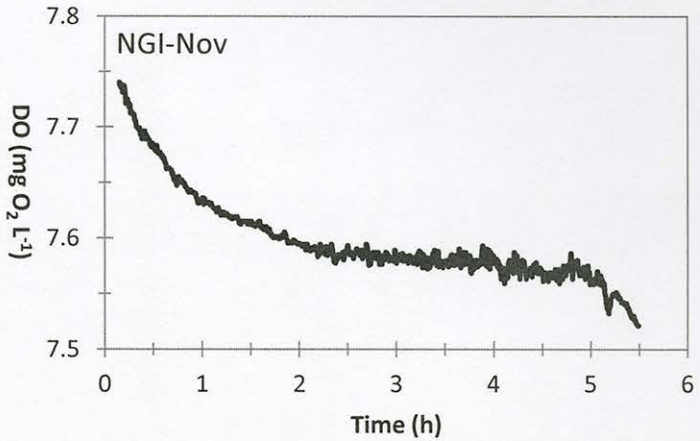
NGI-Nov
DO (mg O2 L-1)
7.8
7.7
7.6
7.5
0
1
2
3
4
5
6
Time (h)

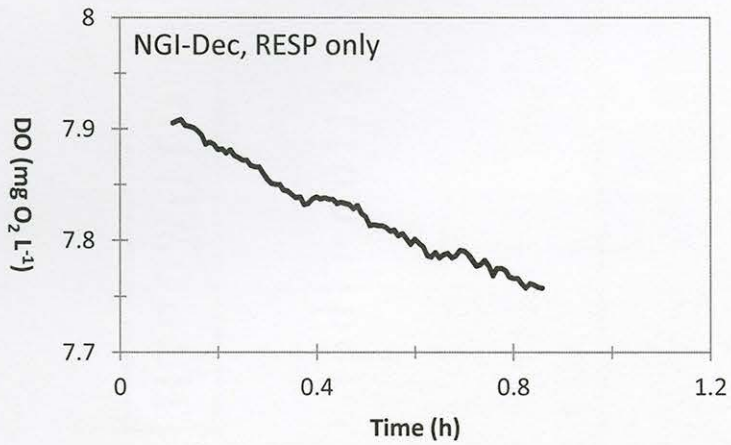
NGI-Dec, RESP only
DO (mg O2 L-1)
8
7.9
7.8
7.7
0
0.4
0.8
1.2
Time (h)

APPENDIX F

DARK AND LIGHT-DEPENDENT RESPIRATION TIME SERIES

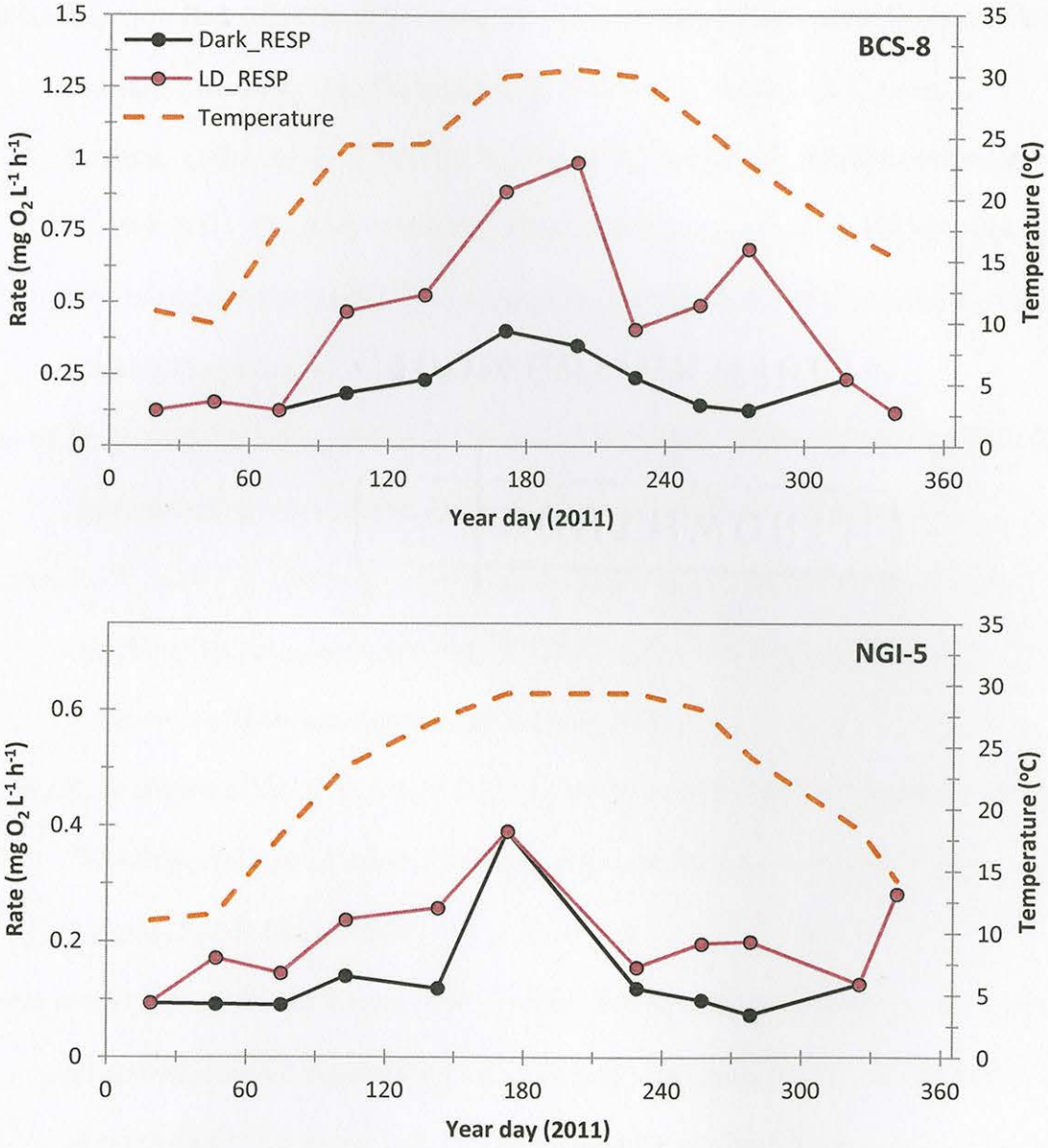

Time series of dark respiration (Dark_RESP) and light-dependent respiration (LD_RESP), with sea surface temperature for reference.

REFERENCES

Abbott, M. R., and R. C. Letelier. 1999. Algorithm theoretical basis document chlorophyll fluorescence (MODIS product number 20). ATBD-MOD-22.

Arellano, A., N. Briggs, F. Cao, A. Chase, H. Chen, A. Dave, C. Goyens, F. Henderikx-Freitas, C. Kearney, M. Kheireddine, S. Mishra, A. Neeley, M. Omand, L. Powers, A. Reisinger, S. Rivero, B. Russell, B. Seegers, R. Vandermeulen, and W. Zhu. 2011. Portfolio of Measurement, Processing, and Analysis Techniques for Optical Oceanography Data. Retrieved from ftp://misclab.umeoce.maine.edu/users/optics/classFTP/Portfolio/portfolio_compiled_final.pdf.

Atwell, B. H. 1973. Mississippi Sound remote sensing study. National Aeronautics and Space Administration, Earth Resources Laboratory. Report Number 048.

Austin, R. W., and T. J. Petzhold. 1986. The determination of the diffuse attenuation coefficient of sea water using the coastal zone color scanner, p. 239-256. *In* J. F. R. Gower [ed.], Oceanography from Space. Springer.

Azam, F., T. Fenchel, J. G. Field, J. S. Gray, L. A. Meyer-Reil, and F. Thingstad. 1983. The ecological role of water-column microbes in the sea. Marine Ecology Progress Series **10**: 257-263.

Bartleson, R. D., and W. M. Kemp. 1991. Preliminary ecosystem simulations of estuarine planktonic-benthic interactions: the planktonic submode, p. 243-261. *In* J. A. Mihursky and A. Chaney [eds.], New perspectives in the Chesapeake system: a research and management partnership. Chesapeake Research Consortium Publication.

Beardall, J., T. Burger-Wiersma, M. Rijkeboer, A. Sukenik, J. Lemoalle, Z. Dubinsky, and D. Fontvielle. 1994. Studies on enhanced post-illumination respiration in microalgae. Journal of Plankton research **16**: 1401-1410.

Beardall, J., E. Young, and S. Roberts. 2001. Approaches for determining phytoplankton nutrient limitation. Aquatic Sciences **63**: 44-69.

Behrenfeld, A. J., and P. G. Falkowski. 1997. A consumer's guide to phytoplankton primary productivity models. Limnology and Oceanography **42**: 1479-1491.

Behrenfeld, M. J., T. K. Westberry, E. Boss, R. T. O'Malley, D. A. Siegel, J. D. Wiggert, B. A. Franz, C. R. McClain, G. C. Feldman, S. C. Doney, J. K. Moore, G. Dall'Olmo, A. J. Milligan, I. Lima, and N. Mahowald. 2009. Satellite-Detected Fluorescence Reveals Global Physiology of Ocean Phytoplankton. Marine Science Faculty Scholarship, Paper 111.

Berger, W. H., V. S. Smetacek, and G. Wefer. 1989. Ocean productivity and paleoproductivity – an overview, p. 1-34. *In* W. H. Berger, V. S. Smetacek, and G. Wefer [eds], Dahlem workshop on productivity in the ocean: present and past. Chichester.

Biddanda, B., S. Opsahl, and R. Benner. 1994. Plankton respiration and carbon flux through bacterioplankton on the Louisiana Shelf. Limnology and Oceanography **39**: 1259-1275.

Blight, S. P., T. L. Bently, D. Lefevre, C. Robinson, R. Rodrigues, J. Rowlands, and P. J. leB. Williams. 1995. Phasing of autotrophic and heterotrophic plankton metabolism in a temperate coastal ecosystem. Marine Ecology Progress Series **128**: 61-75.

Blough, N. V., and R. del Vecchio. 2002. Chromophoric DOM in the coastal environment, p. 509-546. *In* D. A. Hansell and C. A. Carlson [eds.], Biogeochemistry of marine dissolved organic matter. Elsevier.

Boone, P. A. 1973. Depositional systems of the Alabama, Mississippi, and western Florida coastal zone. Transactions of the Gulf Coast Association of Geological Societies **23**: 226-277.

Breitburg, D. L. 1990. Near-shore hypoxia in the Chesapeake Bay: patterns and relationships among physical factors. Estuarine, Coastal and Shelf Science **30**: 593-609.

Bricaud, A., A. Morel, and L. Prieur. 1981. Absorption by dissolved organic matter of the sea (yellow substance) in the UV and visible domains. Limnology and Oceanography **26**: 43-53.

Branco, A. B., and J. N. Kremer. 2005. The relative importance of chlorophyll and colored dissolved organic matter (CDOM) to the prediction of the diffuse attenuation coefficient in shallow estuaries. Estuaries **28**: 643-652.

Bronk, A. A. 2002. Dynamics of DON, p. 153-231. *In* D. A. Hansell and C. A. Carlson [eds.], Biogeochemistry of Marine Dissolved Organic Matter. Elsevier.

Brunner, C. A., J. M. Beall, S. J. Bentley, and Y. Furukawa. Hypoxia hotspots in the Mississippi Bight. Journal of Foraminiferal Research **36**: 95-107.

Burns, C., and F. H. Rigler. 1967. Comparisons of filtering rates of *Daphnia rosea* in lake water and in suspensions of yeast. Limnology and Oceanography **12**: 492-502.

Caffrey J. M. 2003. Production, respiration, and net ecosystem metabolism in U.S. estuaries. Environmental Monitoring and Assessment **81**: 207-219.

Caffrey J. M. 2004. Factors controlling net ecosystem metabolism in U.S. estuaries. Estuaries **27**L 90-101.

Caffrey, J. M., J. E. Cloern, and C. Grenz. 1998. Changes in production and respiration during a spring phytoplankton bloom in San Francisco Bay, California, USA: implications for net ecosystem metabolism. Marine Ecology Progress Series **172**: 1-12.

Cai, Y., L. Guo, X. Wang, A. K. Mojzis, and D. G. Redalje. 2012. The source and distribution of dissolved and particulate organic matter in the Bay of St. Louis, northern Gulf of Mexico. Estuarine, Coastal and Shelf Sciences **96**: 96-104.

Carder, K. L., R. G. Steward, G. R. Harvey, and P. B. Ortner. 1989. Marine humic and fulvic acids: their effects on remote sensing of ocean chlorophyll. Limnology and Oceanography **34**: 68-81.

Carlson, C. A. 2002. Production and removal processes, p. 91-152. *In* D. A. Hansell and C. A. Carlson [eds.], Biogeochemistry of marine dissolved organic matter. Elsevier.

Carter, V., and N. B. Rybicki. 1990. Light attenuation and submersed macrophyte distribution in the tidal Potomac river and estuary. Estuaries **13**: 441-452.

Castro, M. S., C. T. Driscoll, T. T. Jordan, W. G. Reay, and W. R. Boyton. 2003. Sources of nitrogen to estuaries in the United States. Estuaries **26**: 803-814.

Cauwet, G. 2002. DOM in the coastal zone, p. 579-602. *In* D. A. Hansell and C. A. Carlson [eds.], Biogeochemistry of Marine Dissolved Organic Matter. Elsevier.

Christian, D., and Y. P. Sheng. 2003. Relative influence of various water quality parameters on light attenuation in Indian River Lagoon. Estuarine, Coastal and Shelf Science **57**: 961-971.

Christmas, J. Y. 1975. Cooperative Gulf of Mexico estuarine inventory and study, Mississippi. Mississippi Marine Conservation Commission. 1-71.

Cloern, J. E. 1987. Turbidity as a control on phytoplankton biomass and productivity in estuaries. Continental Shelf Research **7**: 1367-1381.

Cole, B. E., and J. E. Cloern. 1987. An empirical model for estimating phytoplankton productivity in estuaries. Marine Ecology Progress Series **36**: 299-305.

D'Avanzo, C., J. N. Kremer, S. C. Wainright. 1996. Ecosystem production and respiration in response to eutrophication in shallow temperate estuaries. Marine Ecology Progress Series **141**: 263-274.

D'Sa, E. J., and R. L. Miller. 2003. Bio-optical properties in waters influenced by the Mississippi River during low flow conditions. Remote Sensing of Environment **84**: 538-549.

Dall'Olmo, G., A. A. Gitelson, D. C. Rundquist, B. Leavitt, T. Barrow, and J. C. Holz. 2005. Assessing the potential of SeaWiFS and MODIS for estimating chlorophyll concentration in turbid productive waters using red and near-infrared bands. Remote Sensing of Environment **96**: 176-187.

del Castillo, C. E. 2005. Remote Sensing of organic matter in coastal waters, p. 157-180. *In* R. L. Miller, C. E. Del Castillo, and B. A. McKee [eds], Remote Sensing of the Aquatic Environment. Springer.

del Giorgio, P. A., and J. J. Cole. 1998. Bacterial growth efficiency in natural aquatic systems. Annual Review of Ecology and Systematics **29**: 503-541.

del Giorgio, P. A., and P. J. leB. Williams. 2005. The global significance of respiration in aquatic ecosystems: from single cells to the biosphere, p. 267-303. *In* P. A. del Giorgio and P. J. leB. Williams [eds.], Respiration in aquatic ecosystems. Oxford.

Dickey, E. D., G. C. Chang, Y. C. Agrawal, A. J. Williams III, and P. S. Hill. 1998. Sediment resuspension in the wakes of Hurricane Edouard and Hortense. Geophysical Research Letter **25**: 3533-3536.

Eleuterius, C. K. 1976. Mississippi Sound temporal and spatial distribution of nutrients. Mississippi-Alabama Sea Grant Consortium, MASGP-76-024.

Engle, V. D., J. K. Summers, and J. M. Macauley. 1999. Dissolved oxygen conditions in the northern Gulf of Mexico estuaries. Environmental Monitoring and Assessment **57**: 1-20.

EPA, 1983. Residue, non-filterable. *In:* Method 160.2. Methods for Chemical Analysis of Water and Wastes, U.S. Environmental Protection Agency, Environmental Monitoring and Support Laboratory, Cincinnati, OH.

Eppley, R. W. 1972. Temperature and phytoplankton growth in the sea. Fishery Bulletin **70**: 1063-1085.

Falkowski, P. G., and T. G. Owens. 1978. Effects of light intensity on photosynthesis in six species of marine phytoplankton. Marine Biology **45**: 289-295.

Falkowski, P. G., Z. Dubinsky, and G. Santostefano. 1985. Light-enhanced dark respiration in phytoplankton. Internationale Vereinigung fuer Theoretische und Angewandte Limnologie Verhandlungen **22**: 2830-2833.

Falkowski, P. G., and J. LaRoche. 1991. Accilmation to spectral irradiance in algae. Journal of Phycology **27**: 8-14.

Falkowski, P. G., and J. A. Raven. 2007. Aquatic Photosynthesis, 2nd ed. Princeton.

Floder, S., J. Urabe, and Z. Kawabata. 2002. The influence of fluctuating light intensities on species composition and diversity of natural phytoplankton communities. Oceologia **133**: 395-401.

Fuhrman, J. A., R. W. Eppley, A. Hagstrom, and F. Azam. 1985. Diel variations in bacterioplankton, phytoplankton, and related parameters in the Southern California Bight. Marine Ecology Progress Series **27**: 9-20.

Gallegos, C. L. 1994. Refining habitat requirements of submersed aquatic vegetation: role of optical models. Estuaries **17**:198-219.

Gallegos, C. and K. A. Moore. 2000. Factors contributing to water-column light attenuation, p. 16-27. *In* R. A. Batiuk, P. Bergstrom, W. M. Kemp, E. Koch, L. Murray, J. C. Stevenson, R. Bartleson, V. Carter, N. B. Rybicki, J. M. Landwehr, C. Gallegos, L. Karrh, M. Naylor, D. Wilcox, K. A. Moore, S. Ailstock, and M. Teichberg [eds.], Chesapeake Bay Submerged Aquatic Vegetation Water Quality and Habitat-based Requirements and Restoration Targets: A Second Technical Synthesis. U.S. Environmental Protection Agency, Chesapeake Bay Program, Annapolis, Maryland.

Gallegos, C. L. 2001. Calculating optical water quality targets to restore and protect submersed aquatic vegetation: overcoming problems in partitioning the diffuse attenuation coefficient for photosynthetically active radiation. Estuaries **24**: 381-397.

Gardner, W. S., M. J. McCarthy, S. A. Carini, and X. Lin. 2010. Evidence of nitrogen limitation of microbial activity in subsurface waters and sediments of the northern Gulf of Mexico hypoxic region. Proceedings from the 2010 AGU Ocean Sciences Meeting. [np] 22-26.

Gazeau, F., J. J. Middelburg, M. Loijens, J. P. Vanderborght, M. D. Pizay, and J. P. Gattuso. 2007. Planktonic primary production in estuaries: comparison of ^{14}C, O_2, and ^{18}O methods. Aquatic Microbial Ecology **46:** 95-106.

Geider, R. J. 1987. Light and temperature dependence of the carbon to chlorophyll *a* ratio in microalgae and cyanobacteria: implications for physiology and growth of phytoplankton. New Phytologist **106**: 1-34.

Geider, R. J. 1992. Respiration: taxation without representation, p. 333-359. *In* P.G. Falkowski and A.D. Woodhead [eds.], Primary Productivity and Biogeochemical Cycles in the Sea. Plenum.

Graham, W. M., F. Pages, and W. M. Hamner. 2001. A physical context for gelatinous zooplankton aggregations: a review. Hydrobiologia **451**: 199-212.

Gregg, W. W., and K. L. Carder. 1990. A simple spectral solar irradiance model for cloudless maritime atmospheres, Limnology and Oceanography **35**: 1657–1675.

Griffith, P. C. 1988. A high-precision respirometer for measuring small rates of change in the oxygen concentration of natural waters. Limnology and Oceanography **33**: 632-638.

Griffith, P. C., D. J. Douglas, and S. C. Wainwright. 1990. Metabolic activity of size-fractionated microbial plankton in estuarine, nearshore, and continental shelf waters of Georgia. Marine Ecology Progress Series **59**: 263-270.

Heinle, D. R. 1969. Temperature and zooplankton. Chesapeake Science **10**: 186-209.

Hernadez-Leon, S., and T. Ikeda. 2005. Zooplankton respiration. p. 57-82. *In* P. A. del Giorgio and P. J. leB. Williams [eds.], Respiration in aquatic ecosystems. Oxford.

Hopkinson Jr., C. S., and E. M. Smith. 2005. Estuarine respiration: an overview of benthic, pelagic, and whole system respiration, p. 122-146. *In* P. A. del Giorgio and P. J. leB. Williams [eds.], Respiration in aquatic ecosystems. Oxford.

Howarth, R. W. 1988. Nutrient limitation of net primary production in marine ecosystems. Annual Review of Ecology and Systematics **19**: 89-110.

Iriarte, A., I. de Madariaga, F. Diez-Garagarza, M. Revilla, and E. Orive. 1996. Primary plankton production, respiration and nitrification in a shallow temperate estuary during summer. Journal of Experimental Marine Biology and Ecology **208**: 127-151.

Irigoien, X., and J. Castel. 1997. Light limitation and distribution of chlorophyll pigments in a highly turbid estuary: the Gironde (SW France). Estuarine, Coastal and Shelf Science **44**: 507-517.

Jensen, L. M., K. Sand-Jensen, S. Marcher, and M. Hansen. 1990. Plankton community respiration along a nutrient gradient in a shallow Danish estuary. Marine Ecology Progress Series **61**: 75-85.

JGOFS. 1996. Protocols for the Joint Global Ocean Flux Study (JGOFS) core measurements. Report number 19.

Johnson, K. S., W. M. Berelson, E. S. Boss, Z. Chase, H. Claustre, S. R. Emerson, N. Gruber, A. Kortzinger, M. J. Perry, and S. C. Riser. 2009. Observing biogeochemical cycles at global scales with profiling floats and gliders, prospects for a global array. Oceanography **22**: 216-225.

Kanwisher, J. 1959. Polarographic oxygen electrode. Limnology and Oceanography **4**: 210-217.

Kemp, W. M., E. M. Smith, M. Marvin-DiPasquale, and W. R. Boyton. 1997. Organic carbon balance and net ecosystem metabolism in Chesapeake bay. Marine Ecology Progress Series **150**: 229-248.

Kirk J. T. O. 1992. The nature and measurement of the light environment in the ocean, p. 9-29. *In* P. G. Falkowski and A. D. Woodhead [eds.], Primary Productivity and Biogeochemical Cycles in the Sea. Plenum.

Kirk, J. T. O. 1994. Light and Photosynthesis in Aquatic Ecosystems. 2nd edition. Cambridge.

Kjerfve, B. 1983. Analysis of synthesis of oceanographic conditions in the Mississippi Sound. Final Report to U.S. Army Engineer District Mobile, AL. 1-229.

Kjerfve, B., and K. E. Magill. 1989. Geographic and hydrodynamic characteristics of shallow coastal lagoons. Marine Geology **88**: 187-199.

Lee, Z. P., K. L. Carder, and R. A. Arnone. 2002. Deriving inherent optical properties from water color: a multiband quasi-analytical algorithm for optically deep waters. Applied optics **41**: 5755-5772.

Lee, Z. P., and K. L. Carder. 2004. Absorption spectrum of phytoplankton pigments derived from hyperspectral remote-sensing reflectance. Remote Sensing of Environment **89**: 361-368.

Lee, Z. P., K. Du, and R. Arnone. 2005a. A model for the diffuse attenuation coefficient of downwelling irrandiance. Journal of Geophysical Research **110**: C02016 1-10.

Lee Z. P., M. Darecki, K. L. Carder, C. O. Davis, D. Stramski, and W. J. Rhea. 2005b. Diffuse attenuation coefficient of downwelling irradiance: an evaluation of remote sensing methods. Journal of Geophysical Research **110**: C02017 1-9.

Lee, Z. P., A. Weidmann, J. Kindle, R. Arnone, K. L. Carder, and C. Davis. 2007. Euphotic zone depth: its derivation and implication to ocean-color remote sensing. Journal of Geophysical Research **112**: C03009 1-11.

Lewis, M. R. 1992. Satellite ocean color observations of global biogeochemical cycles, p. 139-153. *In* P. G. Falkowski and A. D. Woodhead [eds.], Primary Productivity and Biogeochemical Cycles in the Sea. Plenum.

Lewis, M. R., and J. C. Smith. 1983. A small volume, short-incubation-time method for measurement of photosynthesis as a function of incident irradiance. Marine Ecology Progress Series **13**: 99-102.

Lewitus, A. J., and T. M. Kana. 1995. Light respiration in six estuarine phytoplankton species: contrasts under photoautotrophic and mixotrophic growth conditions. Journal of Phycology **31**: 754-761.

Lohrenz, S. E., M. J. Dagg, and T. E. Whitledge. 1990. Enhanced primary production at the plume/oceanic interface of the Mississippi River. Continental Shelf Research **10**: 639-664.

Lohrenz, S. E., G. L. Fahnenstiel, and D. G. Redalje. 1994. Spatial and temporal variations of photosynthetic parameters in relation to environmental conditions in coastal waters of the northern Gulf of Mexico. Estuaries **17**: 779-795.

Lohrenz, S. E., G. L. Fahnestiel, D. G. Redalje, G. A. Lang, M. J. Dagg, T. E. Whitledge, and Q. Dortch. 1999. Nutrients, irradiance, and mixing as factors regulating primary production in coastal waters impacted by the Mississippi River plume. Continental Shelf Research **19**: 1113-1141.

Lohrenz, S. E. and P. G. Verity. 2004. Regional oceanography: Southeastern United States and the Gulf of Mexico, p. 169-223. *In* A. R. Robinson and K. H. Brink [eds.], The Sea. President and Fellows of Harvard College.

Lorenzen, C. J. 1972. Extinction of light in the ocean by phytoplankton. Journal of Conservation **34**: 262–267.

Lytle T. F., and J. S. Lytle. 1983. Pollutant transport in Mississippi Sound. Interim Technical Report IV, MS-AL Sea Grant Consortium. 1-15.

Mallin, M. A., H. W. Paerl, J. Rudek, and P. W. Bates. 1993. Regulation of estuarine primary production by watershed rainfall and river flow. Marine Ecology Progress Series **93**: 199-203.

Miller, C. B. 2004. Biological Oceanography. 1st edition. Blackwell.

Miller, R. L., and B. A. McKee. 2004. Using MODIS Terra 250 m imagery to map concentrations of total suspended matter in coastal waters. Remote Sensing of Environment **93**: 259-266.

Moran, M. A., W. M. Sheldon Jr., and R. G. Zepp. 2000. Carbon loss and optical property changes during long-term photochemical and biological degradation of estuarine dissolved organic matter. Limnology and Oceanography **45**: 1254-1264.

Morel, A. 1988. Optical modeling of the upper ocean in relation to its biogenous matter content (Case I waters), Journal of Geophysical Research **93**: 10,749 – 10,768.

Morel, A., and J. F. Berthon. 1989. Surface pigments, algal biomass profiles, and potential production of the euphotic later: relationships reinvestigates in review of remote-sensing applications. Limnology and Oceanography **34**: 1545-1562.

Morel, A., and S. Maritorena. 2001. Bio-optical properties of oceanic waters: A reappraisal. Journal of Geophysical Research **106**: 7163-7180.

Morel, A., and L. Prieur. 1977. Analysis of variation in ocean color. Limnology and Oceanography **22**: 709-722.

Morel, A., and R. C. Smith. 1982. Terminology and units of optical oceanography. Marine Geodesy **5**: 335-349.

Mortazavi, B., A. A. Riggs, J. M. Caffret, H. Genet, and S. W. Phipps. 2012. The contribution of benthic nutrient regenereation to primary production in a shallow eutrophic estuary, Weeks Bay, Alabama. Estuaries and Coasts **35**: 862-877.

O'Reilly, J. E., S. Maritorena, D. A. Siegel, M. C. O'Brien, D. Toole, B. G. Mitchell, M. Kahru, F. P. Chavez, P. Strutton, G. F. Cota, S. B. Hooker, C. R. McClain, K. L. Carder, F. Muller-Karger, L. Harding, A. Magnuson, D. Phinney, G. F. Moore, J. Aiken, K. R. Arrigo, R. Letelier, and M. Culver. 2000. Ocean color chlorophyll algorithms for SeaWiFS, OC2, and OC4: Version 4, p. 9-27. *In* S. B. Hooker and E. R. Firestone [eds.], SeaWiFS Postlaunch Calibration and Validation Analyses, Part 3, NASA Technical Memorandum.

Outdot, C., R. Gerard, P. Morin, and I. Gningue. 1988. Precise shipboard determination of dissolved oxygen (Winkler procedure) for productivity studies with a commercial system. Limnology and Oceanography **33**: 146-150.

Pennock, J. R., and J. H. Sharp. 1994. Temporal alternation between light-and nutrient-limitation of phytoplankton production in a coastal plain estuary. Marine Ecology Progress Series **111**: 275-288.

Peterson, D. H., and J. P. Festa. 1984. Numerical simulation of phytoplankton productivity in partially mixed estuaries. Estuarine, Coastal and Shelf Science **19**: 563-589.

Platt, T., C. L. Gallegos, and W. G. Harrison. 1980. Photoinhibition of photosynthesis in natural assemblages of marine phytoplankton. Journal of Marine Research **38**: 687-701.

Pomeroy, L. R., and R. E. Johannes. 1968. Occurrence and respiration of ultraplankton in the upper 500 meters of the ocean. Deep-Sea Reasearch **15**: 381-391.

Pomeroy, L. R. 1974. The ocean's food web, a changing paradigm. Bioscience **24**: 499-504.

Qian, Y., A. E. Jochens, M. C. Kennicutt II and D. C. Biggs. 2003. Spatial and temporal variability of phytoplankton biomass and community structure over the continental margin of the northeast Gulf of Mexico based on pigment analysis. Continental Shelf Research **23**: 1-17.

Raven, J. A., and R. J. Geider. 1988. Temperature and algal growth. New phytologist **110**: 441-461.

Redalje, D. G., S. E. Lohrenz, and G. L. Fahnenstiel. 1994. The relationship between primary production and the vertical export of particulate organic matter in a river-impacted coastal ecosystem. Estuaries **17**: 829-838.

Redfield, A. C. 1934. On the proportions of organic derivatives in seawater and their relation to the composition of plankton, p. 177-192. *In* R. J. Daniel [ed.], James Johnstone Memorial Volume. University Press of Liverpool.

Ren, S. 2010. Molecular detection of marine N_2 fixation by cyanobacteria in the northern Gulf of Mexico. M.S. thesis, The Univ. of Southern Mississippi.

Revilla, M., A. Ansotegui, A. Iriarte, I. Madariaga, E. Orive, A. Sarobe, and J. M. Trigueros. 2002. Microplankton metabolism along a trophic gradient in a shallow-temperate estuary. Estuaries **25**: 6-18.

Ryther, J. H. 1956. The measurement of primary production. Limnology and Oceanography **1**: 72-84.

Sampou, P., and W. M. Kemp. 1994. Factors regulating plankton community respiration in Chesapeake Bay. Marine Ecology Progress Series **110**: 249-258.

Sanford, L. P., K. G. Sellner, and D. L. Breitburg. 1990. Covariability of dissolved oxygen with physical processes in the summertime Chesapeake Bay. Journal of Marine Research **48**: 567-590.

Sathyendranath, S., and T. Platt. 1988. The spectral irradiance field at the surface and in the interior of the ocean: A model for applications in oceanography and remote sensing. Journal of Geophysical Research **93**: 9270-9280.

Sawant, P. A., 2009. Factors influencing the environmental quality of the Bay of Saint Louis, Mississippi and implications for evolving coastal management policies. Ph.D. thesis, The Univ. of Southern Mississippi.

Sieburth, J. McN. 1967. Seasonal selection of estuarine bacteria by water temperature. Journal of Experimental Marine Biology and Ecology **1**: 98-121.

Smith Jr., W. O., and D. J. DeMaster. 1996. Phytoplankton biomass and productivity in the Amazon River plume: correlation with seasonal river discharge. Continental Shelf Research **16**: 291-319.

Smith, E. M., and W. M. Kemp. 1995. Seasonal and regional variations in plankton community production and respiration for Chesapeake Bay. Marine Ecology Progress Series **116**: 217-231.

Smith, E. M. and W. M. Kemp. 2001. Size structure and the production/respiration balance in a coastal plankton community. Limnology and Oceanography **46**: 473-485.

Smith E. M., and W. M. Kemp. 2003. Planktonic and bacterial respiration along an estuarine gradient: responses to carbon and nutrient enrichment. Aquatic Microbial Ecology **30**: 251-261.

Solorzano, L., and J. H. Sharp. 1980. Determination of total dissolved phosphorous and particulate phosphorous in natural waters. Limnology and Oceanography **25**: 754-758.

Sterner, R. W., and J. J. Elser. 2002. Ecological Stoichiometry. 1st edition. Princeton.

Strickland, J. D. H., and T. R. Parsons. 1972. A practical handbook of seawater analysis, 2nd edition. Bulletin of the Fisheries Research Board of Canada.

Van Laake, P. E., and G. A. Sanchez-Azofeifa. 2005. Mapping PAR using MODIS atmosphere products. Remote Sensing of Environment **94**: 554-563.

Wang, D., S. Liang, R. Liu, and T. Zheng. 2010. Estimation of dailt-integrated PAR from sparse satellite observations: comparison of temporal scaling methods. International Journal of Remote Sensing **31**: 1661-1677.

Welschmeyer, N. A. 1994. Fluorometric analysis of chlorophyll *a* in the presence of chlorophyll *b* and phaeopigments. Limnology and Oceanography **39**: 1985-1992.

Weger, H. G., R. Herzig, P. G. Falkowski, and D. H. Turpin. 1989. Respiratory losses in the light in a marine diatom: measurements by short-term mass spectrometry. Limnology and Oceanography **34**: 1153-1161.

Williams, P. J. leB. 1981. Microbial contribution to overall marine plankton metabolism: direct measurements of respiration. Oceanologica Acta **4**: 359-364.

Willaims, P. J. leB. 1984. A review of measurements of respiration rates of marine plankton populations, p. 357-389. *In* J. E. Hobbie and P. J. leB. Williams [eds]. Heterotrophy in the Sea. Plenum Press.

Williams, P. J. leB, and N. W. Jenkinson. 1982. A transportable microprocessor-controlled precise Winkler titration suitable for field station and shipboard use. Limnology and Oceanography **27**: 576-585.

Williams P. J. leB., and P. A. del Giorgio. 2005. Respiration in aquatic ecosystems: history and background, p. 1-17. *In* P. A. del Giorgio and P. J. leB. Williams [eds.], Respiration in aquatic ecosystems. Oxford.

Winkler, L. W. 1888. Die Bestimmung des im Wasser gelosten Sauerstoffes. Chemische Berichte **21**: 2843-2855.

Wofsy, S. C. 1983. A simple model to predict extinction coefficients and phytoplankton biomass in eutrophic waters. Limnology and Oceanography **28**: 1144-1155.

Xu, J., R. R. Hood, and S. Chao. 2005. A simple empirical model for simulating light attenuation variability in a partially mixed estuary. Estuaries **28**: 572-580.